2016

Characterization Of Charge Accommodation In Biologically Important Hydrogen-Bonded Clusters

John Thomas Kelly
University of Mississippi

CHARACTERIZATION OF CHARGE ACCOMMODATION IN BIOLOGICALLY
IMPORTANT HYDROGEN-BONDED CLUSTERS

A DISSERTATION SUBMITTED IN PARTIAL FULFILLMENT OF
REQUIREMENTS FOR THE DEGREE OF
DOCTOR OF PHILOSOPHY IN THE DEPARTMENT OF
CHEMISTRY & BIOCHEMISTRY
THE UNIVERSITY OF MISSISSIPPI

BY

JOHN THOMAS KELLY

AUGUST 2016

ABSTRACT

The underlying motivation of chemical physics and physical chemistry is to understand naturally occurring chemical and physical processes from the nanoscopic molecular level to the macroscopic condensed phase. Over the past half-century, experimentalists have developed a number of laser-based analytical techniques to bridge the gap between the bulk phase and the single molecule. Here, we look at bulk phase and gas phase clusters to compare the local hydrogen-bonded network. To better understand the role noncovalent interactions have on biologically relevant building blocks in a natural environment, we compare the microhydration of gas phase cluster ions to condensed phase spectra. The accommodation of excess charge plays an essential character in a number of biochemical processes involving peptides, nucleobases, aerosols, dissolutions, etc. A time-of-flight mass spectrometer was constructed to isolate discrete numbers of solute and solvent molecules for spectroscopic interrogation via light-matter interactions. We also employed high-resolution Raman spectroscopy for vibrational interrogation of temperature dependence in crystalline lattice modes as well as effects of surface-enhanced plasmon resonances. Electronic structure methods were employed for accurate spectral assignment and identification of structural motifs.

DEDICATION

To my loving wife

QUOTE

Every great magic trick consists of three parts or acts. The first part is called "The Pledge". The magician shows you something ordinary: a deck of cards, a bird or a man. He shows you this object. Perhaps he asks you to inspect it to see if it is indeed real, unaltered, normal. But of course... it probably isn't. The second act is called "The Turn". The magician takes the ordinary something and makes it do something extraordinary. Now you're looking for the secret... but you won't find it, because of course you're not really looking. You don't really want to know. You want to be fooled. But you wouldn't clap yet. Because making something disappear isn't enough; you have to bring it back. That's why every magic trick has a third act, the hardest part, the part we call "The Prestige".

Cutter, *The Prestige*

LIST OF ABBREEVIATIONS AND SYMBOLS

”	inch
°	degrees
Å	Angstrom
AEA/AEA_0	adiabatic electron affinity / zero-point corrected AEA
ALS	Advanced Light Source
CF	conflat®
CID	collision-induced dissociation
cm^{-1}	wavenumbers
D	Debye
DC	direct current
DFT	density functional theory
DP	diffusion pump
EA	electron affinity
eBE	electron binding energy
eKE	electron kinetic energy
eV	electron volt
ESI	electrospray ionization
FIR	far infrared
FWHM	full width half maximum
$h\nu$	photon (energy)
HV	high voltage

Hz	Hertz
IR	infrared
IRPD	infrared photodissociation
J	Joule
K	Kelvin (temperature)
KTA	potassium titanyl arsenate (KTiOAsO$_4$)
KTP	potassium titanyl phosphate (KTiOPO$_4$)
LEE	low energy electron
MCP	microchannel plate
MIR	mid infrared
MS	mass spectrometer
m/z	mass-to-charge ratio
Nd:YAG	neodymium-doped yttrium aluminium garnet
NIR	near infrared
nm	nanometer
PES	photoelectron spectroscopy
PES	potential energy surface
psi	pounds per square inch
OPO	optical paramagnetic oscillator
OPA	optical paramagnetic amplifier
TMP	turbomolecular pump
TOF	time-of-flight

UV	ultraviolet
V	volt
VDE	vertical detachment energy
VIS	visible
VMI	velocity map imaging
ZPE	zero-point energy
μs	microsecond
π	pi orbital
π*	anti-bonding pi orbital
Ω	ohm (resistance)

ACKNOWLEDGEMENTS

I would like to thank Professor Nathan Hammer for his magnificent ubiquitous role in my graduate career and early professional career during my time at the University of Mississippi. Nathan has an extremely inimitable approach on science when it comes to the research, incorporating undergraduates, and presentation. Some may misunderstand his "hands-off" approach as apathy, but after spending the better part of a decade as one of his graduate students, I understand his outlook as construction of self-discipline, self-motivation, self-appreciation, and ultimately the life skill of problem solving. Nathan has been more than supportive when it came to investing in his students. He supported my travels throughout my PhD at local, regional, and national American Chemical Society (ACS) meetings, International Symposium of Molecular Spectroscopy (ISMS) meetings, visits to groups with similar experimental setups (Johnson, Duncan, Douberly, Bowen, Compton, von Helden, and Asmis) across the US and also abroad. Though visiting each group had taught me something about experimental procedure or technique, talking with Nathan about fundamental science is what sparked my interested in chemical physics and physical chemistry. Lunch at *Handy Andy's* in Oxford, Mississippi was a history classroom in a sense of hearing about his time at UT working with Bob Compton or the time he spent as a postdoc at Yale with Mark Johnson.

In addition to my experimental spectroscopy research adviser, I would like to thank Professor Greg Tschumper, whose support has been incalculable over the years and was a second research adviser to me when projects involved electronic structure theory. Greg's appreciation for his profession and diligent work ethic is what one should strive for in all parts

of life, but one of his most admirable characteristics would be his ability to separate professional and personal matters. Outside of research, Greg was always an excellent host at his annual summer physical chemistry social with his enthusiasm for red wine and his "Hawaiian Punch" recipe. I thank Greg for encouraging me to move beyond convenient density functional theory and to strive for the correct answer by "hitting it with the sledge-hammer", or more commonly referred to *coupled-cluster* in the basement of Coulter Hall.

I would like to thank a number of extraordinary members of the scientific community that we collaborated with in our research efforts: Dean Guyer (*LaserVision*), Kit Bowen (Johns Hopkins), Keith Hollis (Mississippi State), Mark Johnson (Yale), Ken Jordan (Pittsburg), Bob Compton (Tennessee), Mike Duncan (Georgia), and Gary Douberly (Georgia). I would like to thank graduate students in the Johnson Group: Andrew DeBlase, Conrad Wolke, Patrick Kelleher, and the Duncan Group: Jon Maner. Without the efforts of these individuals, the University of Mississippi would not have the pleasure of mass selecting cluster anions.

The day-to-day discussion with fellow graduate students was truly one of the most important parts of my education. Louis McNamara was an incoming graduate student the same time I came into the department, and his knowledge of various physical phenomena and wizardry with Mathematica is unparalleled (I believe he will be the only person to code Hartree-Fock in Mathematica). Debra Jo Scardino was the senior member of the Hammer research group that really looked out for me while I was young and naive in graduate school. Thomas Ellington was always ready to strike up a debate on computational chemistry and the hours a graduate student should be working. It was our time at the Growler that we sat down and really discussed what we think a graduate student should and should not be doing

TABLE OF CONTENTS

LIST OF FIGURES

LIST OF TABLES

CHAPTER 1

INTRODUCTION

My research achievements as a graduate student in the Department of Chemistry and

Biochemistry at the University of Mississippi have resulted in six published peer-reviewed

articles, one featured on the cover of a January issue of *Physical Chemistry and Chemical

Physics*. Three of these are first author publications in peer-reviewed journals. Two additional

manuscripts are included in this dissertation to be submitted in the future. These achievements

would not have been made possible without the research assistantship through the National

Science Foundation CAREER Award (CHE-0955550) of Prof. Nathan I. Hammer and a

GAANN fellowship.

1.1 MODERN PHYSICAL CHEMISTRY

Many historians credit Wilhelm Ostwald to be the father of physical chemistry for his

efforts and contributions to Haber and Bosch's nitrogen fixation process, patent on

manufacturing nitric acid, and Nobel Prize in Chemistry (1909) in recognition of his work on

catalysis, reaction rates, and chemical equilibrium. By the late 1800's, Ostwald was only a

representative of a vastly growing scientific community in search for rationalization of physical

properties and chemical constitution. Innovation propagated in the areas of molecular kinetics,

chemical thermodynamics, reaction dynamics, and atomic spectroscopy with the greatest

minds of the century. Carnot and Clapeyron described the progression of turning heat (thermal

energy) into work (mechanical energy), Helmholtz and Joule's explanation on conservation of energy, Bernoulli's association of molecular motion with pressure, van der Waals' correction to the ideal gas laws, Maxwell, Boltzmann, and Gibbs' development of statistical mechanics, and lastly Arrhenius' analysis of dissociation of acids, bases and salts in solution.

Many introductory physical chemistry textbooks describe spectroscopy as the interaction between electromagnetic radiation and matter and briefly mention cornerstone experiments: Einstein's explanation of photoelectric effect, Plank's description of blackbody radiation, and de Broglie relations of particle-wave duality. Spectroscopy pre-dates the establishment of chemistry subdivision (physical chemistry) when Brewster characterized the spectral features of pass sunlight through nitrous acid, iodine, and sulfur gases (absorption) or Bunsen studied "bright line" spectrum by passing light from salt solutions in a flame through a prism. Early forms of spectroscopy helped mold and develop the classification of elements and ultimately form the modern day periodic table.

The evolution of modern physical chemistry has fortified what is today known as atomic and molecular spectroscopy. One of the most valuable developments of the 20^{th} century was emissive radiation sources in different areas of the electromagnetic spectrum with exceptionally short bandwidth, such as the laser. Here we employ spectroscopic laser techniques as well as electronic structure theory to characterize molecular cluster and the effects of the formation of a noncovalent network. The arrangement of these types of interactions, such as hydrogen bonds, can lead to observable spectral changes with respect to the quantity or strength. Many chemical properties can be investigated such as inter- an intra-molecular clusters vibrations, partial charge transfer, and large amplitude anharmonic effects.

1.2 ASSESSING EXCESS CHARGE ACCOMMODATION OF AZABENZENE HYDROGEN-BONDED NETWORK WITH WATER IN THE GAS PHASE

Gas phase spectroscopy has significantly developed since award of Nobel Prize in Chemistry announced in 1986 to Dudley R. Herschbach, Yuan T. Lee and John C. Polanyi for their chemical applications of vacuum science and laser techniques. The evolution of examining gaseous molecular assemblies has elucidated a number of chemical enigmas including the hydrated electron,[1-9] Grotthuß mechanism,[10-20] and ion solvation.[21-31] These advancements have provided a basis in which the efforts in this dissertation could characterize chemical properties such as electron affinity (EA) and vertical detachment energy (VDE) by photoelectron spectroscopy (PES), and infrared photodissociation (IRPD) by predissociation spectroscopy.

How Does Water Bind an Excess Electron?

It has been shown that water clusters accommodate an excess electron in a unusual form, where the excess charge does not reside in a valence molecular orbital, but in a diffuse cloud or "dipole-bound" state. Figure 4 shows the delocalized electron binding to the water dimer or $(H_2O)_2{}^-$. Many biological building blocks share a similar binding motif with water cluster and others do not,[32-38] but what yet to be characterized are the effects of hydrogen-bonding between essential biological building blocks and the natural present water molecules with an excess electron.
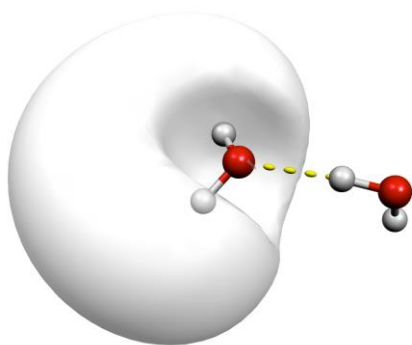
Figure 1.1. The dipole-bound electron for the hydrogen-bonded water cluster dimer, $(H_2O)_2{}^-$.

The surprising transient absorption spectrum of the hydrated electron collected by Hart and Boag [39-42] in the middle of the 20[th] century shed new light on excess charge accommodation for solvents that do not have low lying valence orbital and large molecular dipoles. The featured band at 7000Å (shown in Figure 2), caught the attention of Rentzepis *et al*. who later were the first to study the hydrated electron, e_{aq}^-, by laser spectroscopy.[43,44] A number of motifs have been developed in attempt to describe the molecular structure of e_{aq}^- solvation including dipole-bound, surface-bound, partially embedded and cavity (internally) bound confinement. Historically, experimentalists and theorists have debated the minimum dipole moment of a molecule to bind an excess electron, however the controversial value has resolved to 1.625 Debye. The dipole moment of a single water molecule (H_2O) lies just above this value at 1.85 D. While the ion $(H_2O)^-$ has been isolated via mass spectrometry, it is thought to be a molecular ion cluster.
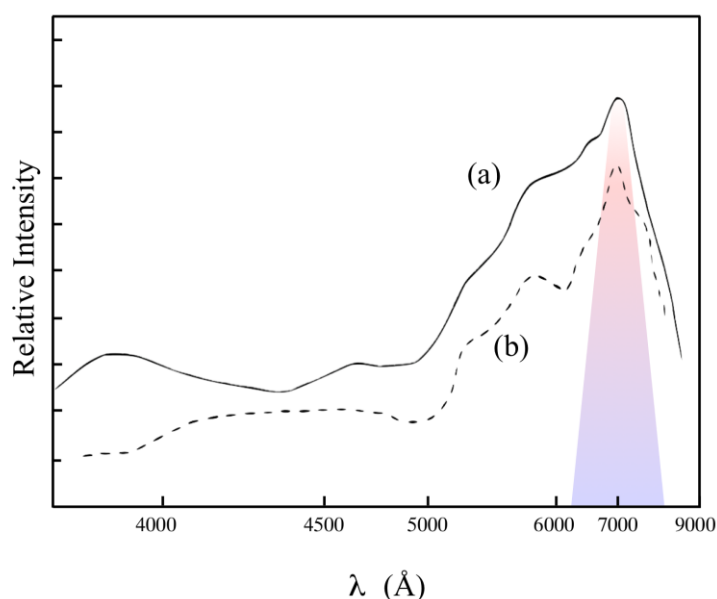
Figure 1.2. Taken from the Hart and Boag experiment, the transient absorption band at 7000 Å in (a) 0.05 M solution of Na_2CO_3 and (b) pure water after being irradiated with spark discharge source. Reprinted with permission from {*J. Am. Chem. Soc.*, **84** (21), 4090–4095} Copyright (1962) American Chemical Society

Coe *et al*. later estimated the vertical detachment energy (VDE) of the water dimer anion, $(H_2O)_2^-$, to ~50 meV as well as identified two additional yet smaller features in the photoelectron spectrum as the bending and stretching vibrational frequencies. This study reported VDE values for the $(H_2O)_n^-$ sequential series for $n = 2, 6, 7,$ and $11 - 69$ and fit

experimental measurements[4] to relations developed by Landman and coworkers[45] years before

seen in Figure 3.
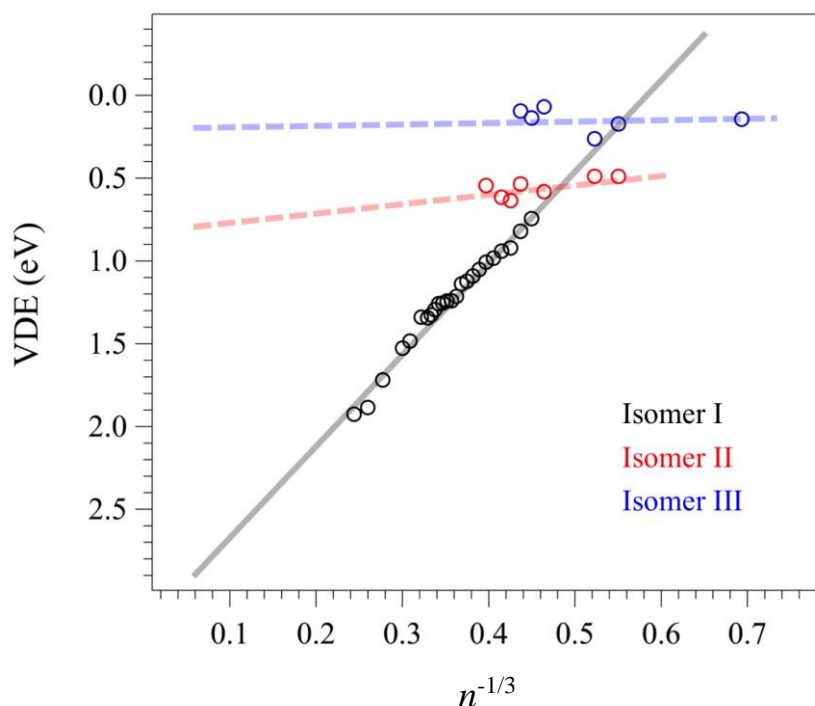
Figure 1.3. Linear relationship between VDEs and $n^{-1/3}$ for $(H_2O)_{n^- = 2-69}$. Reprinted with permission from {*J. Chem. Phys.*, **125**, 014315} Copyright (2006) AIP Publishing LLC

The experimental cross section of absorption is a complimentary to these trends when

comparing the increasing size of cluster anions with photodissociation or photodestruction.

Ayotte and Johnson observed electronic absorption spectra of $(H_2O)_n^-$ cluster anions with fixed

frequency radiation (1064 nm).[46] Figure 4 illustrates the shift to lower energy or "red shift" of

the absorption cross section as n decreases and compares well with a smooth transition from

gaseous ion spectroscopic results to that of the bulk at 2.74 eV. It has been noted that the peak

intensity also grows with decreasing size for the $(H_2O)_n^-$ cluster anions.
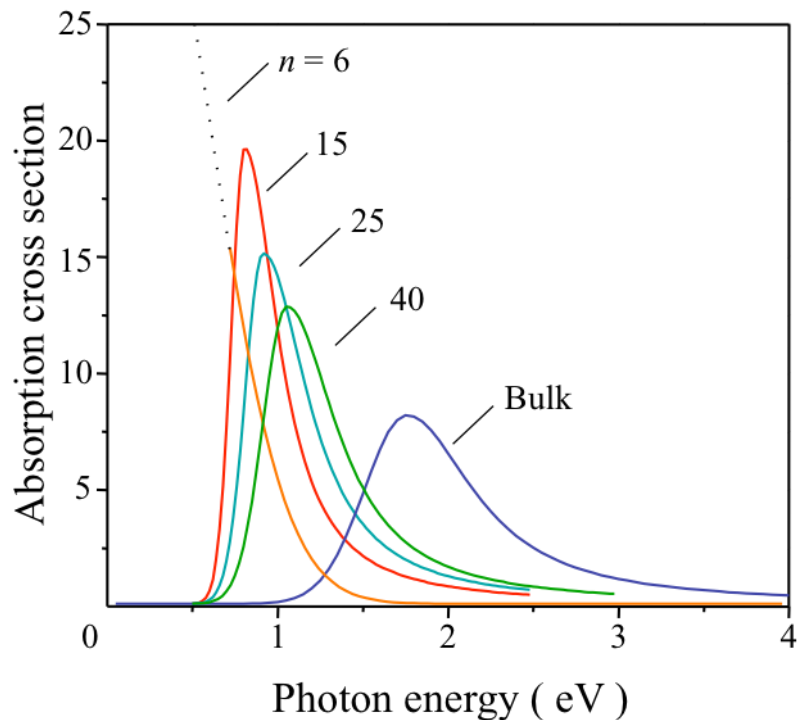
Figure 1.4. Fits of the absorption cross section for the $(H_2O)_n^-$ cluster anions using the 1064 nm laser line. Reprinted with permission from {*J. Chem. Phys.*, **106**, 811} Copyright (1997) AIP Publishing LLC

Excess electron accommodation in nature

Damaging forms of radiation, such as ultraviolet or x-rays, have the ability to pierce the Earth's atmosphere and directly interacting with the DNA of living tissue however the likelihood this event unfolding is poor. The absorption of primary quanta by an intermediate species has been shown to stabilize and even enhance the potentially lethal DNA lesions, such as breaking covalent bonds in the strands of DNA.[47-54] By probing at the nanoscopic level, the spectral signature of transient species has provided evidence to be the culprit in select cases. Advancements in gaseous molecular spectroscopy have shed new light on the ensemble of interactions in biological systems.

Within the past quarter century, many investigators have focused on the formation of transient anions after secondary electron attachment in aqueous conditions.[55-57] Boudaiffa *et al*. observed destructive covalent bond cleavage in single and double DNA strands after

6

exposure to low energy electrons (<20 eV).[58] Complimentary electronic structure computations[59] not only agree with these results but also suggest that excess electron attachment could be a direct result of a combination of resonance in the nucleobase subunit as well solvent stabilization by an extended hydrogen bonded network of water molecules. Recent theoretical efforts have suggested a number of possible bond rupture pathways as a direct result of excess electron attachment. Figure 5 shows how high-energy radiation can form solvated electrons that can quickly be transferred throughout a hydrogen-bonded network in which DNA can accommodate this excess charge leading to transmutations in genomic replication.[60] The destructive pathway for these nanoscopic phenomena are not well-understood, however with our spectroscopic efforts, there is now evidence to suggest that DNA subunits can form transient anions and with neighboring solvent molecules form a stable hydrogen-bonded network.
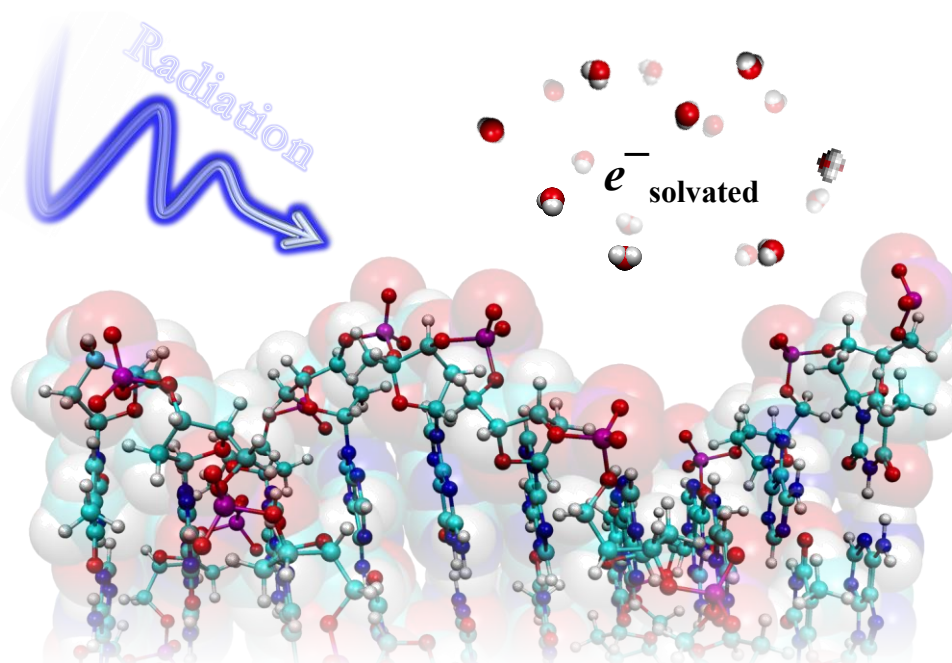
Figure 1.5. Radiation pathway that is known to cause precancerous health concerns by indirect association with solvated electrons.

Spectroscopic and Computational Studies of Anionic Hydrated Azabenzenes

Through collaborations with the research groups of Mark Johnson at Yale, Kit Bowen at Johns Hopkins, and Ken Jordan at Pittsburg, the anionic hydrated azabenzene series was characterized. Our computational contributions provided insight into the construction of the hydrogen-bonded infrastructure that is likely present in gas phase spectroscopic studies. Photoelectron spectra of hydrated azabenzene cluster anions were provided by the research group of Kit Bowen, providing resolved adiabatic electron affinities (AEA) and VDEs. Our contribution to this work is the computational description of the hydrogen bond and solvate on effects for mass-selected ions. Computed VDEs and EAs (also zero point corrected EAs or EA_0) were compared to experimental values resulting in satisfactory agreement. This collaboration resulted in two published articles; one in the *Journal of Physical Chemistry A* while the other was featured on the cover of *Physical Chemistry and Chemical Physics*.

With the intention of studying mass-selected hydrated azabenzene cluster anions using IRPD, well-negotiated communications established an additional collaboration with the Johnson and Jordan group characterizing the vibrational spectra of hydrated pyridine cluster anions, where our contribution was providing optimizing cluster geometries and harmonic frequencies for local minimum. This dissertation will not include this work but can be found in the *Journal of Chemical Physics.*

Excess charge accommodation in atmospheric clusters

Carbon dioxide (CO_2) is a member of a group of atoms and molecules that appear in Earth's atmosphere, and it has been brought to popular attention for being a greenhouse gas that is contributing to global warming. Being among one of the most common of these gases, this inorganic molecule has been spectroscopically interrogated in the gas phase much like the previously discussed H_2O molecule. In 1975, Compton and coworkers quantified the electron

affinity of CO_2 to be -0.60 ± 0.2 eV and the CO_2^- molecular anion is metastable or transient with respect to autodetachment with a lifetime of a fraction of a millisecond. Excess electron attachment to the neutral ground state of the CO_2 molecule ($^1\Sigma_g^+$) results in lengthening of the C=O bonds, lowering the symmetry from $D_{\infty h}$ to C_{2v} by bending the O=C=O angle.

Bowen and coworkers investigated the CO_2^- molecular anion ($^2A_1$) using negative ion photoelectron spectroscopy finding the vertical detachment energy (VDE) to be 1.4 eV. Included in the investigation was evidence of $(CO_2)_2^-$ in which the VDE estimation was found to be more than 2.4 eV due to the fixed photon frequency (2.707 eV). Two potential motifs have been identified for excess electron accommodation in $(CO_2)_n^-$ cluster anions, $(CO_2)^-$ $\cdot(CO_2)_n$ or $(C_2O_4)^-\cdot(CO_2)_n$. Figure 6 illustrates the neutral CO_2 and its anionic counterpart, CO_2^-, as well as the two different $(CO_2)_2^-$ cores of $(CO_2)_n^-$ cluster anions.
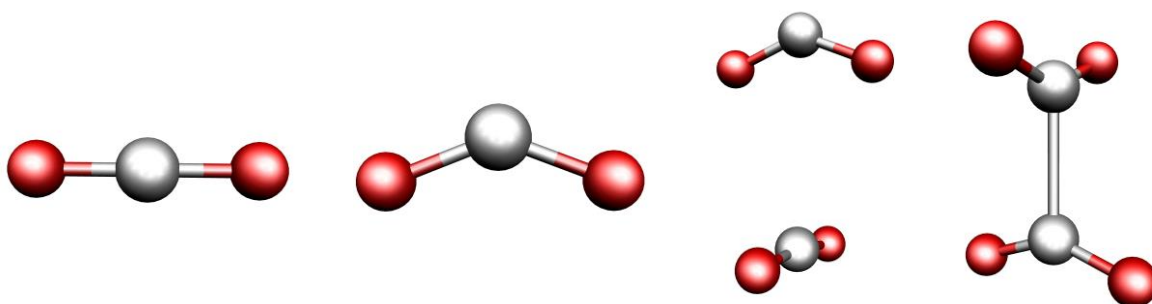
Figure 1.6. The linear CO_2 molecular ($D_{\infty h}$) orientation for the neutral system compared to the bent CO_2^- (C_{2v}) geometry along with dimer cluster anions with C_{2v} and D_{2h} symmetry: (a) CO_2, (b) CO_2^-, (c) $CO_2^-\cdot CO_2$, and (d) $C_2O_4^-$. Reprinted with permission from {*J. Chem. Phys.*, **119**, 7714} Copyright (2003) AIP Publishing LLC

The $(CO_2)_n^-$ cluster anions are considered short lived or meta-stable with respect to electron autodetachment, however fixation of the CO_2^- molecular anions on other electron scavenging systems, such as the nitrogen containing heterocycles studied in our work, have been reported to stabilize the negative charge. In our work, we are interested in the formation of noncovalent interactions between meta-stable anions with other molecular systems increasing the otherwise low-energy dissociative barrier. From previously studies on the

reaction of Pyridine with $(CO_2)_n^-$ the vibrational spectrum suggests the formation of a carbamate radical anion in the gas phase, but we are interested in the contributions of delocalization of the excess electron in the coordination of this bond. A comparative analysis of smaller nitrogen containing system, such as cyanide, could further assess the effects of resonance stabilization as well as evaluate the anharmonic effects with the reduced dimensionality of the larger aromatic system.

1.3 VIBRATIONAL SIGNATURE OF N-HETEROCYCLIC MOLECULES AND CHARGE TRANSFER TO H-BONDED NETWORK

Comprehensive spectroscopic and theoretical studies have lead to substantial insight in the vibrational characterization of the aromatic, organic molecule benzene[61-63] (C_6H_6) as early as the late 1930's. Complementary chemical analysis techniques have been employed early by Lord *et al*. in attempt to compare the highly symmetric benzene vibrational spectra to that of isoelectronic, less symmetric members of the azabenzene series: pyridine, pyrazine, pyrimidine, and pyridazine.[64,65] The infrared and Raman spectra highlight a number of vibrational features that are observed in each of the conjugated molecules, and with the comparative analysis to previously characterized benzene spectra, a majority of vibrational transitions have been assigned. Figure 7 shows (7a) the early infrared spectrograph of pyridine from 1953 as well as a table showing the (7b) qualitative intensities of the vibrational features

(a)

(b)

Pyridine	Pyridine-d_5	Pyridine	Pyridine-d_5
	329 vvw	1482 s	1364 m
405 s	371 m	1572 m	1414 w
604 s	530 vs	1583 vs	1450 w
653 w	567 m	1599 s	1530 vs
675 w	582 s	1633 w	1542 s
703 vvs	625 w	1682 w	1550 m
749	762 m	1872 m	1581 vw
810 vw	798 w	1923 m	1645 m
883 s	823 s	1987 w	1806 vw
938 vvw	833 m	2293 vw	1850 vw
981 w	886 m	2454 vw	1863 vw
991 vs	908 w	2908 w	1918 vw
1030 vs	963 s	2960 m	2042 vw
1068 s	1011 m	3004 s	2117 w
1148 s	1043 w	3036 vs	2254 vs
1217 s	1143 vw	3055 s	2270 s
1296 vw	1228 m	3083 vs	2285 s
1357 w	1302 s		2389 w
1375 m	1322 m		2460 w
1441 vs	1340 w		2566 w

(The qualitative intensities are based on a sample 0.05 mm thick; v = very, w = weak, m = medium, s = strong.)

Figure 1.7. The (a) infrared spectrum of liquid pyridine, the (b) qualitative intensities at each assigned vibrational mode of pyridine, and (c) comparison to the deuterated pyridine-*d5* values. Reprinted with permission from {*J. Chem. Phys.*, **21**, 1170} Copyright (1953) AIP Publishing LLC

(c)

Species and τ-values	Vibration number	Frequency in cm⁻¹	
		Pyridine	Pyridine-d_5
	1	992	962
	2	3054	2293
	6a	605	582
	8a	1580	1530
A_1	9a	1218	887
	12	1029	1006
	13	(3054)	2270
$\tau_{calc} = 5.49$	18a	1068	823
	19a	1482	1340
$\tau_{obs} = 5.38$	20a	3036	2254
B_1	3	(1217)	908
	6b	652	625
	7b	(3054)	2285
$\tau_{calc} = 5.07$	8b	1572	1542
	14	1375	1322
$\tau_{obs} = 4.95$	15	1148	(887)
	18b	(1068)	833
	19b	1439	1301
	20b	3083	(2293)
A_2			
	10a	886	690
$\tau_{calc} = 1.84$	16a	374	329
	17a	981	798
$\tau_{obs} = 1.80$			
B_2	4	675	(625)
	5	942	762
$\tau_{calc} = 2.56$	10b	749	567
	11	703	530
$\tau_{obs} = 2.55$	16b	405	371

( ) indicates a frequency assigned to two vibrations.

in the

IR spectrum and (6c) Wilson's assignment.

Each of the diazine or two nitrogen atom containing heterocyclic molecules were investigated using similar vibrational spectroscopic approaches shortly after pyridine to consider the scrupulous role symmetry has on the vibrational spectrum of such molecules. The reduced symmetry of a benzene molecule by replacing one or more of the C–H with a nitrogen atom has propagating effects on the ability to form hydrogen bonds within a local environment. Takahashi, Mamola and Plyler observed small shifts in the vibrational spectra of the same azabenzene molecules in diluted concentrations in various solvents.[66] These spectral shifts were attributed to the change in electron distribution with respect to the formation of a hydrogen-bonded network. Figure 8 shows such frequency shifts in the dilution from pure pyridine to a solution in pyridine and water.
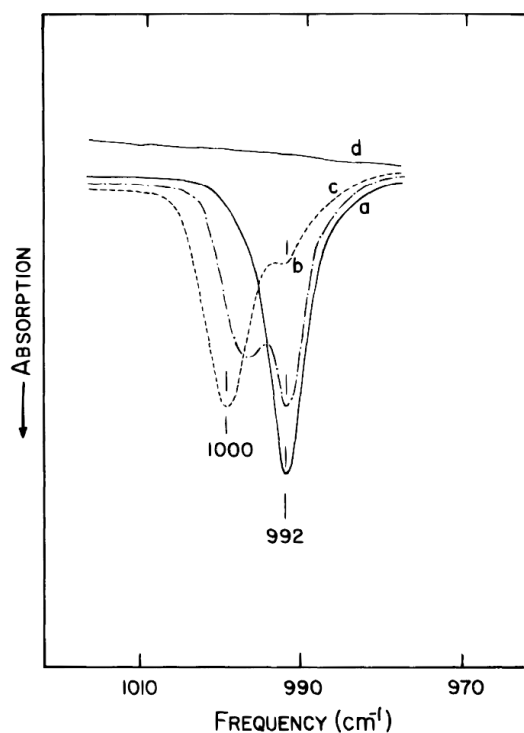
Figure 1.8. The infrared spectrum of liquid pyridine in altering concentration in water solutions: (a) pure pyridine, (b) 10 M pyridine, (c) 5 M pyridine and (d) pure water. Reprinted with permission from {*J. Mol. Spectrosc.*, **21**, 217–230} Copyright (1960) AIP Publishing LLC

Hydrogen bonding is now well known to potentially cause a number of shifts in the vibrational spectra of molecules that can either accept or donate a hydrogen bond. In the case of the azabenzene series, the nitrogen atom plays the role of an electrostatic compass for which

solvent molecules can donate a single hydrogen bond to each nitrogen atom. More recent spectroscopic studies from our group have shown that partial charge transfer from the conjugated heterocycle to the hydrogen bonded donor, give rise to observed shifts in selected vibrations of the diazine pyrimidine. Figure 9 shows the quantitative correlation between charge transfer and shifts in a given vibrational mode (ν_1, the ring breathing).
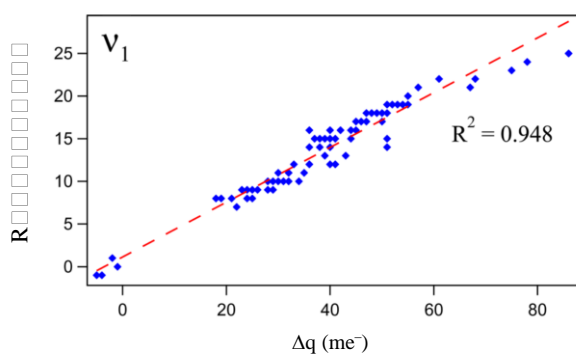
Figure 1.9. Charge transfer from the nitrogen-containing heterocycle to the solvation network of the ring-breathing mode of pyrimidine. Reprinted with permission from {*J. Phys. Chem. A*, **117**, 5435−5446} Copyright (2013) American Chemical Society

Although the definitive cause of modes shifted by noncovalent interactions with surrounding solvent molecules is not clear, there has been a massive effort to explain the phenomenon at the molecular level.[67-74] Here in this dissertation, the effects of charge transfer from the azabenzene series are interrogated using high-resolution spectroscopic techniques and quantum mechanical electronic structure theory in attempt to further characterize the charge transfer and excess charge accommodation for molecular assemblies.

Azabenzene – Silver Interactions

Surface enhanced Raman spectroscopy has evolved vibrational spectroscopy into a new era where not only non-florescent, small molecules can be studied, but extend this recognized as one of the first observed Raman enhancements by adsorption of pyridine on silver electrodes. The proposed theory suggests that the orientation of the water molecules and the "physisorbed" pyridine on the silver surface are the key factors in the phenomenon. Figure 10 is adapted from the original works of Fleischmann demonstrating the association

between solvent, solute and surface with respect to the positive cathode and negative anode

electrodes in the experimental design.[75]
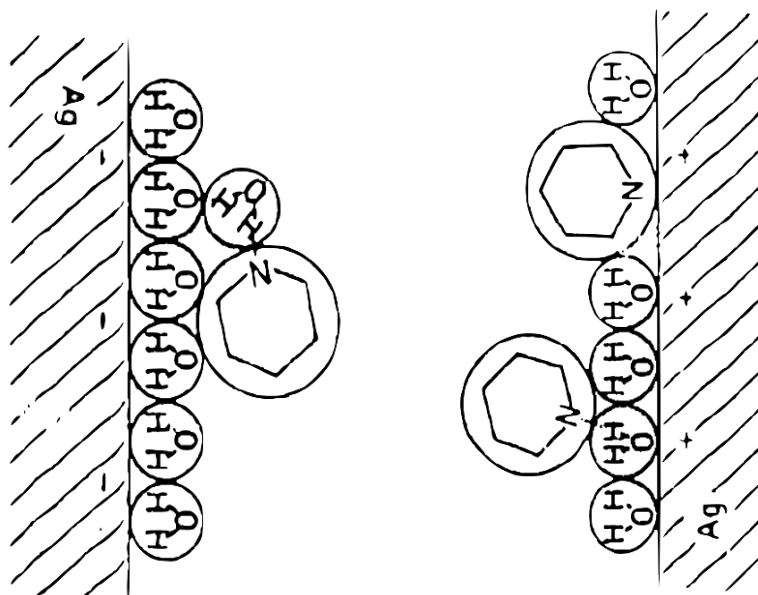
Figure 1.10. The nitrogen-containing heterocycle (pyridine) orients the surrounding hydrogen-bonded network to be in contact with the negative anode but forms an aqueous partition with the cathode. Reprinted with permission from {*Chem. Phys. Lett.,* **26** (2), 163−166} Copyright © 1974 Published by Elsevier B.V.

In this dissertation, the charge transfer from the isoelectronic molecule pyrimidine to a

silver surface as well as compare spectral shifts to those seen in diluted pyrimidine solution in

water using high-resolution Raman spectroscopy and density functional theory (DFT).

Previous work has investigated the charge transfer from pyrimidine to hydrogen-bonded water

clusters, however it has yet to been compared to the same shifts seen in surface-enhanced

Raman spectra that has been attributed to the adsorption on a metal surface and not the

hydrogen-bonded network. Figure 6 shows a hydrated pyrimidine molecule adsorbed to a

representation of silver surface. The agreement between computed shifts and experimental

results suggest that there is a competitive charge transfer event between pyrimidine and the

water and silver surface.

Low Temperature Hydrogen-Bonded Interactions

Raman under nitrogen or RUN spectroscopy is a newly developed procedure that has the ability to interrogate fundamental vibrational transitions as wells as reduced thermal degradation, atmospheric oxidation, and resolve spectral congestion.[76,77] Here we employ RUN spectroscopy to interrogate Raman shifts in the absence and presence of water. Partial charge transfer from to the first solvation shell is demonstrated in the excellent agreement between high-level ab initio computations and high resolution Raman spectroscopy held at 77 K. Many of the same features are resolved in both condensed phase and the crystalline spectra, however the low-temperature spectra is reveals thermally sharpened features by collapsing the non-ground state populations to the zero-point vibrational energy level.

This spectroscopic approach interrogates the vibrational signature of charge transfer in select vibrational modes with high-resolution seen in Figure 11. Between the high resolution of a Raman spectrometer and the low temperature squandering and vibrationally excited molecules, this technique has the ability to resolve the spectral signature of the natural isotope population of carbon tetrachloride (CCl_4) at ambient pressure. The Raman spectrum of carbon tetrachloride is well known and has been fully characterized.

Raman CCl$_4$
RUN CCl$_4$

430   440   450   460   470
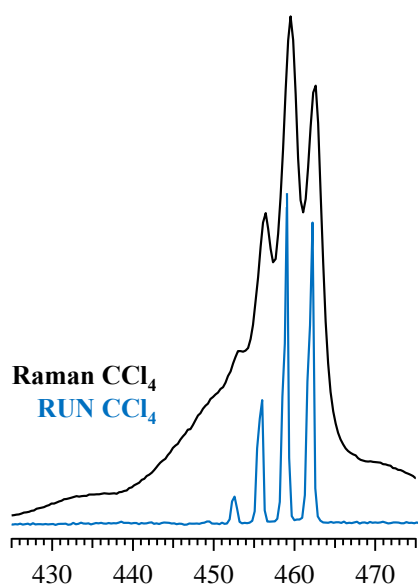
Figure 1.11. The well-known Raman spectrum of carbon tetrachloride (CCl_4) is shown in black (300K) and the Raman spectrum under liquid nitrogen or RUN spectra is in blue. The resolution of room temperature measurement shows some signature of the isotopic distribution but at 77K, each isotopologues has baseline-to-baseline resolution.

In this dissertation, the construction of experimental design of employing Raman spectroscopy under liquid nitrogen is illustrated as well as preliminary results comparing the azabenzene series Raman spectra to RUN spectra at 77 K. The high resolution of the Horiba LabRAM Evo and cryogenic temperatures of the crystalline sample provides narrow vibrational features to be characterized for the mid-IR region as well as the low frequency libron modes below 200 cm^{-1}. The hydrogen-bonded network is interrogated under these extreme experimental conditions revealing further resolved spectral shifts.

CHAPTER 2

MOLECULAR SPECTROSCOPY

2.1 INTRODUCTION TO VIBRATIONAL SPECTROSCOPY

Innovative technological breakthroughs in the spectroscopic techniques allows for vibrational transitions to be studied at the single-molecule level, in isolation or gaseous, condensed solution phase and crystalline phase. Two laureates of the Nobel Prize in Physics Albert Michelson in 1907 and Sir Chandrasekhara Venkata Raman in 1930 pioneered these spectroscopic advancements with techniques and applications in vibrational spectroscopy. The evolution of both complementary analytical approaches, infrared spectroscopy and Raman spectroscopy, has shed new light on a number of paradoxes allowing experimental and theoretical efforts to establish a premise for modern spectroscopy.

Infrared spectroscopy relies on the absorption and transmission of discrete wavelengths to generate a vibrational spectrum, whereas Raman spectroscopy is a scattering technique that relies on detecting photons of a wavelength other than that of the excitation source (*i.e*. Stokes and anti-Stokes scattering). Both techniques abide by selection rules that govern the spectral process in which the activity of the transition is observed. Both transitions can be modeled by the harmonic oscillator paradigm, which will be discussed later in this chapter. It is beneficial to be familiar with the regions of the electromagnetic spectrum that and the corresponding infrared and Raman transitions occur as well as the excitation sources used to perform such measurements. Table 1 shows the visible and infrared regions in applied units of wavelength.

EM Region	λ (nm)	ν (cm^{-1})	$h\nu$ (eV)
Visible	400 – 750	25000 – 13333	3.1 – 1.65
IR$_{near}$	750 – 2500	13333 – 4000	1.65 – 0.50
IR$_{mid}$	2500 – 50000	4000 – 200	0.50 – 0.025
IR$_{far}$	50000 – 1000000	200 – 10	0.025 – 0.00125

Table 1. The visible and infrared regions of the electromagnetic spectrum in units of nanometers (nm), wavenumbers (cm^{-1}), and electron volts (eV).

Quantum Mechanics of Molecular Vibrations

Vibrational spectra have historically been reported in micron or μm it is now conventional for reported values to be in wavenumber or cm^{-1}. The key differences between infrared and Raman spectroscopy are absorption and scattering, respectively. When studying molecular vibrations, it is useful to employ a simple model in which quantum mechanics can be illustrated called the harmonic oscillator. A given vibrational motion of a given molecule can be represented by two balls of masses m_1 and m_2 connected by a spring with a restoring force f shown in Figure 1.
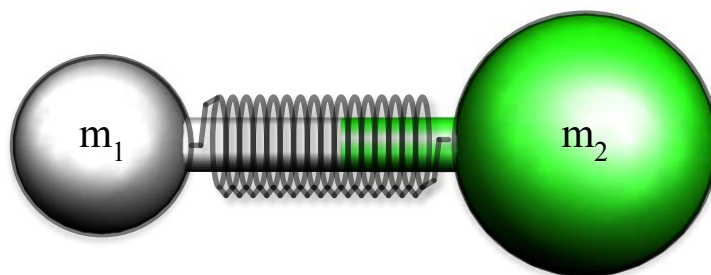
Figure 1. The HCl diatomic molecule with the mass of the white hydrogen atom defined as m_1 and the mass of the chlorine atom defined as m_2.

The quantum mechanical treatment of the ball and spring model presented here is governed by transitions from one vibrational state to the next in naturally defined envelopes of energy called quanta. These discrete transitions, $\nu_n \rightarrow \nu_{n+1}$, are distinct measurable

quantities and can be illustrated with a harmonic potential seen in Figure 2 that is defined by Hooke's law below in Eq. 1:

$$f = -\tfrac{1}{2}\, k\, x^2 \qquad\qquad (\text{Eq. 1})$$

Where f is the force associated with the restoration of the spring to the equilibrium distance, k is the spring constant, and x is the distance displaced from equilibrium. To simplify the harmonic approximation, the reduced mass, μ, is implemented in the place of the two independent masses, m_1 and m_2, seen in Eq. 2.

$$\mu = \frac{m_1 m_2}{m_1 + m_2} \qquad\qquad (\text{Eq. 2})$$

The quantum mechanical model known as the harmonic oscillator is defined by incremental steps between quantized energy levels (ν) and can be expressed in functional form shown is Eq. 3.

$$E = (\nu + \frac{1}{2}) \frac{h}{2\pi} \sqrt{k/\mu} \qquad\qquad (\text{Eq. 3})$$

The values of a vibrational energy level, ν, can be any numerical integer as well as zero. This means that there is a vibrational energy associated with the lowest state, also known as the ground vibrational state. This energy is known as the zero-point vibrational energy level or ν_0. A graphical representation of the harmonic oscillator with vibrational energy levels is provided in Figure 2.
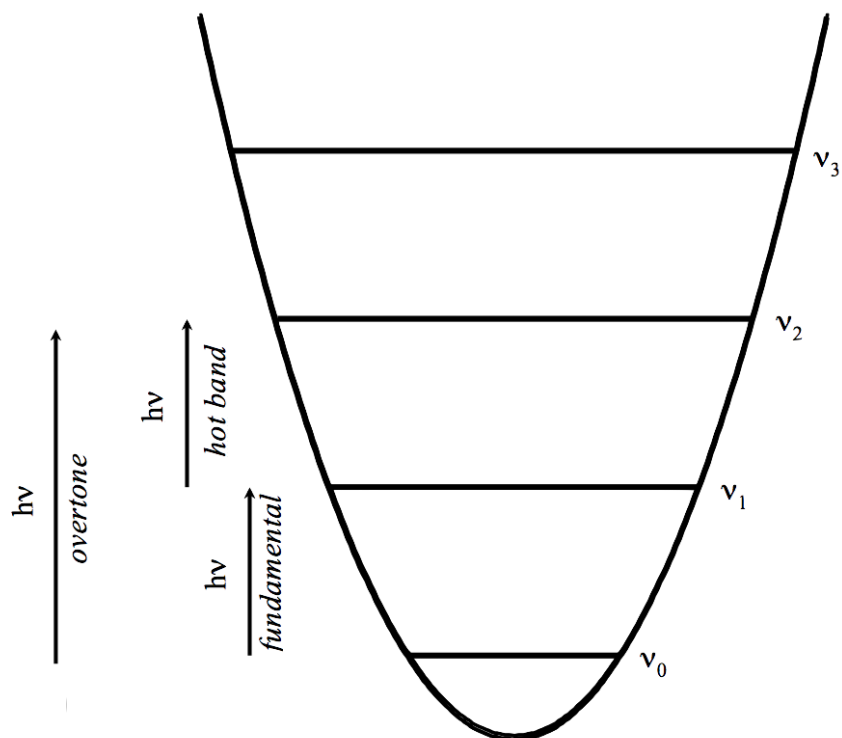
Figure 2. The harmonic potential with labeled vibrational energy levels. Notice the zero point energy is half of the energy associated with the fundamental transition.

The contributions of Phillip Morse and John Lennard-Jones have provided additional mathematical expressions for innovative improvements to the harmonic approximation. Each expression attempts to describe the natural relationship between potential energy and charged atomic nuclei beyond the lower limits of the harmonic potential. Such expressions include the Morse potential energy function and the Lennard-Jones potential energy function.

2.2 GAS PHASE PHOTOELECTRON SPECTROSCOPY

The explanation of the interaction between light and matter resulting in the detachment of an electron, also known as the photoelectron effect, is credited to the Albert Einstein resulting in the 1921 Nobel Prize in Physics. This photo-physical property has been further studied over the year and been applied to gas phase cluster anions. Figure 3 illustrates the transitions: electron affinity (EA), vertical attachment energy (VAE), and vertical detachment energy (VDE). Vibrational and rotational energy levels are also included to depict the qualitative differences to the magnitudes of these transitions.
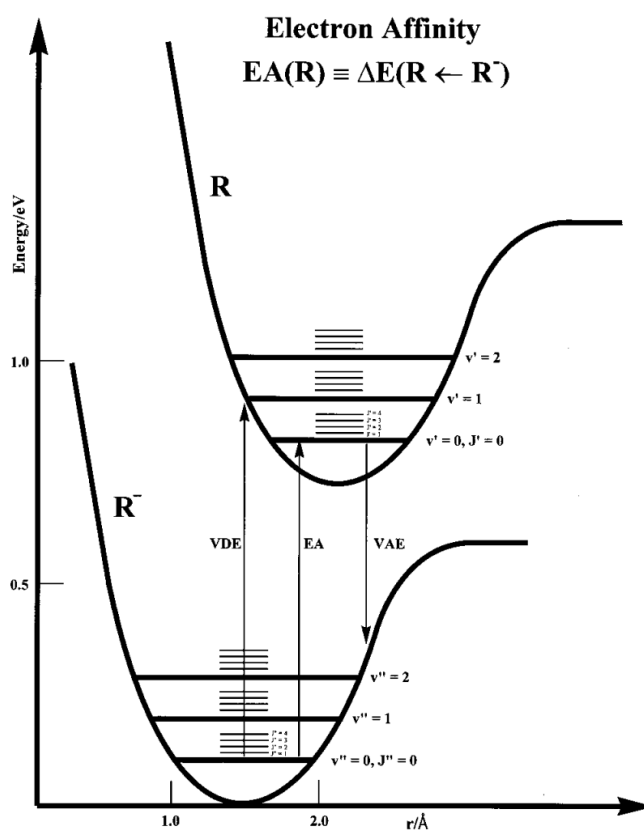
Figure 3. Anion (R⁻) and neutral (R) molecules with associated electronic relations and relative geometric orientations. Reprinted with permission from {*Chem. Rev.*, **102** (1), 231–282} Copyright (2002) American Chemical Society

The spectroscopic signatures of molecular cluster anions have been interrogated by employing laser-based techniques with mass spectrometry to identify cluster size. Figure 4

shows the vibrational resolution of the [NH₄···Cl]⁻ and the correlated pathway to the

photodetached electron providing the photoelectron spectrum.
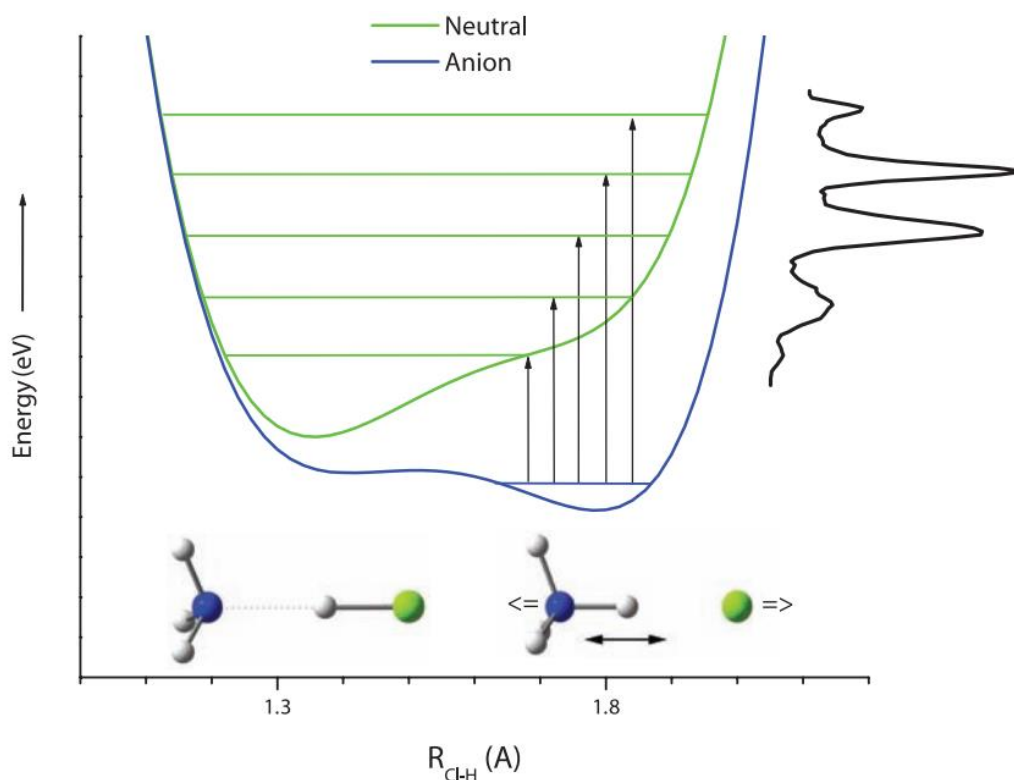
Figure 4. The neutral, NH₃···HCl, (green trace) and negative ion cluster [NH₄···Cl]⁻ (blue trace) 1D potential energy surfaces with vertical arrows (black) outlining Frank-Condon overlap between the ground vibrational state of the cluster anion and the first vibrational states of the neutral. Reprinted with permission from {*Science*, **319** (5865), 936–939} Copyright (2008) American Association for the Advancement of Science

Gas phase photoelectron spectroscopy provides insight in to the overlap between the

ground state of the atomic or molecular cluster anion with respect to the vertical transition to

potential energy surfaces that lay vertically above. One parameter to consider is the energy of

the photon. The photoelectric effect only works if the photon energy is great than the binding

energy of the photoelectron (see Eq. 1)

$$EKE = h\nu - EBE \qquad\qquad (Eq.\ 1)$$

Newly developed detection techniques have allowed for higher resolution (μeV) in the area of gas phase photoelectron spectroscopy. Other advancements, such as electrospray and nano-spray ionization as well as cryogenic ion trapping, have allowed for much larger systems and temperature effects to be studied in the gas phase.

2.3 RAMAN SPECTROSCOPY

The major types of light-matter interaction are absorption, transmission, scattering, reflection and refraction. While infrared spectroscopy primarily is an absorption/transmission technique, Raman spectroscopy relies on inelastic scattering of photons and high-resolution spectrometers to separate excitation photons from scattered photons. The inelastic scattering causes the wavelength or energy of excitation photons to change giving rise to the two common types of non-Rayleigh scattering: Stokes and anti-Stokes. Figure 5 shows the spectral relationship between the Rayleigh line, and stokes and anti-Stokes scattering. The green arrow or Rayleigh line represents the incident wavelength of the laser prior to interaction with the sample. The red line is the loss of energy of the scattered photon also known as Stokes scattering and the blue line represents gained energy by light-matter interaction also known as anti-Stokes scattering. The relative intensities are not proportional to the experimental values for the Stokes scattering and anti-Stokes scattering in relation to the Rayleigh scattering.
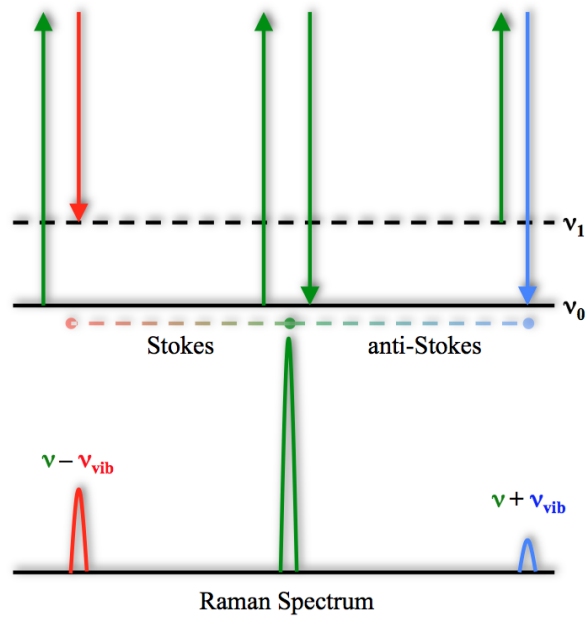
Figure 5. The Raman effect in terms of scattering of incident photons (green) and scattered with the same wavelength (Rayleigh), the loss of energy or Stokes scattering (red) and the gain of energy or anti-Stokes (blue).

CHAPTER 3

COMPUTATIONAL CHEMISTRY

3.1 INTRODUCTION

Computational chemistry has become a new pillar in the scientific approach to problem solving in the 20^{th} and 21^{st} century. By applying quantum mechanical electronic structure theory to the area of atomic and molecular spectroscopy, the understanding of light-matter interactions has tremendously advanced with this particular union. The attempts to solve the Schrodinger equation has been at the fingertips of science for the better part of the 20^{th} century, yet there are tribulations with the addition of a second electron. In this dissertation, there is a significant effort to step beyond the "black box" approach and understand fundamental concepts and theories to rationalize what approximations can be used under given conditions.

3.2 Electronic structure theory

In order to explore a given scientific inquiry, there is a plan of action for a given set of conditions when employing electronic structure theory. A number of commercially available computational software packages have a long list of *ab initio*, density functional theory, semi-empirical, and many other approaches to solve the Schrodinger equation.

Potential energy surface

The potential energy surface or PES is a multidimensional identity of a given chemical complex. In this dissertation, molecular clusters that exhibit hydrogen bonding to a network of water molecules are interrogated to determine how charge or excess charge is accommodated. Figure 6 shows the PES of a molecule comparing the potential energy, $V(r)$, to an arbitrary coordinates, r_x and r_y.
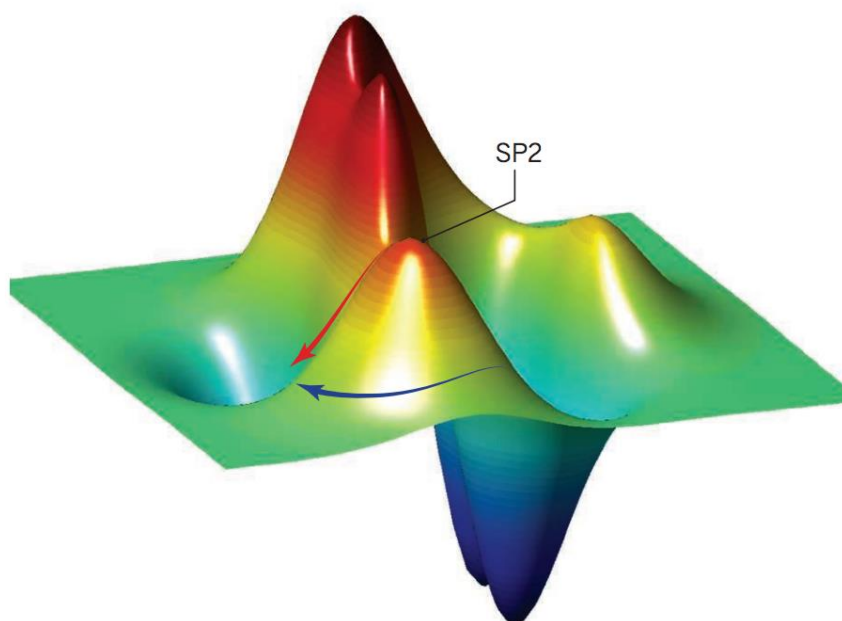
Figure 1. Sample potential energy surface showing the complex dimensionality. Reprinted with permission from {*Science*, **346** (6205), 30 −31} Copyright (2014) American Association for the Advancement of Science

The potential energy surface is commonly condensed to 1D, 2D, or 3D illustrations to help visualize the focus of a select topic. Here, we use the concept of a potential energy surface to descript the optimization procedure performed on each molecular cluster in this dissertation.

Molecular optimization

In order to employ electronic structure theory results to the vibrational and photoelectron spectroscopic experimental values, the transitions must first come from the ground state electronic and vibrational levels, therefore a geometry optimization must be performed. There are a number of optimization approaches in various quantum mechanical

software packages, but nearly all of them use simple differential equations and calculus-based derivatives to solve for the minimum on the potential energy surface. The potential energy surface is a complex multi-dimensional concept in which there are "hills and valleys" or maxima and minima locations. These points on the surface are referred to as stationary points, because there is no slope to the surface, or the first derivative of potential energy with respect to a given coordinate is zero.

Photoelectron computations

Now that minima are identified and characterized on the potential energy surface, there can be spectroscopic transitions from one state to another. The vertical transition that is observed experimentally can be simulated with various levels of electronic structure theory. The example provided in Chapter 2 (Figure 3 and Figure 4) shows the electronic ground state of a cluster anion that has a vertical transition to the corresponding neutral state. Electronic structure theory can quantify the adiabatic electron affinity (AEA) by computing the energetic difference between these two states at optimized geometries. The vertical transitions (VAE or VDE) employ fundamental concepts such as Franck-Condon overlap and Koopmans' theorem with respect to the cluster geometry for a given electronic PES.

CHAPTER 4

EXPERIMENTAL APPROACHES

This chapter gives a comprehensive description of the gas phase infrared photodissociation experimental apparatus as well as the theoretical indirect collection of vibrational action spectra. This chapter also outlines the condensed phase Raman spectroscopy applications including surface-enhanced Raman spectroscopy or SERS and Raman under nitrogen or RUN spectroscopy. The operation of the *LaserVision* OPO/A solid state tunable infrared laser is included as well as the optimization of the laser power at a given frequency.

4.1 MASS SPECTROMETRY

Vacuum chambers and pumps

A Wiley–McLaren time-of-flight mass spectrometer was arranged with alternating positive and negative high voltage stacked, parallel plates in a customized vacuum chamber illustrated in Figure 1. A custom stainless steel vacuum chamber has been assembled operating under a series of mechanical rotary pumps, diffusion pumps, and turbomolecular pumps. Three sectors are present in customized vacuum chamber that is employed in gas phase mass selection: ionization, field-free flight, and molecular ion detection. The ionization chamber is pumped with a Varian M-4 diffusion pump (800 liters/second) connected to an aluminum solid-body slide valve. The field-free flight is pumped with an Edwards DiffStak diffusion pump (300 liters/second) operated with a Humphrey pneumatic valve. The detection chamber is pumped

with a Varian TV-301 Navigator turbomolecular pump (300 liters/second). All high vacuum

pumps are roughed with Edwards's mechanical rotary pumps. Figure 2
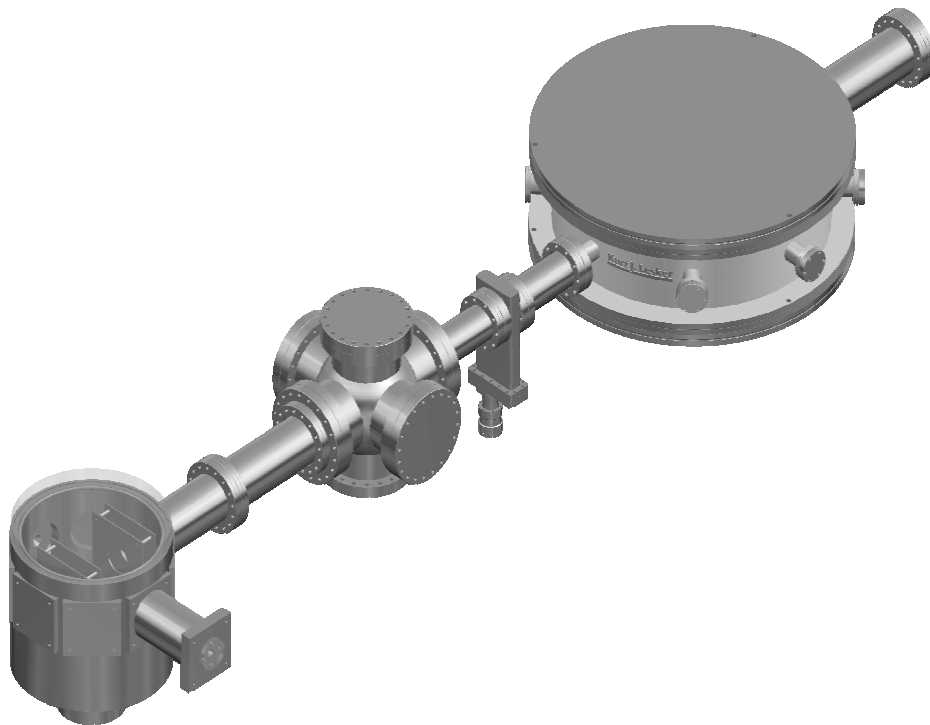
Figure 1. 3D-view of the vacuum chamber previously constructed in the Hammer group.
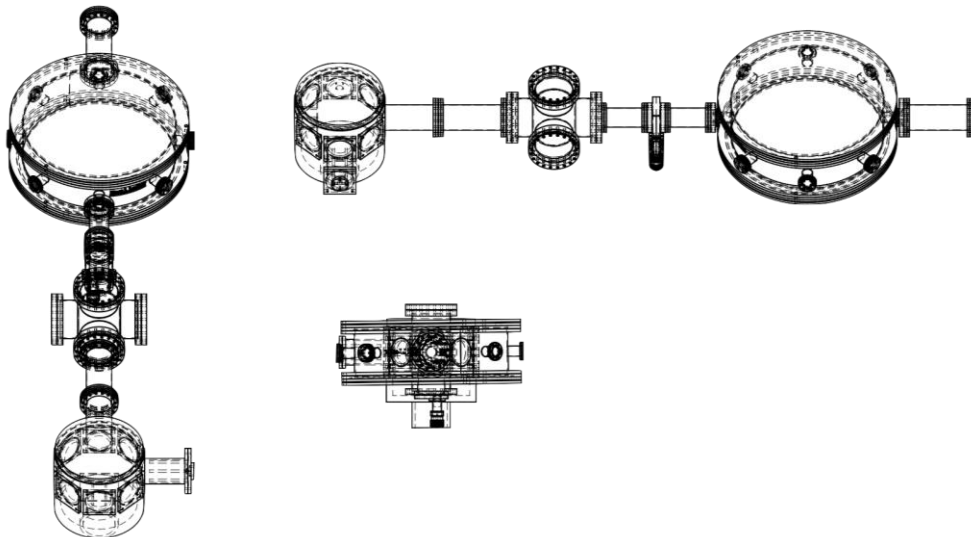
Figure 2. 3D schematic of the vacuum chamber

The Wiley-McLaren triple stack high voltage plates are mounted in a vacuum chamber

donated by Prof. Robert N. Compton from the University of Tennessee and Oak Ridge National

Laboratory (ORNL) shown in Figure 3.
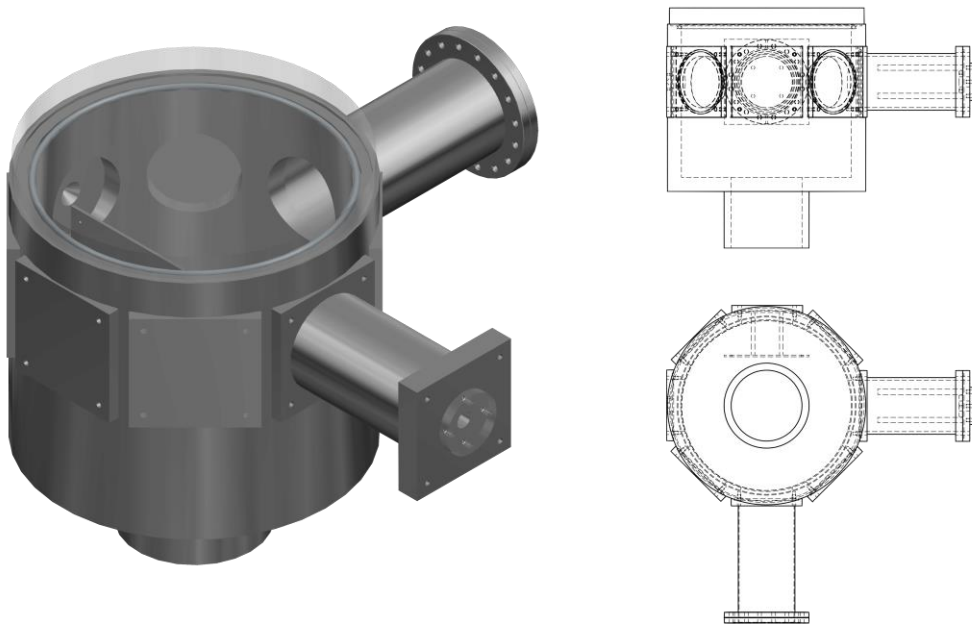
Figure 3. 3D schematic of the ionization vacuum chamber

Ionization by electron impact

The primary ionization technique employed has been electron impact (left on Figure 3) via a Peirce-style electron gun (800 V_{DC} to 1kV_{DC}). A thoriated iridium filament endures a thermionic process in which electrons are ejected from the filament and are focused with a series of electric potentials: Pierce cavity, einzel lens, and high voltage deflectors. This instrumental design provides a continuous short radius electron beam that can be used for ionization of various gases.
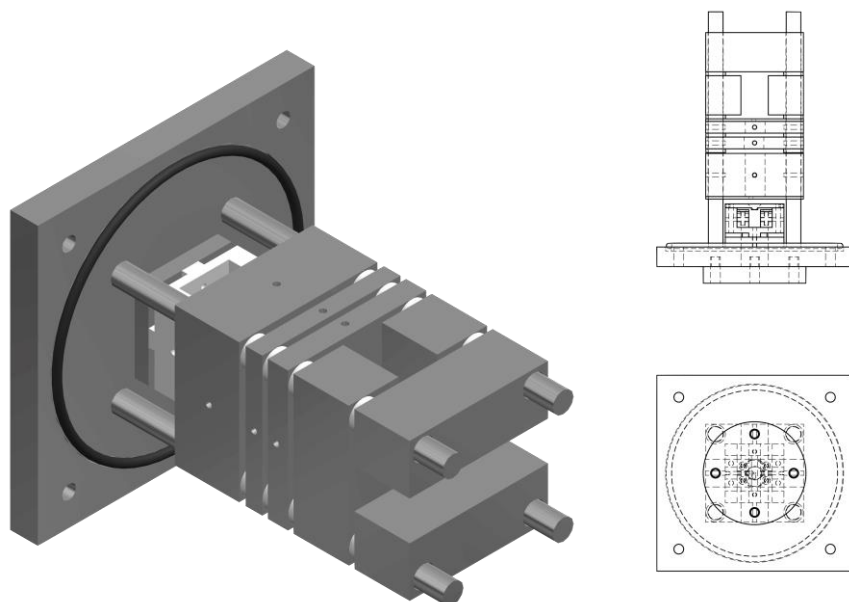
Figure 4: Instrumental designs for ionization source of Pierce-type electron gun

Wiley-McLaren time-of-flight

In order to study the systems of interest, the experiment requires for the sample to have relatively low internal energy; therefore a supersonic jet expansion of gas is employed to yield stable molecular clusters. Sample carried by a rare-gas experience a cooling incident when pulsed from high pressure (~3 atm) through a 0.5-micron orifice into vacuum. The internal (vibrational and rotational) energy of sample is transferred in the expansion event caused by the high number of gaseous collisions. The result of this procedure is a stable source of molecular clusters that can be ionized by electron impact or spark discharge. The direct ionization molecular clusters is rare with the high energy ionization source such as electron bombardment and spark discharge, but lower energy or slow secondary electrons are the principle source of ionization in both techniques. The ionization of the highly abundant carrier gas produces a surplus of secondary electrons that allow fragile, molecular clusters to be ionized. In specific condition, rare-gas can attach to negatively charged clusters by noncovalent interactions. The pulse valve that allows cluster formation and ultimately negatively charged

clusters employs the Parker Fluidics Iota One pulse driver. An equivalent customized circuit was manufactured and commissioned into the experiment allowing convenient controlling of pulse width for the pulse valve.
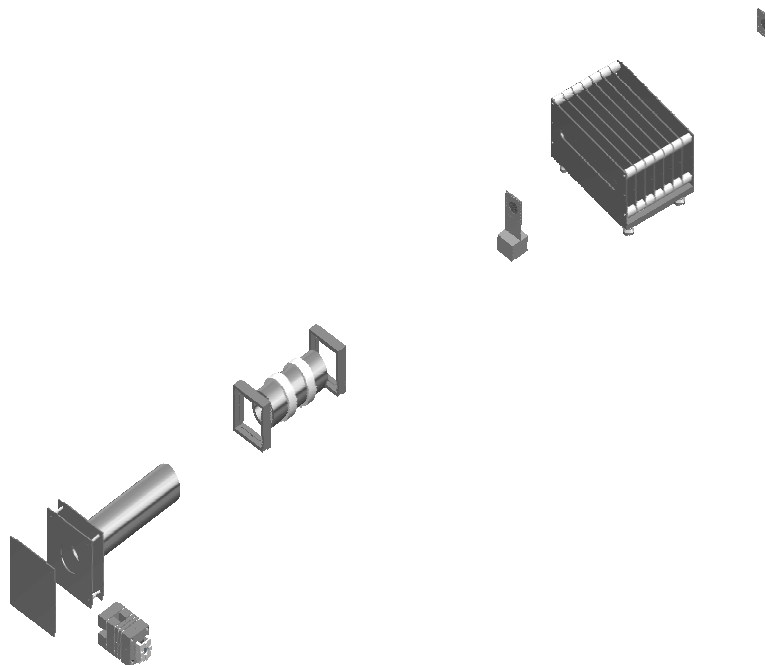
Figure 5: Instrumental designs for Wiley-McLaren plates with electron gun ionization source and ion optics (deflectors and lens)

The Wiley-McLaren style mass spectrometer was adopted for the experimental setup for high-resolution mass separation and the ability to study negative or positive ions with trivial instrument alterations. Mass separation initiates shortly after supersonic expansion of sample and ionization. Extraction of ionic clusters occurs by a short high-voltage pulse that pushes sample ions through an electrically grounded, highly transmissive grid. After extraction, a longer high-voltage pulse that accelerates sample ions into a field free drift region at which a majority of the mass separation occurs. This dual stage separation technique generates a molecular ion beam that can be detected by several schemes. Two possible modes can be utilized with the Wiley-McLaren style mass spectrometer: linear and reflectron. Linear time of

flight permits clusters to be ionized, separated base on the typical mass to charge ration followed by detection via paired microchannel plates.

Tandem Mass Spectrometer – Reflectron

The reflectron time of flight includes all of the same features as the linear time of flight as well as an electric field gradient that turns the molecular ion beam around and re-weighs each ion by the same mass to charge ratio. The reflectron mode allows light-matter interaction to occur resulting in parent ion fragmentation. Re-weighing the molecular beam by employing the reflectron deconvolutes the detection of fragments, daughter ions. Isolation of a single mass-selected cluster is accessible by the use of a mass gate.
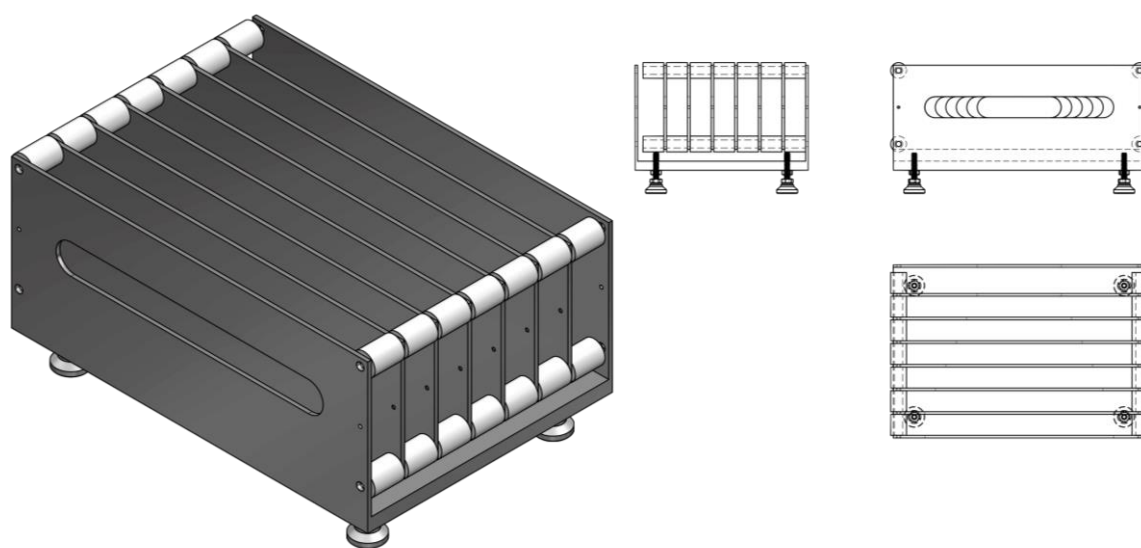
Figure 6: Electrostatic ion mirror, or reflectron.

Gases that do not possess a permanent dipole moment, such as argon, xenon, and molecular hydrogen, are polarizable and can interact with other molecules with a permanent or temporary dipole moment by means of Van der Waals interactions. This unique type of noncovalent interaction is extremely weak and thus allows for the acquisition of data using infrared light to remove the solvated gases. Predissocation spectroscopy capitalizes on this phenomenon and uses the mass difference of argon dissociation to detect infrared absorption. Entrainment of rare gases with sample has been surveyed by multiple pulse valve entrainment of gas prior to ionization. To effectively obtain gas phase infrared spectra of future systems, gas entrainment is required for rare-gas tagging due to increasingly high binding. Figures 7 and 8 are mass spectra from the Wiley-McLaren from the Hammer research group.
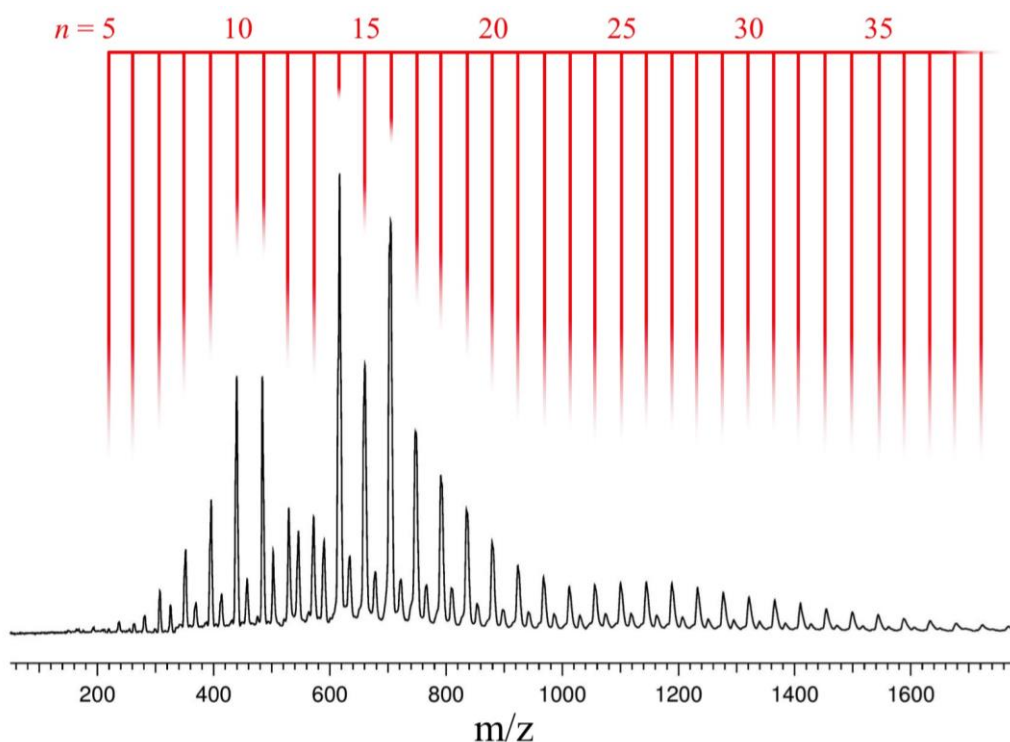
Figure 7: Mass spectrum of $(CO_2)_n{}^-$ cluster anions
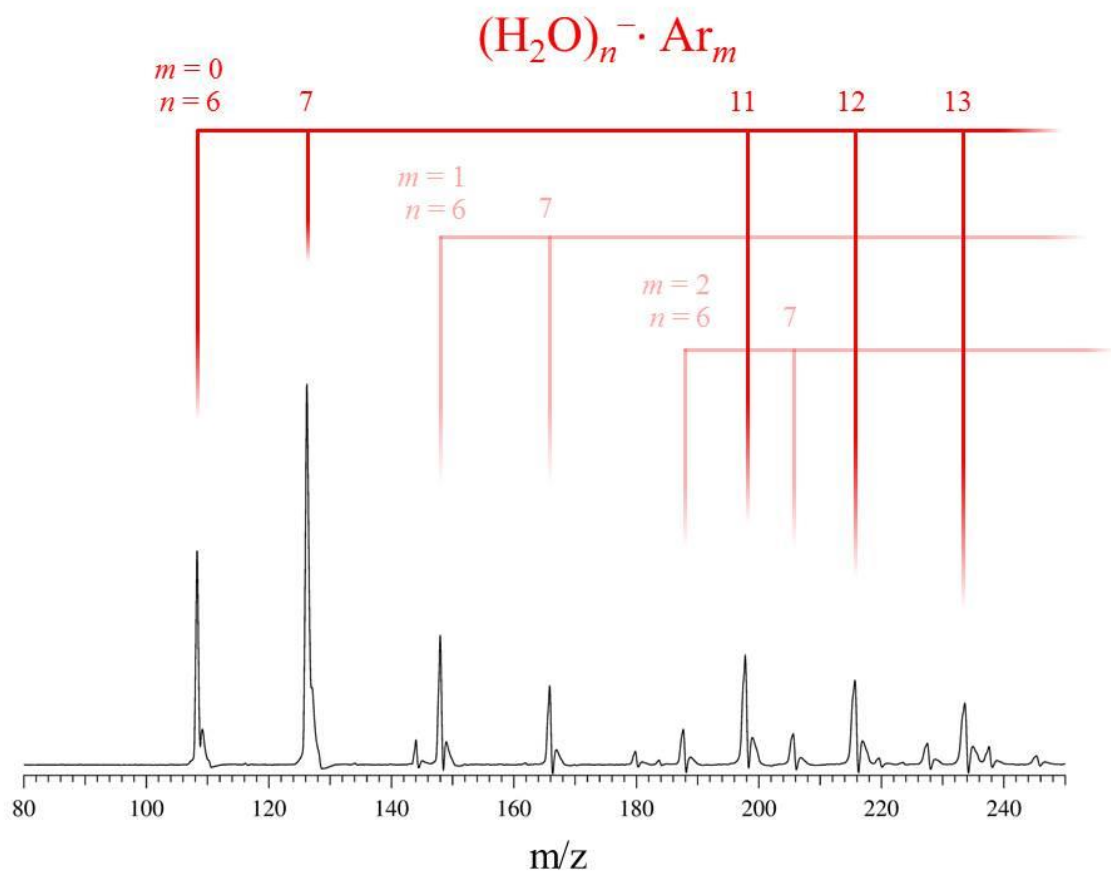
Figure 8: Mass spectrum of H_2O cluster anions
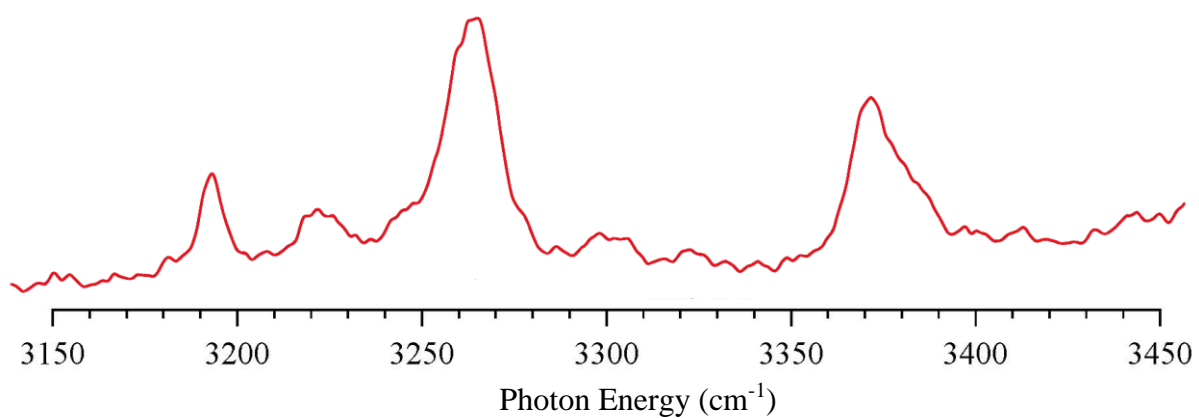
Figure 9: IR spectrum of $(H_2O)_6^-$ cluster anions

Tunable infrared radiation

A tunable radiation source, as seen in Figure 10, will be employed to examine gas phase vibrational interactions of mass selected ions via predissocation and Photodetachment spectroscopy. A Surelite II unseeded Nd:YAG laser (Continuum) supplies 600 mJ/pulse at a rate of 10 Hz to pump an optical parametric oscillator/ optical parametric amplifier laser (OPO/OPA, Laservision, shown in Figure 5). Two dielectric mirrors steer the 1064 nm light into a telescope in which the beam diameters is reduced by 10%. The resulting beam is then split into two beams, one directed at the oscillator stage (40% of total beam), and the other at the amplifier stage (60% of total beam). The OPO beam passes through a potassium titanyl phosphate (KTP) doubling crustal to produce 100 mJ/pulse green, 532 nm.
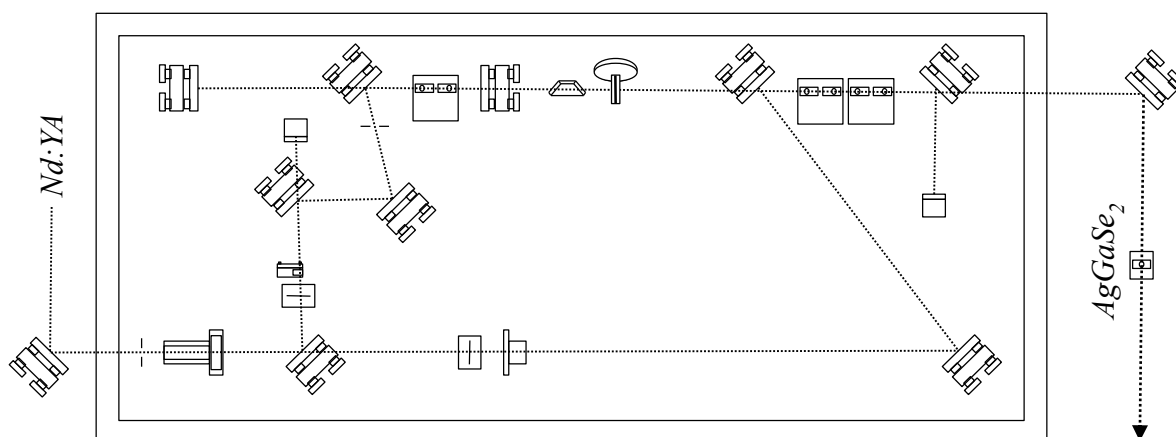
Figure 10: The Laservision OPO/OPA configuration is shown by the schematic above. Oscillation and amplification are permitted in individual regions producing tunable infrared radiation. Low energy vibrational modes require a silver gallium selenite (AgGaSe$_2$) crystal to scan $600 - 2500$ cm^{-1}.

The 532 nm radiation is directed into the oscillator cavity in which two new tunable wavelengths of light are created, the visible 710-880 nm and the idler ~1300-2100 nm (~4700-7500 cm^{-1}). After the OPO stage, over 25 mJ/pulse of total laser light is generated in which all but the idler wavelengths are blocked by a silicon filter. Passing through a series of optics, the

idler beam combines with the OPA 1064 nm beam in four potassium titanyl arsenate (KTA) crystals causing frequency difference generation. The mixing of the idler and the pump beams produce two new wavelengths of infrared radiation: 4700-7500 cm^{-1} (near IR) and 2000-4600 cm^{-1} (mid IR). A Brewster's stack filter can separate the two beams by wavelength to allow for near and mid infrared scanning to take place. All tunable wavelengths are coordinated with motor positions of each crystal and are controlled by an external computer program. Figure 6 compares the absorption of water vapor in the air using the output of the Laservision infrared laser and an FTIR.

Time-of-flight mass spectrometry, in union with a tunable infrared laser, is the approach in which vibrational transitions can be experimentally probed. The mass spectrometer allows for a single mass selected cluster to be isolated and ultimately tagged with a rare-gas. The tunable infrared laser provides $600 - 4700$ cm^{-1} radiation that can be absorbed by negatively charged clusters. After vibrational excitation via infrared absorption, relaxation can be accomplished with two possible paths: fragmentation or electron dissociation. These two paths are competitive yet also happen simultaneously. For preliminary experiments electron dissociation spectra such as that shown in Figure 7 is employed.

If fragmentation of an ion is favorable to electron dissociation, the molecular ion will split into a neutral fragment and a daughter ion. If the electron dissociation energy is lower then the electron will dissociate. Rare-gases are weakly bound to ions and can be fragmented from the parent ion with ~400 cm^{-1} where as fragmenting hydrogen bond of single water molecule takes over 1000 cm^{-1}. Electron dissociation energy varies for each system as seen in the electron photodetachment action spectra Weak dipole bound systems have electron dissociation energies as little 50 cm^{-1}, however valence bound electrons can be well over 10,000 cm^{-1}. When employing rare-gas tagging, the favored path is fragmentation of the Van der Waals bound gas.

The Laservision OPO/OPA tunable infrared laser has an 8 nanosecond output with a diameter the size of a dime where as the molecular ion mass separation varies around 10 microseconds. With calculated timing, light-matter interaction can be easily achieved between the tunable infrared source and the mass selected ions. To maximize the number of photons absorbed by the molecular ion beam, a series of dielectric mirrors were mounted on custom aluminum stands inside of the interaction vacuum chamber with a focal point a few inches in front of the reflectron. By increasing the number of times the laser passes through the molecular ion beam, the detection signal of either neutral or daughter ions is enhanced.

Raman Spectrometer

The Horiba LabRAM Evolution Raman Spectrometer is a recent addition to the Hammer research group and has performed with higher definition for ultra low energy (ULF) transitions, cryogenic Raman under nitrogen or RUN setup, as well as perform full vibrational scans in a fraction of the scanning time. Figure 7 is the newest addition to the research group and employs many new spectroscopic techniques that can be used for future work.
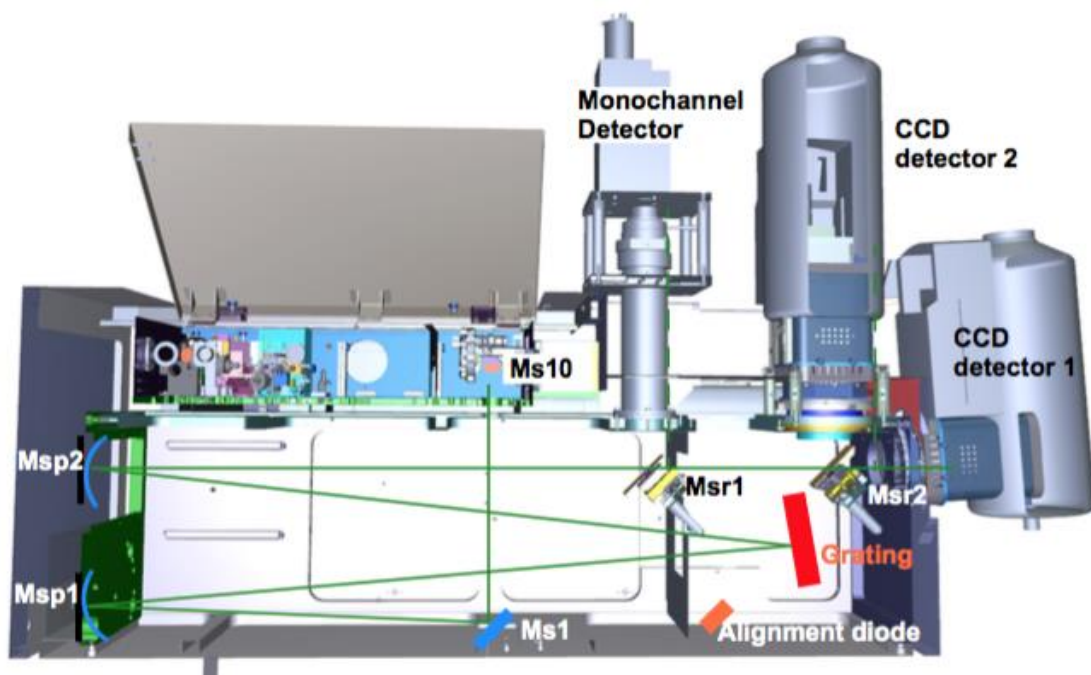
Figure 11: Horiba LabRAM Evolution Raman Spectrometer

These techniques are shown in Figure 12 – 14 for ammonia borane, BH_3NH_3, methanol. and CO_2.

Raman Shift (cm^{-1})
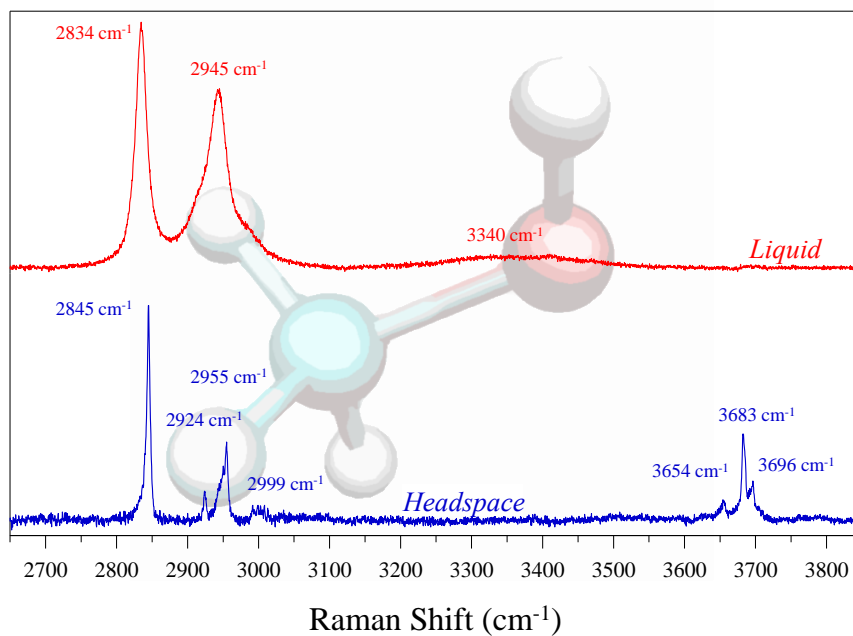
Figure 12: Raman headspace analysis of methanol.

Ammonia Borane ─ BH₃NH₃ (97%)
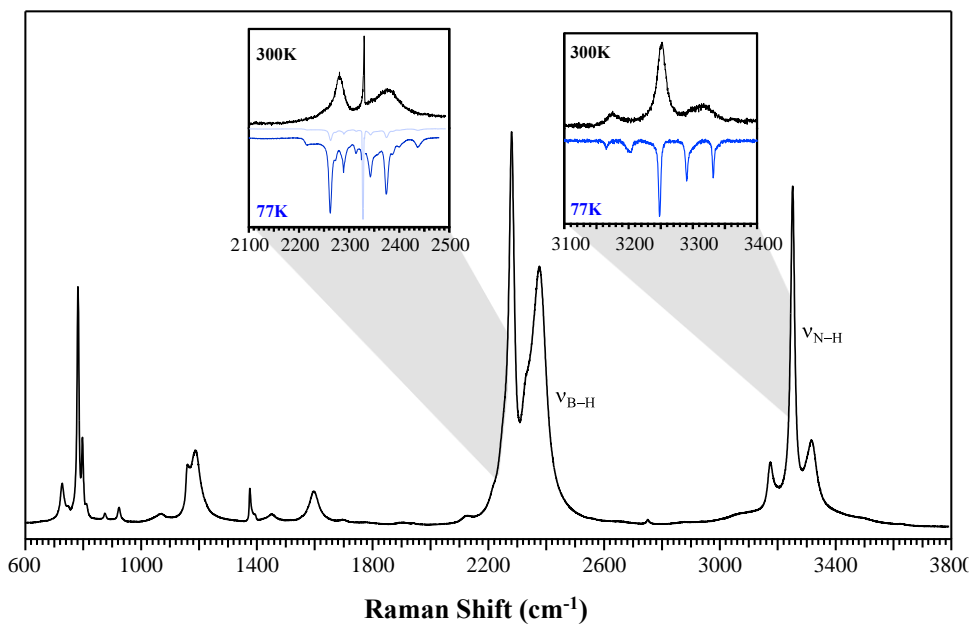
Figure 13: Raman (black trace) and Raman under liquid nitrogen (blue trace) of BH₃NH₃
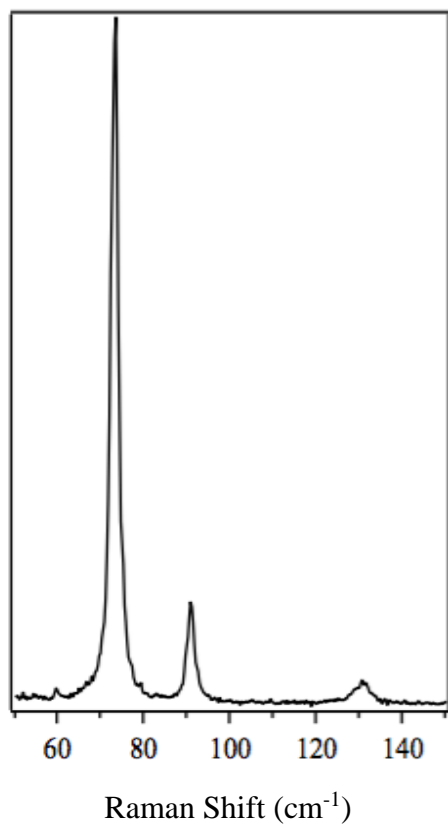
Figure 14: Raman under liquid nitrogen of CO_2

CHAPTER 5

PHOTOELECTRON SPECTROSCOPIC AND COMPUTATIONAL STUDY OF
HYDRATED PYRIMIDINE ANIONS

Preface

The separate contributions of this published work was the experimental photoelectron spectra

of mass selected negative ions by the Bowen group at Johns Hopkins and we performed the

computational investigation of hydrated cluster anions.

Abstract

The stabilization of the pyrimidine anion by the addition of water molecules is studied

experimentally using photoelectron spectroscopy of mass-selected hydrated pyrimidine

clusters and computationally using quantum-mechanical electronic structure theory. Although

the pyrimidine molecular anion is not observed experimentally, the addition of a single water

molecule is sufficient to impart a positive electron affinity. The sequential hydration data have

been used to extrapolate to –0.22 eV for the electron affinity of neutral pyrimidine, which

agrees very well with previous observations. These results for pyrimidine are consistent with

previous studies of the hydrated cluster anions of uridine, cytidine, thymine, adenine, uracil,

and naphthalene. This commonality suggests a universal effect of sequential hydration on the

electron affinity of similar molecules.

Introduction

The interaction of low-energy electrons with nucleic acid bases as a result of interactions with ionizing radiation is known to induce the fragmentation of DNA.[58] Much effort has been made to elucidate the mechanisms at play and the specific site at which fragmentation occurs.[78-80] There is evidence that suggests that pyrimidine nucleobases are the site at which an excess electron can be localized. Pyrimidine is a nitrogen-containing heterocyclic molecule that serves as a structural motif in many important biological molecules. Besides being incorporated in uracil and thymine nucleic acid bases, it is also present in many natural products (e.g., vitamin B_1), synthetic products, and so on.

Pyrimidine is known to possess a negative electron affinity (EA).[81] Anions created from such molecules, whose energies are higher than those of their neutral counterparts, are unstable with respect to autodetachment. However, the interaction of electrons with isolated neutral molecules having negative adiabatic electron affinities can produce short-lived, "temporary" anions in the gas phase,[82,83] and actually become stable in the condensed phase. This phenomenon suggests that interactions between the unbound ion and solvent molecules stabilize the excess charge and lowers the energy of the anion below that of the corresponding neutral. From an energetic standpoint, the interaction of an anion with one or more neutral solvent molecules is more favorable that the interaction of that ion's neutral counterpart with an equal number of those same solvent molecules.

The stabilization of the pyrimidine anion by interactions with different solvent species has previously been investigated by Periquet *et al*.[84] The addition of six argon, five krypton, or four xenon atoms resulted in a stable anion, as did the addition of one water, two ammonia, or three toluene molecules. These results suggest that the magnitude of the EA of the unstable pyrimidine anion is a small negative value. Electron transmissions spectroscopic results from

the mid-1970s also suggest that the pyrimidine anion has an EA close to zero, possibly as far as –0.25 eV.[81]

Here we use negative ion photoelectron spectroscopy to quantify the stabilization effect that water has on the otherwise unstable pyrimidine anion. This solvent-induced anion stabilization has been observed in similar molecules including uridine, cytidine, thymine, adenine, uracil, and naphthalene.[35,85-87] When studying solvent stabilization effects on unstable anions, mass analysis allows for the systematic addition of solvent molecules, along with the determination of the minimum number of solvent molecules necessary to stabilize the negative ion. Analysis of photoelectron spectra of solvated cluster anions also offers a direct method of measuring the stabilization of the anion by interrogation of the EAs of the clusters.

Experimental Methods

Negative ion photoelectron spectroscopy is conducted by crossing the mass-selected negative ion beam with a fixed frequency laser and energy analyzing the resulting photodetached electrons. This process is governed by the equation:

$$h\nu = \text{EKE} + \text{EBE} \qquad (1)$$

where EKE is the electron kinetic energy and EBE is the electron binding energy, The negative ion photoelectron spectrometer as Johns Hopkins University has been described previously.[88] Anions were formed at its supersonic expansion source. There, the mixture of pyrimidine and water was heated to ~60º C and expanded together with argon gas through the 20 μm nozzle orifice. The low-energy electrons from a biased filament were injected into the expanding jet in the presence of a weak magnetic field. The apparatus utilized a Wien filter for mass selection. A magnetic sector mass spectrometer was also used for mass analysis. Photodetachment was accomplished with 2.54 eV (488 nm) photons of an intracavity laser. Photodetached electrons were analyzed with a hemispherical electron energy analyzer with a typical resolution of ~25 meV. The well-known photoelectron spectra of O^- and NO^- were used for calibration.[89-91]

Computational Methods

Full geometry optimizations and harmonic frequency calculations were performed on all hydrated pyrimidine cluster anion structures using the spin-unrestricted UB3LYP density functional theory (DFT) method[92-94] and 6-31++G(2df,2pd) double-ζ basis set as implemented in the Gaussian09 software package.[95] Pure angular momentum (5d,7f) atomic orbital basis functions were utilized rather than the Cartesian counterparts (6d,10f). A pruned numerical integration grid composed of 99 radial shells and 590 angular points per shell was employed with a threshold of 10^{-10} for the RMS change in the density matrix during the self-consistent field procedure. The maximum Cartesian force for each optimized structure did not exceed 1.4×10^{-6} Hartrees/Bohr. Our previous optimized neutral pyrimidine/water structures[96] were taken as starting geometries for the [Py·(H$_2$O)$_n$]$^-$ ($n = 1 - 5$) anions. Additional starting structures were created by taking known hydrated electron cluster geometries[6,97-99] [(H$_2$O)$_n$ $^-$] and attaching a pyrimidine molecule to a free hydrogen atom via an HOH···N hydrogen bond. Although this procedure is by no means an exhaustive exploration of the complicated potential energy surfaces associated with these clusters, it should, at the very least, identify representative minima close to the global minimum.

Vertical detachment energies (VDEs) of low-lying UB3LYP optimized structures were calculated as the difference between the electronic energy anion and that of the corresponding neutral species (constrained to the anion geometry). All computations used to determine VDEs employed the same 6-31++G(2df,2pd) basis set. The electronic energies of the neutral clusters were computed with the spin-restricted RB3LYP DFT method.

The optimized geometries and harmonic frequencies of the corresponding neutral clusters were also computed with the spin-restricted RB3LYP DFT method and the 6-31++G(2df,2pd) basis set to evaluate the adiabatic electron affinity (AEA) of the [Py·(H$_2$O)$_n$] series. To preserve the hydrogen bonding motifs and minimize solvent reorganization, we used the optimized

anion structures as starting points for subsequent geometry optimizations of the neutral cluster. These neutral structures were all identified in our previous work but do not necessarily correspond to the lowest-energy configuration. AEAs corrected for zero-point vibrational energy (ZPVE) of both the anion and neutral were also determined from the unscaled B3LYP/6-31++G(2*df*,2*pd*) harmonic vibrational frequencies. Extensive calibration[100] has determined the electron affinities computed with the B3LYP DFT method, and a comparable double-ζ basis set is typically within four tenths of an electronvolt of the experimental values for valence bound anions.

Experimental Results

Figure 1 shows a typical mass spectrum of the pyrimidine/water cluster anion system. The first observed member of the $[Py \cdot (H_2O)_n]^-$ series is the $[Py \cdot (H_2O)]^-$ anion. The pyrimidine molecular anion was not observed. This result suggests that just one water molecule was sufficient to stabilize the negative ion of pyrimidine, in agreement with the previous results of Periquet et al. The intensity of the second member of the series, $[Py \cdot (H_2O)_2]^-$, is stronger than that of $[Py \cdot (H_2O)]^-$, which is a characteristic common to all of the solvent-stabilized systems we have previously studied.[35,85-87] The first solvent-stabilized cluster in the series is likely to be only weakly bound, and this low stability is manifested by the weaker signal in the mass spectrum. The intensity of the hydrated series decreases sharply after $n = 2$ but levels off after $n = 5$. $[Py_2 \cdot (H_2O)_m]^-$ clusters can also be seen in our mass spectrum between the peaks for $n = m + 4$ and $n = m + 5$ (e.g., $[Py_2 \cdot (H_2O)_2]^-$ between $n = 6, 7$). Intensities of these clusters containing two or more pyrimidine molecules are significantly weaker compared with the largest peaks associated with the $[Py \cdot (H_2O)]^-$ clusters. As such, clusters containing more than one pyrimidine will not be discussed or analyzed here.
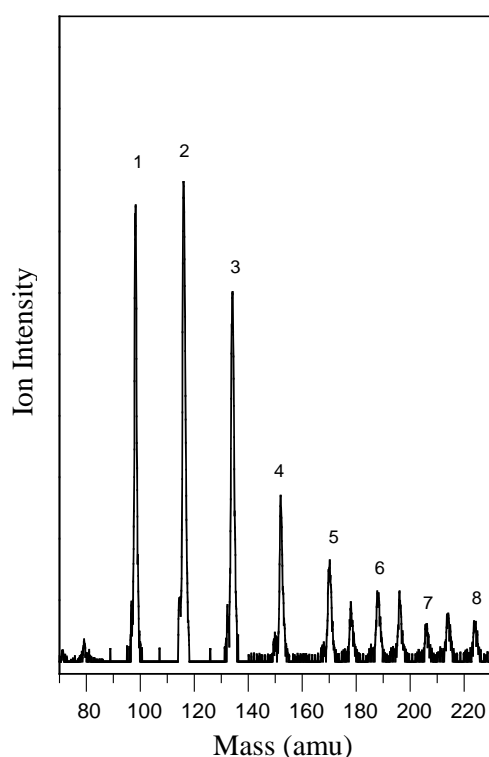
Figure 1. Mass spectrum of $[Py \cdot (H_2O)_n]$ − cluster anions, $n = 1 - 8$.

The photoelectron spectra of the first eight members of the hydrated series $[Py \cdot (H_2O)_n]^-$ are presented in Figure 2. The experimental threshold energies (E_{th}) and EAs are presented in Table 1, along with the stepwise increase in the EAs with sequential hydration (ΔEA). The spectra have very broad features, typical of solvated valence anions. The spectral profile is conserved through the series, but there is a nonlinear shift to higher binding energy and additional broadening with increasing cluster size. The first member of the series ($n = 1$) is characterized with two peaks at 0.23 and 0.41 eV. We assigned the lower binding energy peak as a transition origin, taking the center of this peak as an experimental EA of $Py \cdot (H_2O)$ cluster. The spacing between the origin transition and the higher energy peak (1449 ± 80 cm^{-1}) indicates that the higher binding energy peak could be caused by the vibrations of pyrimidine.[73,96,101-103] We assigned the EBEs of the next five members of the hydrated series by comparing and overlaying the adjacent pairs of the series, $n = 1$, $n = 2$, and $n = 3$, and so on. This procedure has proved to be fairly reliable in the systems we have previously studied.[87] In the photoelectron spectrum of $[Py \cdot (H_2O)_5]^-$ negative ion, there is an additional broad feature around 0.75 eV. A summary of these results is presented in Table 1.
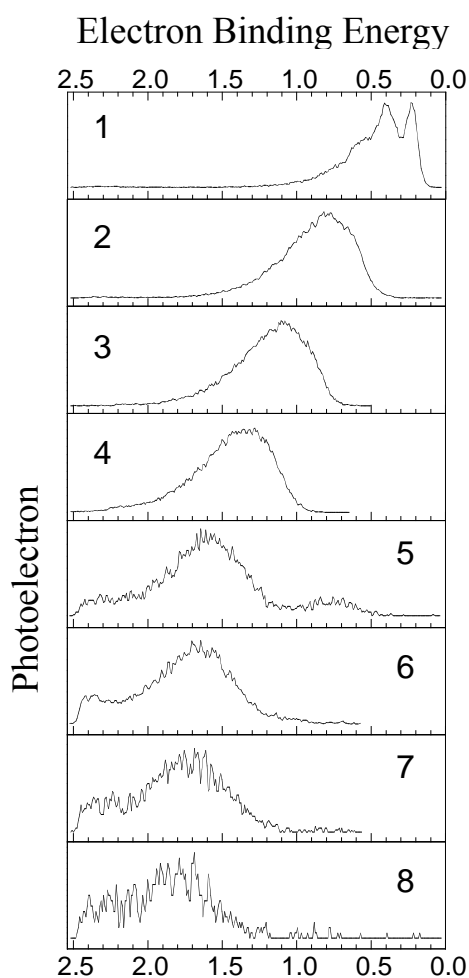
Figure 2. Photoelectron spectra of $[Py \cdot (H_2O)_n]^-$, $n = 1 - 8$ cluster anions recorded with 2.54 eV photons.

Table 1. The experimental electron affinities (EA) of hydrated pyrimidine clusters $[Py \cdot (H_2O)_n]^-$, their stepwise increase $\Delta EA = (EA_{(n)} - EA_{(n-1)})$, and the threshold energies (E_{th}) of their negative ion photoelectron spectra. All energy values are in eV.

n	E_{th}	EA	ΔEA
1	0.10	0.23	
2	0.32	0.62	0.39
3	0.64	0.93	0.29
4	0.87	1.16	0.23
5	1.04	1.36	0.20
6	1.10	1.45	0.09
7	1.11	1.51	0.06
8	1.17	1.59	0.08

[a]All energy values are in electronvolts.

Computational Results

Figure 3 shows select optimized structures for low-energy $[Py \cdot (H_2O)_n]^-$ ($n = 1 - 5$) cluster anions identified in this study, and Table 2 lists their computed vertical detachment energies (VDEs) for the anions and AEAs with (AEA_0) and without (AEA) the zero-point vibrational energy corrections for the corresponding neutrals. Only a single low-energy $[Py \cdot (H_2O)]^-$ minimum was found (Figure 3a), and it is characterized by an OH$\cdots$N hydrogen bond donated from water to pyrimidine. The VDE of this structure was found to be 0.43 eV, while corresponding neutral has an AEA and AEA^0 of 0.14 and 0.28 eV, respectively. The latter value is slightly larger than the lowest energy experimental feature at 0.22 eV but smaller than the second lowest experimental feature at 0.41 eV. The magnitude of the corrections for the ZPVE is essentially the same for all of the clusters examined in this work. The AEA^0 is consistently 0.14 to 0.19 eV larger than the AEA, and , as such, the latter quantity is largely omitted from the remaining discussion.

	VDE	AEA	AEA^0
$[Py \cdot H_2O]^-$	0.43	0.14	0.28
$[Py \cdot (H_2O)_2]^-$-A	0.91	0.56	0.69
$[Py \cdot (H_2O)_2]^-$-B	0.77	0.29	0.46
$[Py \cdot (H_2O)_2]^-$-C	0.77	0.34	0.51
$[Py \cdot (H_2O)_3]^-$-A	1.22	0.68	0.83
$[Py \cdot (H_2O)_3]^-$-B	1.21	0.68	0.83
$[Py \cdot (H_2O)_3]^-$-C	1.99	0.44	0.63
$[Py \cdot (H_2O)_4]^-$-A	2.34	0.88	1.03
$[Py \cdot (H_2O)_4]^-$-B	1.50	0.78	0.96
$[Py \cdot (H_2O)_4]^-$-C	1.50	0.78	0.95
$[Py \cdot (H_2O)_5]^-$-A	1.74	0.85	1.03
$[Py \cdot (H_2O)_5]^-$-B	2.17	0.65	0.84
$[Py \cdot (H_2O)_5]^-$-C	0.99	0.47	0.58

Table 2. Vertical Detachment Energies for Select $[Py \cdot (H_2O)_n]^-$ ($n = 1 - 5$) Cluster Anions and Adiabatic Electron Affinities of the Corresponding Neutral Clusters Calculated Using B3LYP/6-31++G($2df,2pd$) Level of Theory

The three lowest-lying $[Py \cdot (H_2O)_2]^-$ minimum energy structures identified on the B3LYP/6-31++G($2df$,$2pd$) potential energy surface are shown in Figure 3b-d. The lowest energy structure (Figure 3b) has water molecules donating hydrogen bonds to each of the nitrogen atoms of the pyrimidine ring and exhibits a VDE of 0.91 eV, while the analogous neutral has an AEA^0 of 0.69 eV. The two other low-energy $[Py \cdot (H_2O)_2]^-$ isomers (Figures 3c,d) share the same structural motif where a water dimer is hydrogen-bonded to one of the nitrogen atoms (i.e., both waters on the same side of the pyrimidine ring). Both structures are 2.6 kcal mol-1 higher in energy than $[Py \cdot (H_2O)_2]^-$–A according to the B3LYP/6-31++G($2df$,$2pd$) electronic energies. These two structures have identical VDEs of 0.77 eV but slightly different corresponding neutral AEA^0 values (0.46 eV for $[Py \cdot (H_2O)_2]^-$–B and 0.51 eV for $[Py \cdot (H_2O)_2]^-$–C). These calculated values agree very well with experiment (0.62 eV) and suggest that multiple structural isomers could be present experimentally. No anion structures were found that form cyclic hydrogen bonding networks involving both CH$\cdots$O and OH$\cdots$N interactions as previously identified for neutral $Py \cdot (H_2O)_2$ clusters.[96]
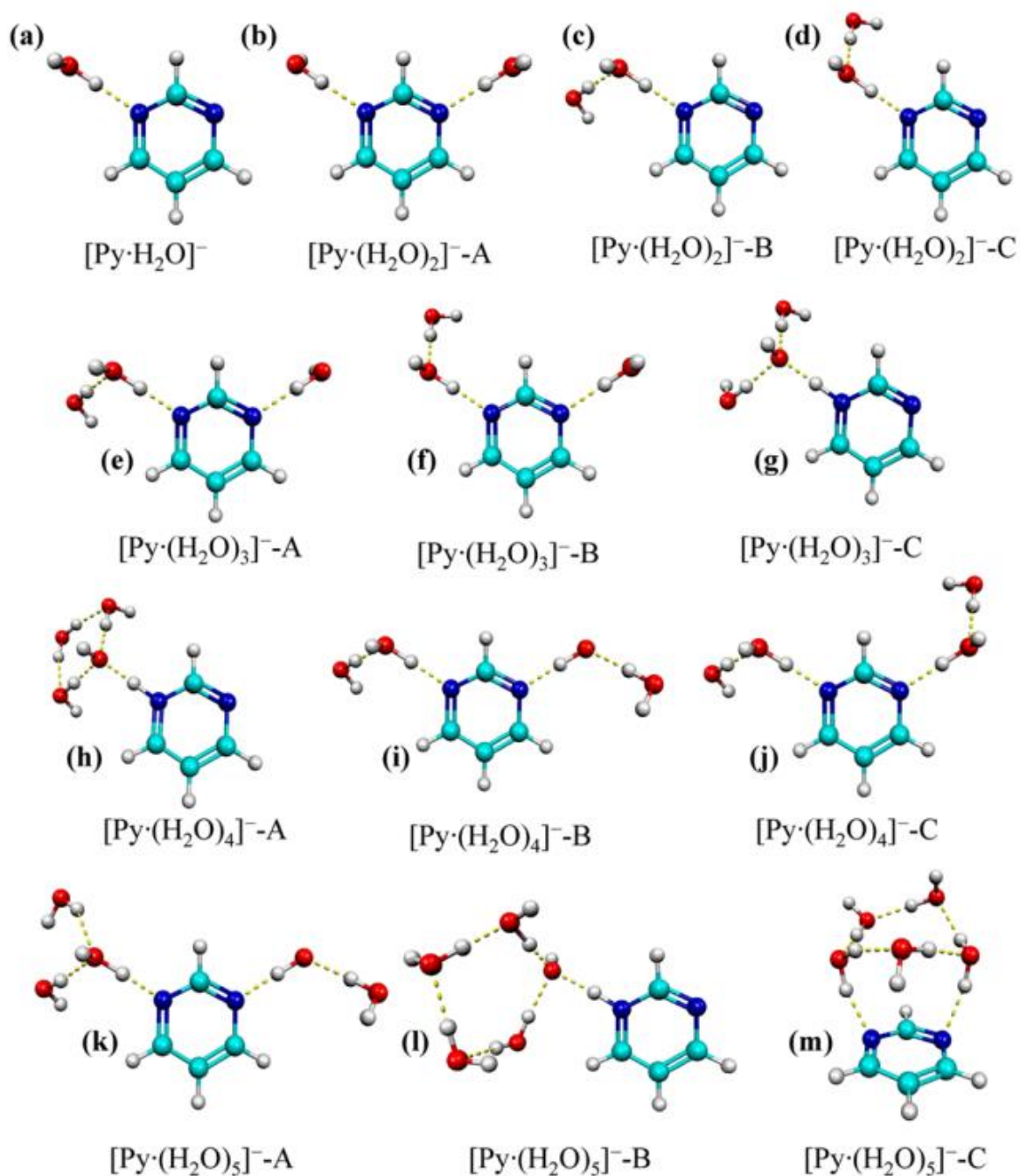
Figure 3. Structures of select $[Py \cdot (H_2O)_n]^-$ ($n = 1 - 5$) cluster anions optimized at the B3LYP/6-31++G($2df,2pd$) level of theory.

Several $[Py \cdot (H_2O)_3]^-$ minima were identified. The two lowest energy structures, $[Py \cdot (H_2O)_3]^-$–A and $[Py \cdot (H_2O)_3]^-$–B, are nearly isoenergetic and are shown in Figure 3e,f, respectively. These structures essentially have a water dimer hydrogen bonded to one nitrogen atom and a water monomer donating a hydrogen bond to the other nitrogen atom of the pyrimidine ring. Some higher energy structures were identified that exhibit proton transfer from water to pyrimidine, such as $[Py \cdot (H_2O)_3]^-$–C in Figure 3g. Additional structures with all three water molecules on the same side of the ring and interacting with just one nitrogen atom (not shown) were identified and found to be appreciably higher in energy. The VDE and AEA^0 for the corresponding neutral computed for $[Py \cdot (H_2O)_3]^-$–A are 1.22 and 0.83 eV, respectively. The values of those for $[Py \cdot (H_2O)_3]^-$–B are virtually identical (within 0.01 eV), and both values agree very well with the experimental EA of 0.93 eV. The structure that exhibits proton transfer, $[Py \cdot (H_2O)_3]^-$–C is only 1.8 kcal mol^{-1} higher in energy than the other two isomers at the B3LYP/6-31++G($2df$,$2pd$) level of theory. Its VDE is much higher at 1.99 eV, while the AEA^0 of the analogous neutral is 0.63 eV due to significant rearrangement upon the loss of the excess electron.

Over 20 $[Py \cdot (H_2O)_n]^-$ ($n = 4,5$) minima were identified that exhibit structural motifs similar to these observed for the smaller hydrated structures. For $n = 4$, the two lowest energy structures that were found are structurally similar and exhibit proton transfer from water to pyrimidine, as shown by $[Py \cdot (H_2O)_4]^-$–A in Figure 3h. The VDE and AEA^0 of the neutral for this structure are 2.34 and 1.03 eV, respectively, compared with an experimental EA value of 1.16 eV. The two structures $[Py \cdot (H_2O)_4]^-$–B and $[Py \cdot (H_2O)_4]^-$–C lie within < 1 kcal mol^{-1} according to B3LYP/6-31++G($2df$,$2pd$) electronic energies (Figure 3i,j, respectively). These two structures are characterized by a pair of water dimers donating a single hydrogen bond to one of the nitrogen atoms in pyrimidine. The VDE and AEA^0 of the corresponding neutral are 1.50 and 1.03 eV for $[Py \cdot (H_2O)_4]^-$–B, respectively, and those for $[Py \cdot (H_2O)_4]^-$–C differ by no more than

0.01 eV. All of the AEA_0 values are similar to the experimental EA of 1.16 eV, and these B3LYP computations suggest that either structural motif could be present in the experiment.

The lowest energy $[Py \cdot (H_2O)_5]^-$ structure ($[Py \cdot (H_2O)_5]^-$–A) that was identified is shown in Figure 3k and exhibits a water dimer hydrogen bonded to one nitrogen atom of the pyrimidine ring and a water trimer cluster hydrogen bonded to the other nitrogen atom. The computed VDE and AEA^0 for the corresponding neutral are 1.74 and 1.03 eV, which agree with the experimental EA of 1.36 eV. Penta-hydrated structures exhibiting proton transfer such as $[Py \cdot (H_2O)_5]^-$–B in Figure 3l were also found. $[Py \cdot (H_2O)_5]^-$–B is < 1 kcal mol^{-1} higher in energy than $[Py \cdot (H_2O)_5]^-$–A at the B3LYP/6-31++G(2df,2pd) level of theory and has a VDE of 2.17 eV and a AEA^0 of 0.84 eV for the analogous neutral. Figure 3m shows a higher energy $[Py \cdot (H_2O)_5]^-$ isomer that is characterized by a cyclic water pentamer ring hydrogen bonded to both of pyrimidine's nitrogen atoms. $[Py \cdot (H_2O)_5]^-$–C is the lowest energy isomer identified that displays this structural motif. Although it is 3.9 kcal mol^{-1} higher in energy than $[Py \cdot (H_2O)_5]^-$–A at this level of theory, it has a calculated VDE of 0.99 eV and AEA0 of 0.58 eV for the related neutral that could account for the experimental feature at 0.80 eV in the experimental spectrum of $[Py \cdot (H_2O)_5]^-$.

Interestingly. The hydrogen bonding motifs of the lowest energy $[Py \cdot (H_2O)_n]^-$ structures identified in this work are somewhat different than for their neutral counterparts. The lowest-energy neutral $Py \cdot (H_2O)_n$ clusters prefer to have all of the water molecules on one side of the pyrimidine ring, interacting with only one of the nitrogen atoms.[96] In contrast, the lowest-energy anions identified in this study lead to either the water molecules interacting with both nitrogen atoms of the pyrimidine ring or aggregating to donate a proton to one of the nitrogen atoms in the ring.

Discussion

The electron affinity of the $[Py \cdot (H_2O)_n]$ series increases with increasing n, and this can be described with the thermodynamic cycle

$$EA[X(Y)_n] = EA[Y] + \sum_{m=0}^{n-1} D_0[X^-(Y)_m \cdots Y] - \sum_{m=0}^{n-1} D_0[X(Y)_m \cdots Y] \qquad (2)$$

where X represents the solvated molecule of interest, Y represents the solvent, $D_0[X^-(Y)_m \cdots Y]$ is the ion-neutral dissociation energy for the loss of one solvent molecule from the anion cluster, and $D_0[X(Y)_m \cdots Y]$ is the neutral-neutral dissociation energy for the loss of one solvent molecule from the neutral cluster. The description relies on the condition that the excess electron in the $[Py \cdot (H_2O)_n]^-$ cluster is primarily localized on pyrimidine in valence bound orbitals and not delocalized to any great extent in the solvent network. From eq. 2, the sequential energy change per solvent molecule can be expressed as

$$\Delta EA = EA[X(Y)_n] - EA[X(Y)_{n-1}]$$

$$= D_0[X(Y)_n] - D_0[X(Y)_{n-1}] \qquad (3)$$

Negative ion photoelectron spectroscopy can therefore yield the necessary information for the quantization of the energy change for solvation if the excess electron is not significantly interacting with the solvent network.

The solvation of pyrimidine with one water molecule results in a positive electron affinity.[84] Additional water molecules to the cluster stabilize the excess charge and increase the electron affinity of the pyrimidine monomer in a predictable trend, as shown in Figure 4. Using Eqs. 2 and 3, extrapolation of the electron affinity as a function of the number of water molecules back to $n = 0$ yields the electron affinity of the pyrimidine monomer to be –0.22 eV. This approximation agrees very with the previous electron transmission spectroscopic measurement

of –0.25 eV.[81] Figure 5 quantifies the change in electron affinity (ΔEA) with each additional water molecule added. The first water molecule addition has the largest impact on the anion cluster going from –0.22 to 0.21 eV, a 0.43 eV difference, but as the number of water molecules increases the ΔEA decreases. These results are consistent with those for uridine, cytidine, thymine, adenine, uracil, and naphthalene.[35,85-87] In each of these systems, the sequential addition of water molecules increases the electron binding energy of the cluster, with the first water molecule having the largest impact on the electron affinity. In the cases of uridine, cytidine, adenine, and uracil, molecular anions exist, and hydration serves to increase the electron binding energy of the negative charged cluster. The case of naphthalene, however, is nearly identical to pyrimidine in that although the neutral molecule has a negative electron affinity, the addition of one water molecule creates a stable negative ion. [87]
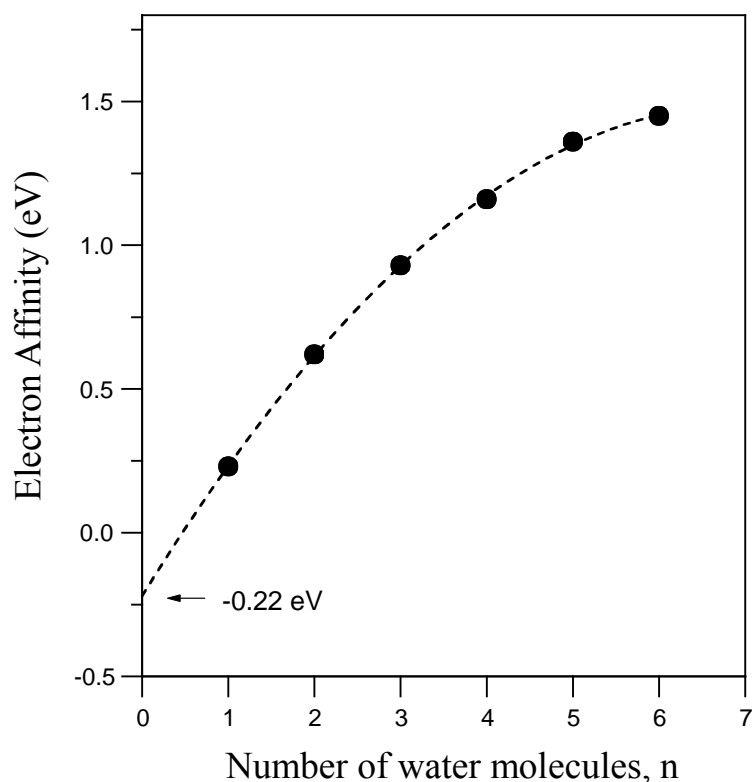
Figure 4. Plot of the experimental electron affinities (EAs) of hydrated pyrimidine clusters as a function of cluster size, *n*.

Interestingly, the computational results reveal that the localization of excess charge in the [Py·(H₂O)$_n$]⁻ cluster anions does not change appreciably with increasing n. Starting with the smallest experimentally observed pyrimidine anion cluster, [Py·(H₂O)]⁻ B3LYP computations show the excess electron residing in a singly occupied molecular orbital (SOMO) that is characterized as a valence π* orbital on pyrimidine. This character does not change with increasing n even though the photoelectron spectra evolve to more closely resemble that of bulk water.[104] This suggests that the addition of subsequent water molecules simply increase the overall binding energy of the entire anionic cluster.
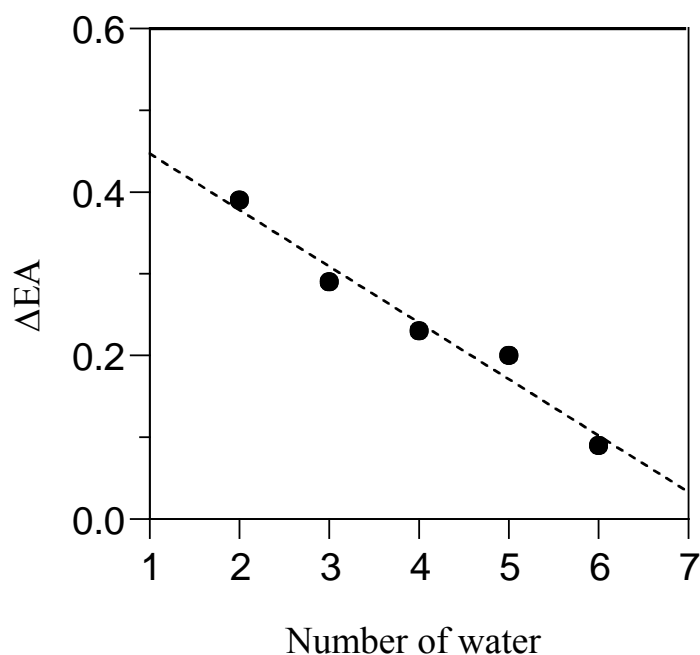
Figure 5. Plot of the sequential spectral shifts (ΔEA) of [Py·(H₂O)$_n$]− photoelectron spectra as a function of cluster size, *n*.

Conclusions

Although the pyrimidine molecular anion is shown to be energetically unstable, only a single water molecule is required to stabilize a negative ion state. B3LYP computations indicate that the excess electron primarily resides in a pyrimidine antibonding π^* orbital, and the character of this SOMO does not change appreciable even after the addition of five water molecules. This localization of excess charge on pyrimidine allows us to extrapolate the electron affinity of the pyrimidine monomer out to –0.22 eV, which is in good agreement with a pervious experimental estimate. The addition of the first water molecule has the largest impact on the electron affinity of the cluster, in agreement with our previous uridine, cytidine, thymine, adenine, uracil, and naphthalene. Although agreement between experimental PES spectra and our theoretical predictions is very good, infrared spectroscopic studies of $[Py \cdot (H_2O)_n]^-$ clusters would provide much insight into the structural motifs of the anion clusters present in the experiment.

CHAPTER 6

THE ONSET OF ELECTRON-INDUCED PROTON TRANSFER IN HYDRATED
AZABENZENE CLUSTER ANIONS

Preface

This work is part of an ongoing collaboration in which the authors at Johns Hopkins University

acquire high-resolution photoelectron spectra of mass-selected ions and the authors from the

University of Mississippi perform quantum mechanical electronic structure computations.

Abstract

   The prospect that protons from water may be transferred to N-heterocyclic molecules due to

the presence of an excess electron is studied in hydrated azabenzene cluster anions using

photoelectron spectroscopy and computational chemistry. In the case of s-triazine ($C_3H_3N_3$),

which has a positive adiabatic electron affinity, proton transfer is not energetically favored nor

observed experimentally. Heterocyclic rings with only 1 or 2 nitrogen atoms have negative

electron affinities, but the addition of solvating water molecules can yield stable negative ions.

In the case of the diazines ($C_4H_4N_2$: pyrazine, pyrimidine, and pyridazine) the addition of one

water molecule is enough to stabilize the negative ion, with the majority of the excess electron

density in a π^* orbital of the heterocycle but not significantly extended over the hydrogen

bonded water network. Pyridine (C_5H_5N), with the most negative electron affinity, requires three water molecules to stabilize its negative ion. Although our computations suggest proton transfer to be energetically viable in all five N-heterocyclic systems studied here when three or more water molecules are present, *i.e.*, both motifs are observed. Pyridine clusters containing four or more water molecules almost exclusively exhibit proton transfer along with solvated $[C_{6-x}H_{6-x+1}N_x \cdot OH]^-$ ions.

Introductions

Subtle non-covalent interactions between nitrogen-containing heterocyclic molecular building blocks, such as the azabenzenes shown in Fig. 1, and hydrogen bonded aqueous environments play important roles in both biological structure and function. Such interactions are fundamental to the nature of macromolecular assemblies, ranging from DNA to proteins. [105-111] The interactions between water and ions are likewise important in many biochemical processes, in aqueous electrolyte chemistry, and in atmospheric chemistry. [112-114] Such hydrogen-bonded networks have been studied at the nanoscopic level for decades in order to understand such interactions. [115,116] The addition of an excess electron to these systems further alters their energetic landscapes. Here, we explore how excess electrons are stabilized in hydrated azabenzene cluster anions as a function of stepwise hydration. Fig. 1 shows the structures of the five N-heterocyclic molecules studied here.

The vertical electron affinities (EA_v) of several azabenzenes were determined by electron transmission spectroscopy (ETS) and compared to benzene. EA_v of benzene (−1.15 eV) was found to be more negative than that of pyridine (−0.62 eV), while the EA_v values of the diazines were determined to be near zero. [81] When ETS was applied to the related molecule, naphthalene, both its EA_v and its adiabatic electron affinity (EA_a) values were both found to be –0.19 eV. [117] Anion photoelectron spectroscopy determined the EA_a value of _s_-triazine to be positive at +0.03 eV, [118] while by extrapolation, it estimated the EAa values of Py to be between –0.67 eV and –0.15 eV and of Pz to be –0.01 eV. [84,119] Mass spectra of hydrated pyridine cluster anions showed that water was stabilizing otherwise unstable pyridine anions. [120] Other mass spectra measurements showed the minimum number of water molecules needed to stabilize pyridine (3), and the diazines (1), and also estimated the negative electron affinity values for each of them. [84] Theory also computed both EA_v and EA_a (negative) values for pyridine, pyrimidine, and related molecules. [118] Both Rydberg electron transfer and anion photoelectron spectroscopy

were also used to study hydrated nucleobase anions.[35,86,119,121] Anion photoelectron spectroscopy was also used to study hydrated 7-azaindole cluster anions for their threshold size at three water molecules through six of them.[122] Negative ion photoelectron spectroscopic studies were also conducted on hydrated amino acid anions,[38] on hydrated naphthalene anions,[87] and on other hydrated aromatic molecular anions.[123] Recently, in combined anion photoelectron and computational study, we studied hydrated pyrimidine (Pm) cluster anions, were we found that a single water molecule stabilized the Pm negative ion.[124] The azabenzene series has also shown interesting "associative" bond formation with CO_2 upon excess electron attachment.[125,126]

Here, in combined anion photoelectron spectroscopic study, we explore and compare the structures and energetics of sequentially hydrated azabenzene cluster anions, where the N-heterocyclic molecules under investigation were *s*-triazine, pyridazine, pyrimidine, pyrazine, and pyridine. While *s*-triazine forms stable parent anions without hydration, the above listed diazines require solvation by at least one water molecule in order to stabilize their anions, and pyridine needs at least three. The focus of this study is on determining the number of water solvent molecules needed to induce proton transfer from H_2O to a given N-heterocyclic molecular anion. This work continues our practice of studying electron-induced proton transfer (EIPT), where in this case water is the proton donor.[32,37,127-141]
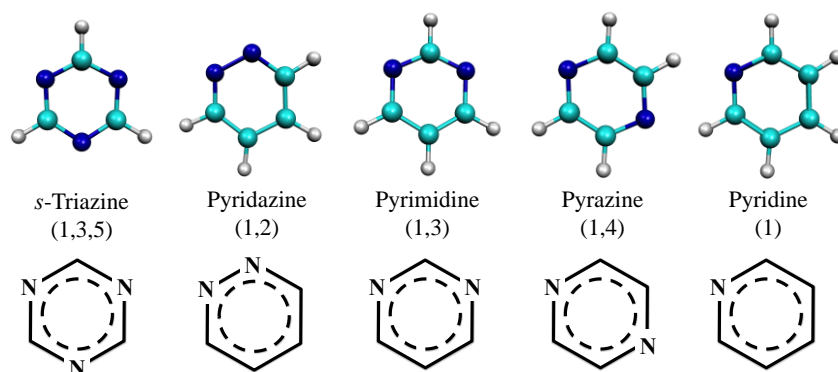
Figure 1. The five N-heterocyclic azabenzene anions studied in this work: *s*-triazine (Tz), pyridazine (Pd), pyrimidine (Pm), pyrazine (Pz), and pyridine (Py).

Experimental Details

Anion photoelectron spectroscopy is conducted by crossing a mass-selected beam of negative ions with a fixed-frequency photon beam and energy-analyzing the resultant photoelectrons. It is governed by the energy-conserved relationship, $h\nu$ = EBE + EKE, where $h\nu$ is the photon energy, EBE is the electron binding (transition) energy, and EKE is the electron kinetic energy.

The hydrated N-heterocycle cluster anions were produced by two different kinds of anion photoelectron spectrometers in our lab. Hydrated s-triazine cluster anions were produced and characterized on our pulsed photoelectron instrument.[142] In general the anions were generated in a photoemission ion source by focusing a pulsed (10 Hz), second harmonic (532 nm) beam of a Nd:YAG laser onto a continuously rotating, translating copper rod. The ultrahigh purity He carrier gas was pulsed though a pulsed valve with a backing pressure of ~ 150 psi. The mixture and s-triazine were directly put into the pulsed valve. The resultant anions were then extracted into a linear time-of-flight mass spectrometer, mass-selected by a mass gate, decelerated by a momentum decelerator, and photodetached by a Nd:YAG laser operated at third harmonic (355 nm, 3.49 eV). The resultant photoelectrons were analyzed by a magnetic bottle electron energy analyzer with a resolution of 35 meV at EKE = 1 eV. The photoelectron spectra were calibrated against the well-known photoelectron spectrum of Cu^-.[143]

All of the other cluster anions were produced and characterized on our continuous anion photoelectron spectrometer. As previously described,[88] a nozzle expansion source was used. Briefly, the N-heterocyclic samples along with water were heated to 70 – 80 ˚C in a stagnation chamber (biased at –500 V) and co-expanded together with 30 – 50 psig argon gas through the 23 μm nozzle orifice into ~10^{-4} Torr vacuum. Low-energy electrons from a biased thoriated-iridium filament were injected into the expanding jet to form negative ions in the presence of a weak magnetic field. The anions were then extracted and transported via a series of ion lenses through the flight tube if a 90˚magnetic sector mass spectrometer (mass resolution, ~ 400).

Mass-selected anions were then crossed with an intra-cavity argon ion laser beam, where photodetachment occurred. The resultant photoelectrons were then analyzed by a hemispherical electron energy analyzer with a resolution of 25 meV. The photoelectron spectrum reported here was recorded with 488 nm (2.540 eV) photons and calibrated against the well-known photoelectron spectrum of the O⁻ anion.[89]

Computational Details

A similar computational approach from our previous study has been employed using the Gaussian09 software package[144] to perform full geometry optimizations as well as harmonic frequency calculations. A hybrid meta-GGA functional,[145-147] M06-2X, was employed for the hydrated azabenzene anions to compare relative energetics as well as to compute vertical detachment energies (VDEs). Pure angular momentum ($5d$, $7f$) atomic orbital basis functions along with a pruned numerical grid integration grid composed of 99 radical shells and 590 angular pointes per shell were employed. All electronic structure methods utilized a Pople-style double-ζ basis set, 6-31++G(d,p). Our previously optimized neutral[96] and anionic[124] structures were taken as starting geometries for al of the hydrated azabenzene series. Additional starting point geometries were generated by attaching an azabenzene molecule to a free hydrogen atom from known water cluster geometries[148-154] and hydrated electron clusters. [37,88,104,134-143,155,156] Though not an exhaustive conformational search, this study identifies low energy structures that should be close to the global minimum. VDE values were calculated as the difference between the optimized geometries electronic energy of the anion and that of the corresponding neutral species with identical geometry. A previously developed solvent polarized continuum model (PCM) linear extrapolation[157] revealed that the ordering for the vertical electron affinities is as follows: pyridine (1) < pyrimidine (1,3) < pyridazine (1,2) < pyrazine (1,4) < s-triazine (1,3,5).

Experimental Results

Fig. 2 shows the photoelectron spectra (PES) of four of the five hydrated azabenzene cluster anions studied here. Additional photoelectron spectra are included in the ESI. Also, we recently reported PES of the hydrated pyrimidine series for $n = 1 - 8$, and we have included those results here for comparison.[124] Broad, vibrationally unresolved spectral features are typical of such hydrated valence anions. Moreover, their spectral onsets (E_o) increase with each additional water solvent that is added, $i.e.$, $A^- \cdot (H_2O)_n + H_2O \rightarrow A^- \cdot (H_2O)_{n+1}$.[158,159] In cases where there is Frank-Condon overlap between the lowest vibrational levels of the cluster anion and its neutral counterpart and where there are no vibrational hot bands present, the EBE of the onset is equal to the adiabatic electron affinity (EA_a). In that case $E_0 = EA_a$. However, in the absence of a clear spectral assignment or explicit computational results it is best not to assume that they are the same. In anion photoelectron spectroscopy, the vertical detachment energy (VDE) is the EBE value at the photoelectron intensity maximum, $i.e.$, where the Frank-Condon overlap in a given transmission is maximized. The EA_a value, which is the thermodynamic energy difference between the lowest vibrational levels of the anion and its corresponding neutral, can only be determined with confidence under the conditions described above.[100] Between VDE and EA_a value, the former is usually the better defined, when no vibrational structure is present. The vertical electron affinity (EA_v) is the energy measured from the lowest vibrational level of a neutral molecule or cluster vertically to its corresponding anion at the structure of the relaxed neutral. While the VDE is a detachment quantity, EA_v is an electron attachment quantity. Anion photodetachment spectra do not reveal direct information about EA_v values. Only in the case where the anion and its neutral counterpart have identical (relaxed) structures is the EA_v equal to the EA_a, and there $VDE = EA_a = EA_v$.

| | s-Triazine (1,3,5) | Pyridazine (1,2) | Pyrimidine (1,3) | Pyrazine (1,4) |

Electron Binding Energy (eV)
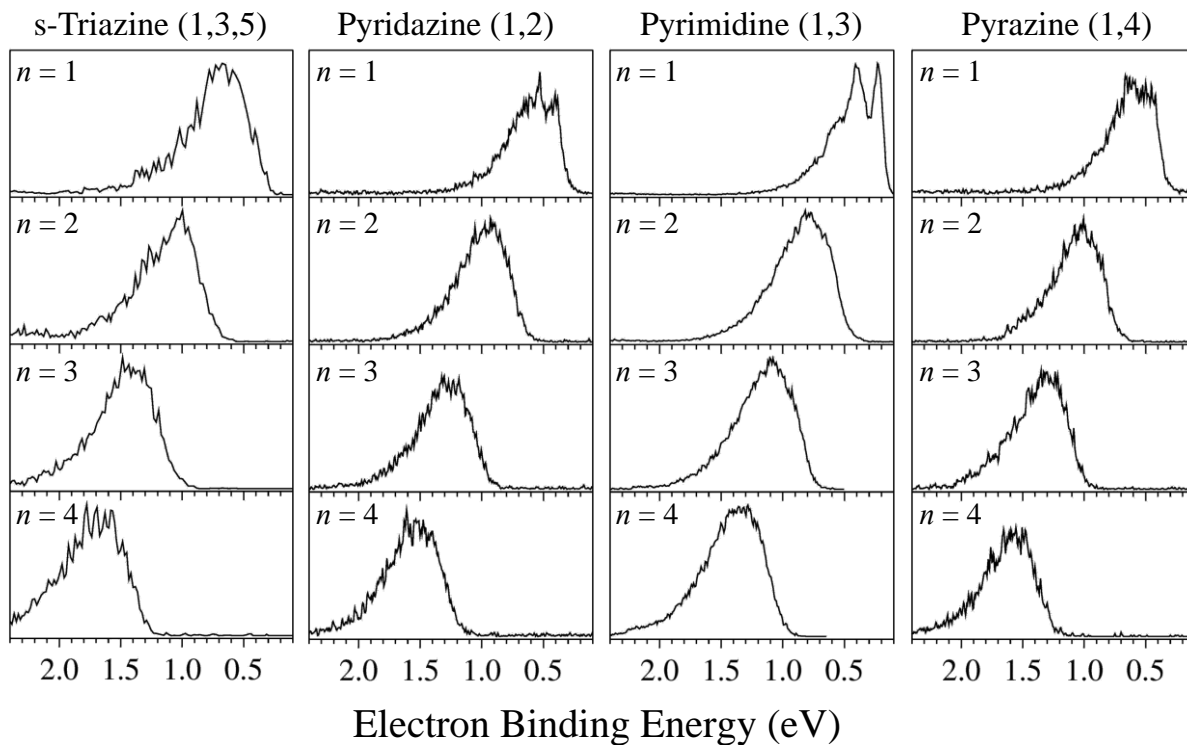
Figure 2. Photoelectron spectra of four of the five hydrated azabenzene cluster anions studied here: $Tz^- \cdot (H_2O)_n$, $Pd^- \cdot (H_2O)_n$, $Pm^- \cdot (H_2O)_n$, and $Pz^- \cdot (H_2O)_n$, where $n = 1 - 4$.

Hydrated s-triazine anions

The *s*-triazine anion, Tz^-, is the only azabenzene considered here that exhibits a stable bound state with respect to autodetachment, *i.e.*, it has a positive EA_a value. Kim *et al.* previously reported the gas phase photoelectron spectrum of the Tz^- molecular anion and determined its electron affinity to be +0.03 eV.[160] The photoelectron spectra of the hydrated *s*-triazine cluster anion series are shown in Fig. 2. Its experimental VDE for $n = 1$ is 0.68 eV. The VDE values are observed to increase continuously with hydration and are 1.01 eV, 1.41 eV, 1.69, eV 1.89 eV, and 2.09 eV for $n = 2 - 6$, respectively.

Hydrated pyridazine, pyrimidine, and pyrazine anions

Pyridazine is the diazine derivative of pyridine with the second nitrogen atom in the *ortho*-position (*i.e.* 1,2 diazine). The electron affinity of the pyridazine molecular anion is though to be slightly negative.[81] With the addition of a single water molecule, the

monohydrated cluster anion is stabilized and exhibits a VDE of 0.53 eV. Addition of subsequent water molecules leads to VDE values of 0.93 eV, 1.27 eV, and 1.53 eV for the $n = 2 - 4$, respectively.

Previously, we reported PES of the hydrated pyrimidine (1,3 diazine) cluster anion series up to $n = 8$ and we included those results here. The VDEs of the hydrated pyrimidine cluster anion series are 0.42 eV, 0.75 eV, 1.11 eV, 1.34 eV, 1.58 eV, and 1.62 eV, respectively, while the extrapolated electron affinity (E_0) of the pyrimidine monomer was –0.2 eV.

Pyrazine is another derivative of pyridine, but with its second nitrogen atom in the *para-* or 1,4 position of the heterocycle (see Fig. 1). Kim measured the PES of $Pz^- \cdot (H_2O)$. Using a sequential argon extrapolation method, the adiabatic electron affinity of pyrazine is estimated to be -0.01 ± 0.01 eV.[161] The photoelectron spectra of hydrated Pz values for n = 1 – 4 are 0.66 eV, 1.05 eV, 1.32 eV, and 1.60 eV, respectively.

Hydrated pyridine anions

The photoelectron spectra of hydrated pyridine cluster anions are shown in Fig. 3. The $[A \cdot (H_2O)_n]^-$, $n = 1, 2$, clusters are unstable in the gas phase with respect to autodetachment. The PES for $n = 3$ exhibits two broad overlapping features with the smaller feature (shoulder) located between 0.5 and 1.0 eV and with the stronger feature (peak) centered at 1.56 eV, its VDE value. The photoelectron spectra for $n = 4 - 6$ species each exhibit single broad peaks with VDE values of 1.79 eV, 1.98 eV, 2.18 eV, respectively.

Pyridine
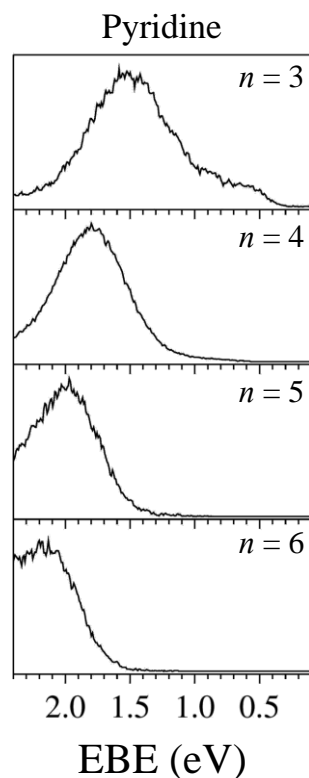
Figure 3. Photoelectron spectra of $[Py \cdot (H_2O)_n]^-$ cluster anions, $n = 3-6$.

Theoretical Results

Over 80 hydrated cluster anion structures, these corresponding to minima (no imaginary frequencies), were characterized and are included in the ESI. The lowest energy structures identified though this calibrated DFT procedure[162] exhibited two motifs. One group of structures can simply be classified as hydrated azabenzene anions, $A^- \cdot (H_2O)_n$ in which a water molecule (or hydrogen bonded network of water molecules) tend to form a hydrogen bond with one N atom of the heterocycle. DFT computations indicate that the majority of the excess electron density resides in a p* orbital of the azabenzene rather than significantly interacting with the extended hydrogen bonded network of water molecules. The lowest-energy $A^- \cdot (H_2O)_n$ structures exhibited this motif are shown in Fig. 4. For $n = 1 - 4$ and A = Tz, Pd, Pm, and Pz.

Starting at $n = 3$ for Py and for Pd and at $n = 4$ in Pm, Pz, and Tz, the other interaction motif begins to emerge. This second class of structures exhibits proton transfer from a water molecule to the azabenzene effectively creating a solvated anion complex, $[AH \cdot OH]^- \cdot (H_2O)_{n-1}$. The M06-2X/6-31G($d,p$) computations suggest neither the charge nor the spin of the excess

69

electron is appreciably localized on either fragment of the [AH·OH]$^-$ complex (although this characteristic could change with the method and/or basis set). In the cases of Tz, Pd, Pm, and Pz, the structures exhibiting proton transfer are not the lowest energy structures (with the exception of Pz for n = 5, 6), as shown in Table 1. However, in the case of Py, the lowest energy structures identified in this study for each cluster size ($n \geq 3$) all exhibit proton transfer, although Py$^-$·(H$_2$O)$_3$ also has a low-lying, hydrogen bonded solvation network, i.e., non-proton transfer, structure. These are shown in Fig. 5, and both motifs described in greater detail in the following sections for the various azabenzene systems.

Hydrated s-triazine anions

The heterocycle, *s*-triazine is the only azabenzene in this study that has a positive electron affinity. The addition of an excess electron lowers the symmetry of *s*-triazine from D$_{3h}$ to C$_{2v}$ due to Jahn–Teller distortions.[160] The Tz$^-$·(H$_2$O)$_{n=1-6}$ cluster anions have calculated VDE values of 0.74 eV, 1.16 eV, 1.45 eV, 1.50 eV, 1.87 eV, and 2.09 eV respectively. Our relative energy calculations suggest that 2 or 3 water molecules tend to prefer interacting with s-triazine at a single nitrogen atom, instead of individually forming hydrogen bonds with the heterocycle at multiple sites (see first column of Fig. 4).

Hydrated pyridazine, pyrimidine, and pyrazine anions

For the hydrated diazine series, the position of the two nitrogen atoms plays an important role in the solvation of the anion at each hydration step (see second, third and fourth column of Fig. 4). Unlike the stable Tz$^-$ anion, all three of the diazine (Pd, Pm and Pz) monomeric anions are unstable with respect to autodetachment of the excess electron. However, with the addition of a single water molecule, the energy of the hydrated cluster anion

becomes lower than that of its corresponding neutral molecular cluster in each case. Only one structure for each of the monohydrated diazines, $A^- \cdot (H_2O)$ was found at the M06-2X/6-31++G(d,p) level of theory, with computed VDE values of 0.61 eV, 0.59 eV, and 0.69 eV for Pd, Pm and Pz, respectively. Stepwise hydration of each negatively charged diazine cluster anion, $A^- \cdot (H_2O)_n$, resulted in increasing VDE values. Interestingly, the hydrated Pm cluster anions, $Pm^- \cdot (H_2O)_n$, have lower computed VDE values than those of the hydrated Pz and Pd cluster anions at the same values of n. Structures exhibiting proton transfer for a given value of n have computed VDE values that are up to 0.7 eV higher than those that do not. Moreover, hydrated diazine cluster anion structures that display proton transfer are not their lowest energy minima (with the exception of Pz for $n = 5, 6$).

Hydrated pyridine anions

Dozens of low-lying minimum energy structures were identified for the negatively charged hydrated pyridine series, and many of them exhibit proton transfer from associated water molecules. For $n = 3$, even though the lowest energy structure exhibits proton transfer (shown in Fig. 5), another structure only 0.02 kcal mol^{-1} lower in energy (also shown in Fig. 5) does not. For $n = 3$, the computed VDE value of the non-proton transfer structure is 0.84 eV, whereas the middle of the shoulder region in the actual photoelectron spectrum is ~0.75 eV. Also for $n = 3$, the computed VDE value for the proton transferred structure is 1.44 eV, whereas the VDE value for the main peak is 1.56 eV. The computed and experimental VDE values for both interaction motifs are in good agreement. For $n = 4 - 6$, the lowest energy structures possess a transferred proton from a water molecule and have calculated VDE values of 1.70 eV, 1.87 eV, and 2.07 eV, respectively. These are shown in Fig. 5. For $n = 4 - 6$, these compare well with experimentally-determined VDE values of 1.79 eV, 1.98 eV, and 2.18 eV, respectively. The corresponding lowest energy structures with intact water molecules lie at least 1 kcal mol^{-1} higher in energy and have computed VDE values of 1.13 eV, 1.33 eV, and

1.51 eV, respectively. For structures exhibiting proton transfer, only a single deprotonated water molecule interacts directly with the heterocycle. While the other $n-1$ water molecules form a hydrogen-bonded network around the deprotonated water molecule.
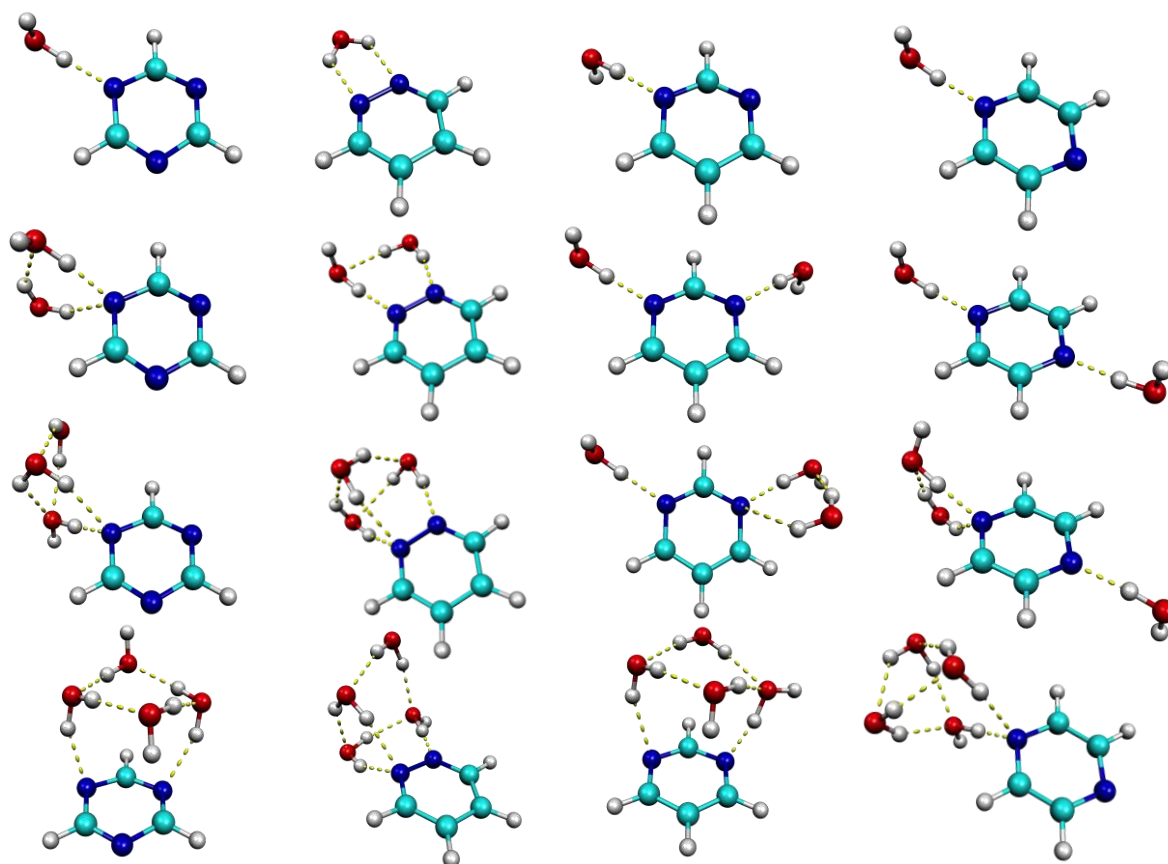
Figure 4. Lowest energy structures of $Tz^-\cdot(H_2O)_n$, $Pd^-\cdot(H_2O)_n$, $Pm^-\cdot(H_2O)_n$, and $Pz^-\cdot(H_2O)_n$ cluster anions for $n = 1-4$ using M06-2X/6-31++G(d,p) level of theory

Discussion

Assignment of photoelectron spectral features

The combination of negative ion photoelectron spectroscopy with density functional theory provides insight into important molecular interactions at play in negatively charged cluster anions. In the case of the N-heterocyclic molecular anion clusters studied here, two types of structural motifs are theoretically predicted to occur as a result of the attachment of an excess electron. In one case, the excess electron density primarily resides in a π^* orbital with n intact water molecules solvating the azabenzene anion at nitrogen atom sites. The other case involves the transfer of a proton from a water solvent to the azabenzene sub-anion solute: $A \cdot (H_2O)_n + e^- \rightarrow [AH \cdot OH]^- \cdot (H_2O)_{n-1}$. Table 1 summarizes the experimental and theoretical results of this study. For Tz, Pd, Pm, and Pz the quantitative agreement between the computed VDE values for non-proton transfer isomers and the experimental VDE values is relatively good, whereas the agreement between the computed VDE values for proton transferred isomers and experiment is poor. This suggests that proton transfer is not occurring in these systems. In the case of $n = 3$ for Py, however, the same comparison indicates both structural motifs are likely to be present. For the Py systems with $n > 3$, the VDE data suggests that only structures exhibiting proton transfer, $[PyH \cdot OH]^- \cdot (H_2O)_{n-1}$, are present. These results are strongly supported by unpublished infrared spectroscopic studies on the same clusters anions by Johnson and co-workers.

	n	A⁻·(H₂O)ₙ VDE	[AH·OH]⁻·(H₂O)ₙ₋₁ VDE	ΔE_rel	E₀	VDE
		Theoretical			Experimental	
Tz	1	0.74	—	—	0.38	0.68
	2	1.16	—	—	0.72	1.01
	3	1.45	—	—	1.03	1.41
	4	1.50	2.04	4.20	1.28	1.69
	5	1.87	2.63	1.91	1.43	1.89
	6	2.09	2.84	1.40	1.51	2.09
Pd	1	0.61	—	—	0.40	0.53
	2	1.12	—	—	0.67	0.93
	3	1.46	2.02	6.48	1.09	1.27
	4	1.79	2.37	4.05	1.30	1.53
	5	1.96	2.55	4.14	—	—
	6	1.95	2.79	2.22	—	—
Pm	1	0.59	—	—	0.23	0.42
	2	0.87	—	—	0.62	0.78
	3	1.26	—	—	0.93	1.11
	4	1.36	2.07	3.00	1.16	1.34
	5	1.37	2.34	1.24	1.36	1.58
	6	1.64	2.42	0.00	1.45	1.62
Pz	1	0.69	—	—	0.34	0.66
	2	1.24	—	—	0.73	1.05
	3	1.64	—	—	1.05	1.32
	4	1.67	2.40	2.25	1.31	1.60
	5	1.66	2.55	−3.37	—	—
	6	2.21	2.75	−0.13	—	—
Py	1	−0.04	—	—	—	—
	2	0.41	—	—	—	—
	3	0.84	1.44	−0.02	0.93	0.75, 1.56
	4	1.13	1.70	−1.21	1.23	1.79
	5	1.33	1.87	−4.32	1.48	1.98
	6	1.51	2.07	1.96	1.61	2.18

Table 1. Computed VDE values for the lowest energy structural isomers for A⁻·(H₂O)ₙ and [AH·OH]⁻(H₂O)ₙ₋₁ (A = Tz, Pd, Pm, Pz, and Py); ΔE_rel, the energy difference between the isomers (in kcal mol⁻¹, where a negative value indicates a structure exhibiting proton transfer is lower in energy); and the experimentally-determined spectral onsets, E₀, as well as vertical detachment energies, VDE

Role of symmetry

The *s*-triazine is the only negatively-charged azabenzene molecule in this study that is stable with respect to autodetachment. Previous work on *s*-triazine and its anion compared the high symmetry neutral s-triazine (D_{3h}) to the reduced symmetry anion (C_{2v}).[118] A nascent Jahn–Teller distortion has also been recently reported in buckminsterfullerene, C_{60}, upon the addition of an excess electron perturbing the electronic structure.[163-168] This structural change

transforms a number of chemical properties, including but not limited to electron affinities, vertical detachment energies, electronic states, charge distributions, and relative energetics between isomers. There are instances, however, where the addition of an excess electron to a closed-shell neutral system can increase the symmetry of the molecular framework.[169] The diazines (Pd, Pm, Pz) maintain their symmetric geometries upon excess electron attachment. Delocalization of the excess charge over the ring minimizes changes in the structure of the anion relative to its neutral. The 1,4 diazine monomer has D_{2h} symmetry in its neutral state, whereas both the 1,3 and 1,2 diazine monomers have C_{2v} symmetry.

Extrapolation of experimentally-determined E_0 values

Previously, we utilized the experimental E_0 values of the $Pm^- \cdot (H_2O)_n$ cluster anion series to extrapolate to $n = 0$, giving an E_0 value of 0.2 eV for the Pm molecule.[124] As described earlier, in the absence of a vibrational assignment of the origin transition, there is no *a priori* assurance that EA_0 values are equal to EA_a values. Often, in fact, they are not due to a lack of Franck–Condon overlap between the lowest vibrational levels of the anion and its neutral counterpart. Nevertheless, the 0.2 eV value agreed well with the earlier electron transmission spectroscopy (ETS) measurement of $EA_v = 0.25$ eV. (Technically, ETS provides EA_v values.) The value of EA_a only equals the value of EA_v when the structures of the anion and its neutral counterpart are similar. As noted in previous studies, however, this is the case for pyrimidine and the other diazines studied here. Thus, the implication is that the measured E_0 values of $Pm^- \cdot (H_2O)_n$ spectra were close to EA_a values. The structural similarity between these anions and their neutral counterparts is the reason that both $E_0 \sim EA_a$ and $EA_a \sim EA_v$. Nevertheless, the anion and corresponding neutral structures are not identical, since if they were the observed photoelectron spectral bands would be quite narrow, not broadened, as in fact they are. Similar extrapolations of experimental E_0 values for the $Pd \cdot (H_2O)_n$, $Pz \cdot (H_2O)_n$, and $Py \cdot (H_2O)_n$ cluster

anion series gave E_0 values at $n = 0$ of ~0.0 eV, –0.1 eV, and –0.5 eV respectively. The E_0 value of 0.5 eV for the pyridine molecule is comparable to the previously measured ETS value of $EA_v = 0.67$ eV for pyridine.[81]
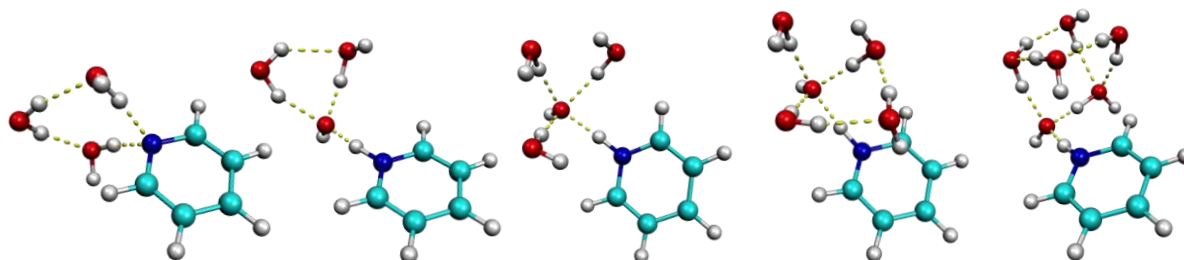
Figure 5. From left to right: Low-energy structures for Py⁻·(H₂O)₃, [PyH·OH]⁻·(H₂O)₂, [PyH·OH]⁻·(H₂O)₃, [PyH·OH]⁻·(H₂O)₄, and [PyH·OH]⁻·(H₂O)₅.

Electron induced proton transfer

The work presented here continues a line of work that focuses on electron-induced proton-transfer (EIPT) in the electronic ground state.[32,37,127-141] Among these are the thymine–glycine dimeric anion complex, (TG), where the excess electron first goes to the thymine base. This then enables the extraction of a proton from the glycine, resulting in a complex composed of a ''thymine hydride'' and a deprotonated glycine.[32] Another example of EIPT involves the ammonia–hydrogen chloride dimeric anion complex, [NH₃·(HCl)]⁻. In this case, the excess electron first goes to the ammonia side of the linear, high dipole moment ammonia–hydrogen chloride dimeric (neutral) complex, leading to the formation of a temporary dipole bound anion. The additional negative charge, associated with the ammonia molecule, then helps to pull the proton from the HCl and onto ammonia, which in turn becomes NH₄⁺, albeit with the diffuse excess electron still nearby. These latter two entities then form the neutral Rydberg molecule, NH₄. Thus, the formal nature of the ammonium chloride molecular anion is a neutral

NH$_4$ Rydberg molecule interacting with a Cl$^-$ anion, which in turn polarizes the NH$_4$, *viz*., NH$_4\cdots$Cl$^-$.[128] Yet another example of EIPT may be the hydrated electron itself, although unlike those mentioned above, this one may be hypothetical. While the cavity model is the generally accepted picture of the hydrated electron, an alternative model was espoused by Robinson *et al*.[170] and then studied theoretically by Domcke *et al*.[171,172] In that model, an excess electron induces a water molecule, which resides in a sea of other water molecules, to donate a proton to a neighboring water molecule, thereby forming H$_3$O$^+$, with the excess electron nearby. Together, the latter two entities are envisioned as forming the H$_3$O Rydberg molecule. Since an OH$^-$ anion was also formed in the deprotonation step, the net outcome is the hydrated radical–anion complex, (H$_3$O$\cdots$OH$^-$)$_{aq}$. Unlike the other examples mentioned above, however, this species has not been demonstrated experimentally. Perhaps, this is a higher energy isomer of the hydrated electron. In all of these examples, the lowest EBE photodetached electron would be expected to originate from the net neutral ''base hydride'', *i.e*., ''thymine hydride'', NH$_4$, or H$_3$O, rather than from the deprotonated ''acid'', *i.e*., deprotonated glycine, Cl$^-$, or OH$^-$.

The present study differs from our previous work with EIPT in that here, water is the proton donor. Proton transfer by water is facilitated by the fact that, while neutral N-heterocyclic molecules are themselves bases, negatively-charged N-heterocyclic molecules are even better bases (proton acceptors). Of the hydrated azabenzene anions studied here, pyridine is the most prone to accept a proton from water, because pyridine has the most negative value of EA$_v$, the pyridine anion is the best Lewis base among them. As in other EIPT examples discussed above, the excess electron goes first to the base, after which proton transfer from the ''acid'' occurs. Thus, we believe that proton transfer from water occurred only after the solvated pyridine anion had formed at $n = 3$. For the four non-pyridine, hydrated azabenzene cluster anions studied here, notice that the VDE values for their threshold cluster anion sizes

are all significantly smaller than the VDE value of $Py^-(H_2O)_3$. Once enough water is present to initiate proton transfer, the resulting cluster anion is greatly stabilized compared to the stabilization afforded by simple solvation. A relatively high VDE value at a given cluster anion's threshold size is a signature of proton transfer having occurred. In fact, in photoelectron work on 7 – azaindole – water cluster anions by Nakajima *et al.*,[122] where the VDE value was found to be ~1.3 eV at the $n = 3$ threshold size, this was likely an unrecognized indication that electron induced proton transfer had occurred.

Cover of PCCP for the 18th volume in the Jan. 14th issue.

PCCP

Physical Chemistry Chemical Physics

ROYAL SOCIETY
OF CHEMISTRY
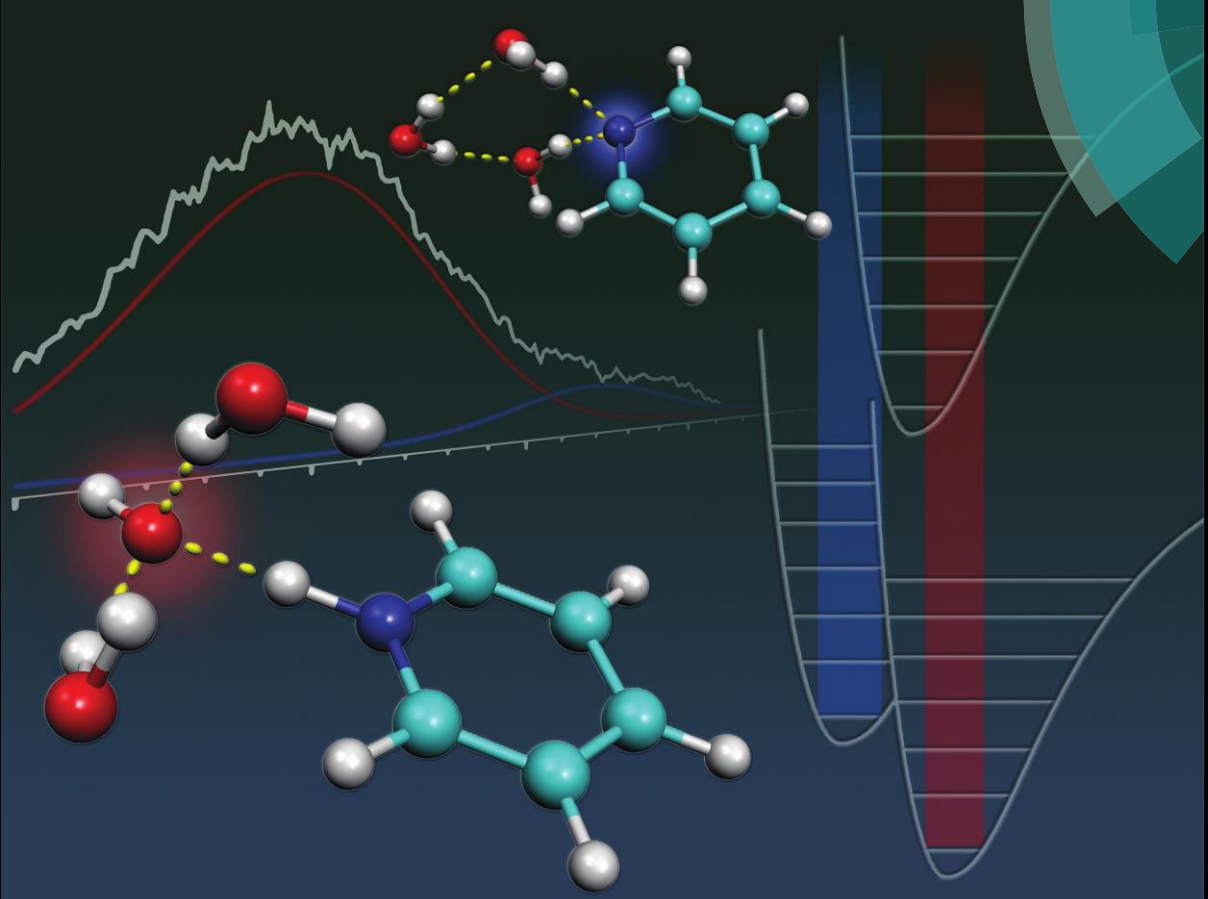
175 YEARS

CHAPTER 7

COMPETITION BETWEEN HYDROPHOLIC AND ARGYROPHILIC INTERACTIONS
IN SURFACE ENHANCED RAMAN SPECTROSCOPY

Abstract

The competition for binding and charge-transfer (CT) from the nitrogen containing heterocycle

pyrimidine to either silver or to water in surface enhanced Raman spectroscopy (SERS) is

discussed. The correlation between the shifting observed for vibrational normal modes and CT

is analyzed both experimentally using Raman spectroscopy and theoretically using electronic

structure theory. Discrete features in the Raman spectrum correspond to the binding of either

water or silver to each of pyrimidine's nitrogen atoms with comparable frequency shifts.

Natural bond orbital (NBO) calculations in each chemical environment reveals that the

magnitude of charge transfer from pyrimidine to adjacent silver atoms is only about twice that

for water alone. These results suggest that the choice of solvent plays a role in determining the

vibrational frequencies of nitrogen containing molecules in SERS experiments.

Introduction

Although the exact mechanism is not fully understood, Fleischmann *et al*. made a lasting impression in the scientific community with the spectroscopic observation of "physisorbed" pyridine on a silver surface nearly half of a century ago.[75] Today, surface- enhanced Raman spectroscopy (SERS) is employed in a wide range of applications to characterize both inter- and intramolecular interactions.[173-181] Many biologically relevant molecules have weak Raman scattering and/or exhibit problematic fluorescence, making structural assignment difficult.[182] SERS helps facilitate the detection and analysis of such molecules by increasing the scattering intensity on the order of 10^6 times[183-186] and this enhancement makes SERS a powerful analytical technique. Despite all of the progress, the contributions from electromagnetic (EM) and charge-transfer (CT) enhancements to the SERS effect continues to be debated.[184,187-190]

The nitrogen containing heterocycle pyridine is probably the most studied SERS active molecule, and its vibrational spectrum is still examined today both experimentally and theoretically in efforts to better understand the fundamental molecular interactions that give rise to this nascent enhancement.[191-195] Here, in order to study the interactions of a nitrogen containing heterocycle with silver and water we choose to study the two nitrogen atom analogue pyrimidine. Pyrimidine is a more biologically relevant building block and offers two binding sites to silver and water. Previously, we employed a combination of Raman spectroscopy and the results of electronic structure calculations to show that partial CT from pyrimidine to extended hydrogen bonded solvent networks resulted in blue-shifted Raman peaks in pyrimidine,[96,101,103] where blue- and red-shifted modes are those that either increase or decrease in energy, respectively. In those studies, we considered over 100 micro-solvated molecular clusters and eight different solvent molecules and showed a direct correlation between the magnitude of charge transfer and the resulting frequency shifts. Such shifts are common in SERS spectra and also likely originate from partial charge-transfer.[196-198]

Centano et al. previously investigated the SERS spectra of nitrogen containing heterocycles including pyrimidine in aqueous solutions.[199,200] These authors noted shifts in the Raman spectra of the nitrogen containing heterocycles in these solutions and compared their experimental results to the results of electronic structure calculations. They focused their analysis on the interactions between the metal and the absorbate and quantified the SERS enhancements. Here, in order to separate the contributions of CT from pyrimidine to silver and pyrimidine to the hydrogen bonded water network, we compare the Raman spectra of solvated pyrimidine (Pm/H2O) to the SERS spectra of both neat pyrimidine on silver substrate (Pm/Ag) and pyrimidine on silver substrate in the presence of water (Pm/H2O/Ag), both experimentally and theoretically. We also compare these results to our earlier studies.

Figure 1 compares the experimental Raman spectra of a (a) 1 M pyrimidine/water mixture with that of (b) pure pyrimidine as well as the SERS spectra of a (c) 1 M pyrimidine/water mixture on a silver island film with that of (d) pure pyrimidine on a silver island film. Water's bending and stretching modes are apparent in the aqueous pyrimidine/water mixture in Fig. 1(a). Details of the experimental techniques are included in the Supporting Information. Certain vibrational normal modes of pyrimidine are observed to either blue shift (shift to higher energy) or red shift (shift to lower energy) in the presence of water, by up to 14 cm^{-1}. Similar shifts are observed in the SERS spectra of both pyrimidine and the pyrimidine/water mixture when absorbed to a silver substrate. These vibrational energy level shifts are tabulated in Table 1. In our earlier works we analyzed our experimental results with the use of natural bond orbital (NBO) analyses and attributed this blue shifting to result from electron density transfer from pyrimidine's lone pairs to the hydrogen-bonded network.[101,103] Here, we apply this same computational approach to study interactions with the silver substrate.
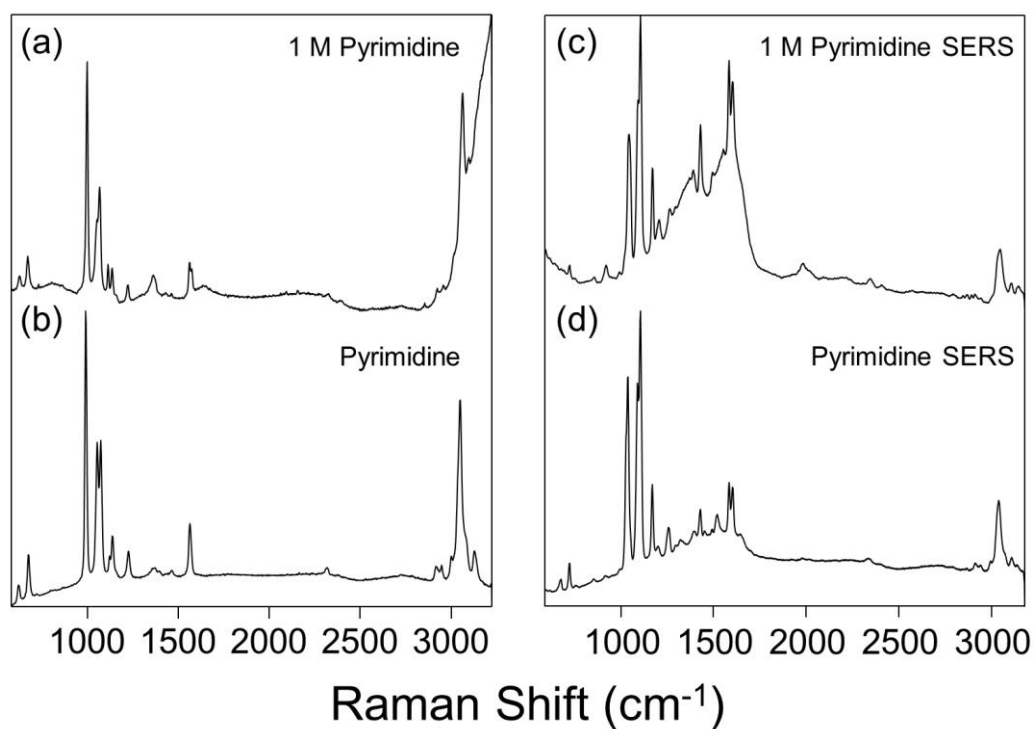
Figure 1. Raman spectra of (a) a 1M aqueous pyrimidine solution, (b) neat pyrimidine and SERS spectra of (c) a 1M aqueous pyrimidine solution and (d) neat pyrimidine.

Symmetry	mode	Pm ν	Pm/H$_2$O $\Delta\nu$	Pm/Ag $\Delta\nu$	Pm/H$_2$O/Ag $\Delta\nu$
A$_1$	ν_{6a}	681	+5	+3	---
	ν_1	990	+14	+13/+25	+14
	ν_{9a}	1139	+5	-1	+1
	ν_{8a}	1564	+6	-4	-4
B$_2$	ν_3	1228	+3	+6	+5
	ν_{8b}	1571	+12	+7/+11	+9

Table 1. Normal modes, symmetries, and shifts ($\Delta\nu$, in cm^{-1}) of pyrimidine (Pm) in the presence of water (Pm/H2O), silver (Pm/Ag), and water and silver (Pm/H2O/Ag).

Both Raman and SERS spectra of pyrimidine include a prominent feature at 990 cm^{-1} (ν_1), which is pyrimidine's ring breathing mode. This mode is common to all benzene-like molecules and exhibits the largest change in polarizability upon excitation and therefore the largest Raman cross-section. A high-resolution comparison of this region is shown in Figure

2. We,[101,103] and others,[201-203] previously showed in the cases of pyrimidine interacting with water, methanol, and ethylene glycol, that the features labeled here by α, β, and γ originate from interactions with 0, 1, and 2 hydrogen bonded groups, respectively. In the cases with water, these features are broader due to the many possible hydrogen-bonded geometries. With methanol, however, these features are more distinct and similar to the case of Figure 2(c), suggesting that, in addition to free pyrimidine molecules (α), pyrimidine molecules also exhibit interactions with silver by both one (β) or both nitrogen atoms (γ). The differences in the ratios of α, β, and γ between Figures 2(c) and 2(d) suggest that both water and silver are interacting with pyrimidine.

Also in this region, centered at 1060 cm^{-1}, are two peaks that are equal in intensity in the Raman spectrum of pure pyrimidine. This feature has been assigned by different authors as a Fermi resonance (FR) including ν_{12} and a combination band, most usually $\nu_{10b} + \nu_{16b}$, although the actual assignment is still debated in the literature. We previously showed that ν_{16b} (centered at 351 cm^{-1} in pure pyrimidine) exhibits a shift of +2 cm^{-1} in the presence of water. Interestingly, in the cases of pyrimidine interacting with water, silver, and silver and water together, these peaks get closer together and their relative intensities changes, indicating that the overlap in the energies of these modes is no longer favorable.

Figure 3 shows higher resolution spectra of the symmetric and asymmetric ring-stretching modes of pyrimidine ν_{8a} and ν_{8b}, respectively, near 1560 cm^{-1}. In the SERS spectra of pyrimidine, there is also a substantial enhancement of these features. This is especially true in aqueous solution as shown in Figure 1(c). As in the case of ν_1, multiple spectral components are apparent in ν_{8b} when pyrimidine interacts with silver, suggesting that binding by silver to either one or two nitrogen atoms yields different vibrational energy shifts. However, it is also apparent from the smaller blue shift in Figure 3(d) that water effectively competes with silver for binding with pyrimidine.
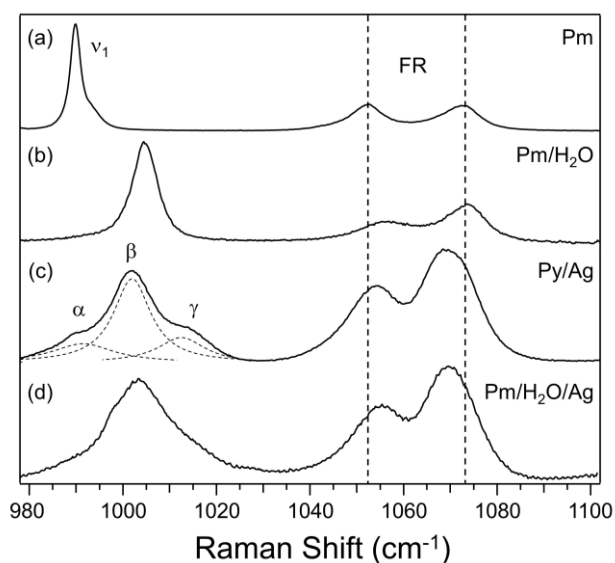
Figure 2. Higher resolution Raman and SERS spectra of pyrimidine and aqueous pyrimidine solutions in the region of pyrimidine's ring breathing mode ν1 and Fermi resonance (FR). Peaks labeled by α, β, and γ indicate 0, 1, or 2, respectively, interactions with silver and the Lorentzian fits in (c) indicate contributions from three distinct binding motifs.
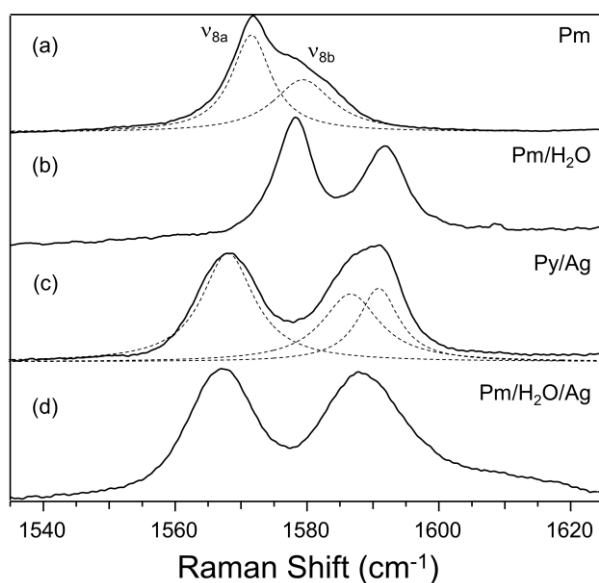
Figure 3. Higher resolution Raman and SERS spectra of pyrimidine and aqueous pyrimidine solutions showing the symmetric and asymmetric ring- stretching modes ν8a and ν8b, respectively.

Centeno *et al*. previously suggested that the increase in Raman activity of ν8a and ν8b has its origins in resonance Raman effects, Herzberg-Teller intensity borrowing, and Frank-Condon factor enhancements.[204] It is important to point out that this effect is much more

pronounced in the presence of water, suggesting that the solvent is playing an important role in this enhancement.

A number of different electronic structure approaches have been reported in the literature for the description of silver clusters. Harmonic vibrational frequencies have been computed using a variety of Density Functional Theory (DFT) methods[205,206] with different basis sets. Here, Becke's 3-parameter exchange functional with the Lee-Yang-Parr correlation [92-94,207] is employed with several basis sets in an attempt to accurately describe charge-transfer between silver clusters, solute, and water. Full geometry optimizations and frequency analyses were performed using the B3LYP hybrid density functional along with suitable triple-ζ quality basis sets and the Gaussian09 software package.[144] For comparison, calculations were also performed using the M06-2X and M06-L functionals and results are included in the supporting information. Figure 4 shows optimized molecule cluster geometries for pyrimidine interacting with water, Ag2, or water and Ag2. Although the number of silver atoms for a given nanocluster is known to affect the structure and resulting vibrational frequencies in nitrogen containing molecules, Schatz showed that this variation is relatively small and also depends on the placement of the silver atoms.[208] Here we explore the interactions between pyrimidine and silver using Ag_2 because the deviation expected from choice of the number of silver atoms is less than the absolute error expected from the choice of the level of theory and this selection allows a convenient comparison with interactions with water.
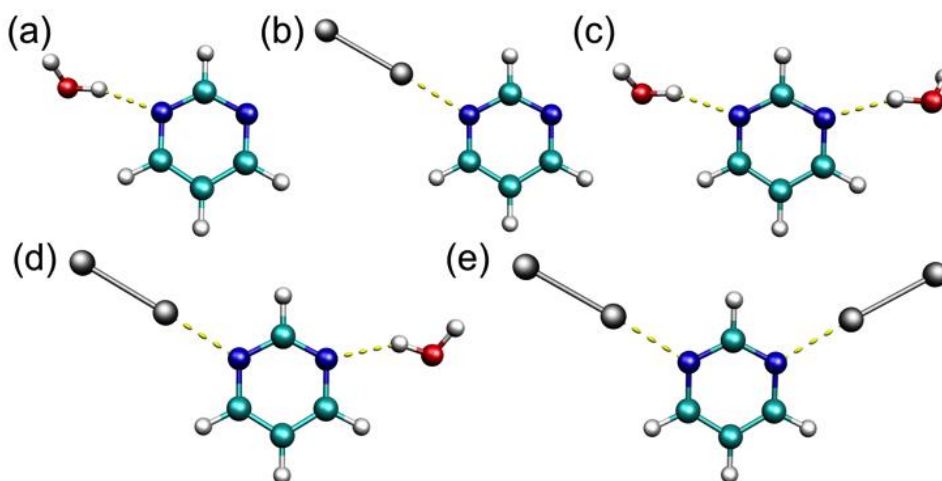
Figure 4. Optimized minimum energy geometries of (1) pyrimidine hydrogen bonded to one water molecule, (b) pyrimidine interacting with a silver dimer, (c) pyrimidine hydrogen bonded to two water molecules, (d) pyrimidine interacting with both a silver dimer and a water molecule, and (e) pyrimidine interacting with two silver dimers

We previously showed that symmetrically-solvated pyrimidine clusters reproduced experimental shifts in the cases of water, methanol, and other hydrogen- bonded solvents.[196-198] In each of these cases, these hydrogen-bonded complexes, including the structure shown in Figure 4(c), are energetically more stable than the individual monomers. This interaction energy is computed to be 10.6 kcal mol^{-1} at the B3LYP/aug–cc–pVTZ level of theory. In the case of silver binding to both nitrogen atoms as in Figure 4(c), this energy is 20.18 kcal mol^{-1}, roughly twice that of water.

Tables 2 and 3 compare the observed Raman shifts upon hydration and interactions with silver with computed harmonic vibrational frequencies using the structures in Figure 3(b), 3(c), and 3(d). Although a number of basis sets were employed here for comparison using the density functional method B3LYP, the Dunning correlation consistent aug-cc- pVTZ basis set with a pseudopotential for silver atoms exhibited the best agreement with experimental results. This basis set is also expected to yield the most reproducible results. Results with other basis sets are included in the Supporting Information. The agreement between theory and experiment

in the case of pyrimidine interacting with silver is very good. This is especially true of the in the case of the spectral features β and γ in Figure 2 (c), which are experimentally +13 and +25 cm^{-1}, respectively. These agree very well with the computed values of +13 and +22 cm^{-1} for binding by silver to either one or both of pyrimidine's nitrogen atoms.

Mode		Pm/H$_2$O	Pm·H$_2$O	H$_2$O·Pm·H$_2$O
A$_1$	ν_{6a}	+5	+4	+7
	ν_1	+14	+8	+15
	ν_{9a}	+5	+2	+4
	ν_{8a}	+6	-1	+3
B$_2$	ν_3	+3	+4	+9
	ν_{8b}	+12	+9	+11

Table 2. Comparison of the experimental (Pm/H$_2$O) and the computed (Pm·H$_2$O and H$_2$O·Pm·H$_2$O) vibrational energy shifts (in cm^{-1}) of certain normal modes of pyrimidine when interacting with water using the B3LYP method and the aug-cc-pVTZ basis set.

Mode		Pm/Ag	Pm·Ag$_2$	Ag$_2$·Pm·Ag$_2$	Pm/H$_2$O/Ag	H$_2$O·Pm·Ag$_2$
A$_1$	ν_{6a}	+3	+2	-4	-	+4
	ν_1	+13/+25	+13	+22	+13	+19
	ν_{9a}	-1	-1	-6	+1	+2
	ν_{8a}	-4	-4	+5	-4	-1
B$_2$	ν_3	+6	+4	+15	+5	+9
	ν_{8b}	+7/+11	+14	+20	+9	+15

Table 3. Comparison of the experimental (Pm/Ag and Pm/H$_2$O/Ag) and the computed (Pm·Ag$_2$, Ag$_2$·Pm·Ag$_2$, and H$_2$O·Pm·Ag$_2$) vibrational energy shifts (in cm-1) of certain normal modes of pyrimidine when interacting with silver and water and silver using the B3LYP method and the aug-cc-pVTZ basis set.

The NBO results shown in Table 3 suggest partial electron transfer from the pyrimidine to both adjacent water molecules and the silver island films.[209] This CT is the origin of the spectral blue shifts in a number of normal modes in pyrimidine. The analysis of these results quantifies for the first time the magnitude at which partial charge transfer plays a role in this

widely applied technique in competition with the solvent, in this case water. Although charge transfer to silver dominates, consideration of the solvent, especially water, should not be neglected. Over 10% of the charge transfer is redistributed to the water network when both silver and water are interacting at the same time with pyrimidine.

In summary, we demonstrate that the interactions of the nitrogen containing building block pyrimidine with either silver or water are remarkably similar in terms of blue-shifted vibrational frequencies and partial CT. We also demonstrate that the agreement between experiment and theory is very good in these systems. Although the binding of pyrimidine to silver is preferential to that with water, binding with water still competes as evidenced by differences in the SERS spectra of $\nu 1$ and pyrimidine's Fermi resonance. Over 10% of charge transfer from the pyrimidine molecule has been shown by NBO analyses to localize around the solvent, and not silver, when both are present. Together, these results suggest that interactions with both silver and water account for the spectral features observed experimentally in SERS experiments and that the choice of solvent in SERS likely plays an important role in the observed vibrational spectra of nitrogen containing heterocyclic molecules.

CHAPTER 8

FUNDAMENTAL DIFFERENCES OF CARBON FIXATION ON HALIDE AND PSEUDOHALIDE SPECIES: X– + CO_2 → $[XCO_2]^-$ FOR X = F, CN

Abstract

The purpose of this work is to shine new light on the anharmonic effects of CO_2 fixation on the elusive fluorocarbonate and cyanoformate ion complexes with *ab initio* methods. Previously, Murphy *et al*. established a quantum mechanical comparison between the $[FCO_2]^-$ and $[NCCO_2]^-$ by electronic structure theory [*Science* **2014** *344* (6179) 75-78]. Here, we perform second-order vibrational perturbation theory (VPT2) to obtain anharmonic corrections on closed-shell systems by the coupled-cluster singles and doubles method with perturbative connected triples, CCSD(T).

Introduction

Noncovalent interactions between atmospheric gases and the "naked" fluoride ion have shown to exhibit partial or full coordinate-covalent bonding. The fluorocarbonate, $[FCO_2]^-$, was unveiled in 1972 by Spears in attempt to compare alkali and halide ions bonding energies and entropies of association with atmospheric gases (i.e. O_2, N_2, and CO_2). Halogen anion solvation by a carbon dioxide molecule, $X^-(CO_2)$ where X=F, Cl, Br, and I, was interrogated by negative ion spectroscopy ultimately confirming the formation of a weak C–F chemical bond. This anomaly is not featured in the spectra $Cl^-(CO_2)$, $Br^-(CO_2)$, or $I^-(CO_2)$ cluster anions. There has been interest in the scientific community regarding the parallel dynamics between the halide-CO_2 fluorocarbonate ion and pseudohalide-CO_2 cyanoformate ion: $[FCO_2]^-$ and $[NCCO_2]^-$ respectively.

Early spectroscopic investigations detected the transient CO_2^- radical anion in rare gas matrices but more recent studies have shown cluster anions that include CO_2 coordinate covalent bonds. Kim and coworkers identified this feature by negative ion photoelectron spectroscopy in the co-expansion of CO_2, argon, and pyridine vapor forming $[C_5H_5N - CO_2]^-$. Analogous nitrogen containing heterocycles (pyrazine, pyrimidine, pyridazine and *s*-triazine) cluster anions exhibited similar bond formation. The simplest analogue of the azabenzene molecular anions is cyanide (CN^-), which has also been shown to exhibit bond formation, but not $C - N$ bonding like the aromatic counterpart. The products of this interaction is either a (1) non-covalent bonded $CN^- \cdots CO_2$ cluster anion or (2) coordinated covalently bonded $[NCCO_2]^-$ much like the molecular ion analogue, $[FCO_2]^-$.

In this work, we compare the coordination of the covalently bonded CO_2 to a fluorine ion (F^-) to that of the cyanide radial anion (CN^-) with coupled-cluster methods. Computed anharmonic frequencies are also compared to experimental values and the associative reaction

coordinate between the ion and CO_2 molecule with respect to the CO_2 bond angle is theoretically modeled.

Theoretical Methods

By employing *ab initio* methods in the CFOUR software suite, full geometry optimizations and harmonic vibrational frequencies were computed with correlation consistent basis sets (aug-cc-pVXZ where X = D, T, and Q). All closed shell systems that were considered utilized the coupled-cluster method, CCSD(T) for all computations including anharmonic corrections by using the second-order perturbation theory (VPT2). All calculations were performed using pure angular momentum functions ($5d$, $7f$, $9g$) rather than Cartesian counterparts ($6d$, $10f$, $15g$) under the "frozen core" approximation. Gaussian09 was employed for single-point energy to generate scans of the potential energy surface.
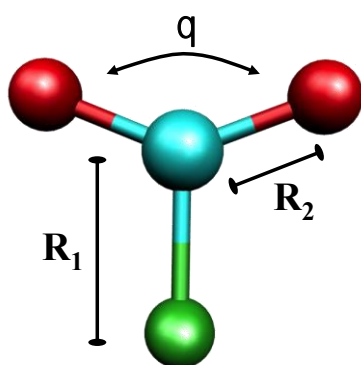
Figure 1. Minimum energy structures for the FCO_2^- molecular anion with C_{2v} symmetry with parameters R_1 (C – F bond length), R_2 (C – O bond length), and θ (O – C – O bond angle).

C_{2v}	mode	Ault	Zhang	Nguyen	This work
A_1	n_1	1316	1275	1339	1253
A_1	n_2		752	816	743
A_1	n_3	883	570	625	551
B_1	n_4		795	838	806
B_2	n_5	1749	1798	1860	1804
B_2	n_6		610	587	560

Table 1. Comparison of previous experimental and theoretical values to our results (CCSD(T) / aug-cc-pVXZ) of the vibrational frequencies for FCO_2^- cluster anion with C_{2v} symmetry.

Results and Discussion

The noncovalent coordination of the fluorine ion (F^-) and a carbon dioxide molecule (CO_2) results in the formation of a covalent bond creating a fluorocarbonate molecular anion (FCO_2^-). High level ab initio computations shed new light on the spectroscopic investigation of carbon fixation by small molecular anions. In 2000, Kim and coworkers reported negative ion photoelectron spectra of mixed pyridine:CO_2 cluster anions along with computed vertical detachment energies. A Photodissociation spectrum was later reported and verified the covalent nature of the $PyCO_2^-$ interaction and extending the study to n number of solvating CO_2 molecules for $PyCO_2^-(CO_2)_n$. Several other spectroscopic and computational studies have looked at this phenomenon regarding covalent bond formation to cluster anions including other nitrogen containing heterocycles. Coupled-cluster methods on systems this large are not feasible, however reducing the size of the ionic complex allows for a higher level of theoretical treatments.

FCO_2^- energetics and vibrational frequencies

A single stationary point for the fluorocarbonate anion was found at the current level of theory. The previously determined point group was conserved in geometry optimization and frequency analysis at all levels of theory. Figure 1 shows the geometric variables we are

concerned with in this study and the computed. Harmonic vibrational frequencies were computer at the CCSD(T)/aug-cc-pVXZ (where X = D, T, and Q) for the fluorocarbonate anion (FCO_2^-) and was VPT2 anharmonic contributions were considered in comparison to infrared spectra.

Ault reported the first experimental spectrum of the fluorocarbonate or "fluoroformate" anion in 1981 in argon matrices along with isotopologues spectra preluded only by an ion cyclotron resonance spectrometric study. The C–F stretching mode, ν_3, was reassigned by Zhang *et al.* to a much lower frequency, supporting the evidence of a longer bond. These authors also comment on the large difference between the symmetric and asymmetric CO_2 stretching modes (ν_1 and ν_5) as a results of the large bond angle. Early *ab initio* approaches were performed to compute harmonic vibrational frequencies and "stabilization energies" on geometrically optimized structures for the HCO_2^- and FCO_2^- molecular anions. Table 1 is a survey of values found in the literature compared to our coupled-cluster values for vibrational frequencies that include anharmonic contribution of the FCO_2^- molecular anion. McMahon and Northcott report the fluoride affinity of CO_2 to be 33 kcal mol^{-1}, Larson and McMahom report the bond dissociation to be 31.7 ± 0.2 kcal mol^{-1}, and we compute the dissociation energy to be 32.7 kcal mol^{-1} at the CCSD(T)/aug-cc-pVQZ level of theory.

There is minimal dissimilarity between the previously reported experimental vibrational frequencies of the FCO_2^- molecular anion and our computed coupled-cluster values corrected for anharmonicity. Artificial symmetry lowering of the solid argon matrix may be a source of the minor differences between experiment and theory. Our assignment of the C – F stretching mode, ν_3, is in disagreement with the previously reported value provided by Ault, but supports the assignment provided by Zhang *et al.* Select combination band and overtone frequencies can be found in the Supporting Information (SI). The computed coupled-cluster vibrational frequencies for the FCO_2^- molecular anion is in good agreement with experimental

results and this theoretical approach can be extended to the CO_2 adducting pseudohalide analogue, $NCCO_2^-$.

[NCCO2]$^-$ and [CN·CO2]$^-$ energetics and vibrational frequencies

The cyanide anion is a member of an exclusive class of small molecules called *pseudohalides* for being closed shell ions with high electron binding energies (eBE). The sequential addition of CO_2 molecules on small ionic species is known to increase the eBE as an inherent solvation effect, however Weber and Bowen point out that two moieties are manifested with the addition of a single CO_2 molecule: chemisorption and physisorption. In the case of the cyanide, two isomeric structures were found to be minima, each exhibiting one of the two possible moieties as seen in Figure 2.
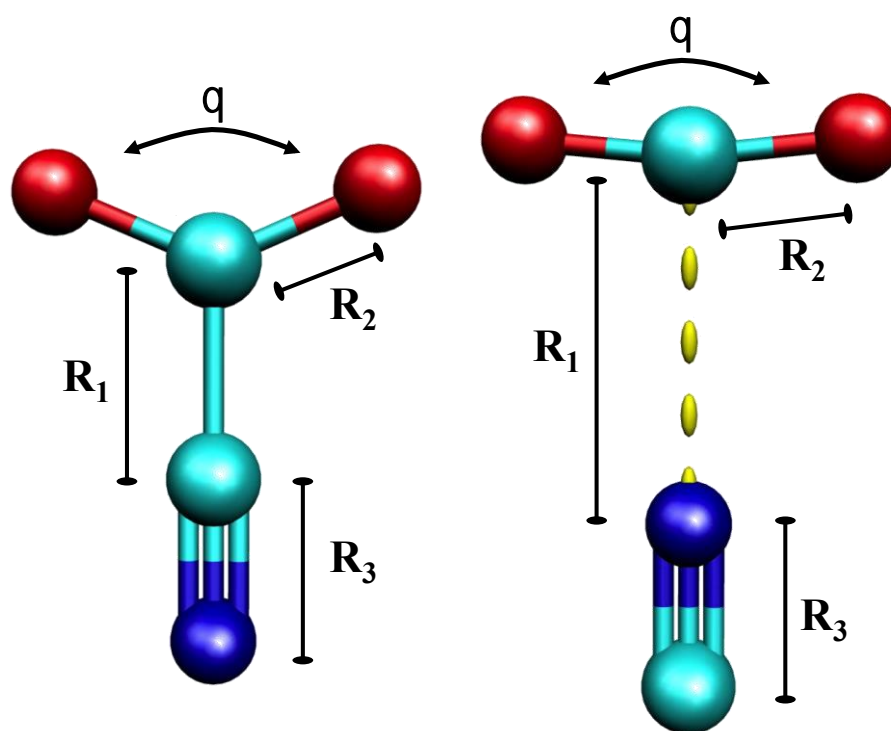
Figure 2. Minimum energy structures for the $NCCO_2^-$ and $CN·CO_2^-$ cluster anions with C_{2v} symmetry with parameters R_1 (C − F bond length), R_2 (C − O bond length), R_3 (C − N bond length), and θ(O − C − O bond angle).

Earlier spectroscopic studies have interrogated the photofragmentation pathway of $ICN^-(CO_2)_n$ cluster anions finding the major photoproduct to be either $NCCO_2^-$ and $CN·CO_2^-$

where $n \leq 2$. These authors employed density functional theory to identify the same minimum energy structures we present in this work. We apply the same coupled- cluster approach to the $NCCO_2^-$ molecular anion and $CN \cdot CO_2^-$ cluster anion, including geometry optimizations and frequency analysis correcting for anharmonicity. Though the infrared spectra of the $NCCO_2^-$ molecular anion and $CN \cdot CO_2^-$ cluster anion has yet to be acquired, our results compare well with previously reported experimental values of the $NCCO_2^-$ from reacting $[PPh_4]CN$ with carbon dioxide (tetraphenylphosphonium salt).

Potential energy surfaces: $[NCCO_2]^-$ vs. $[FCO_2]^-$

The nonlinear $O - C - O$ bond angle is inherent upon addition of an excess electron to the triatomic species, however this characteristic is also observed in when partial electron density is shared with the CO_2 molecule. With regards to the XCO_2^- potential energy surfaces where X = F or CN, the bond angle of the CO_2 molecule is dictated by the coordination with the negatively charged ion. Figure 3 illustrates that nonlinear dependency of $O - C - O$ bond angle as a function of distance from the fluoride anion. An important qualitative interpretation

is the dissociation energy of the molecular anion increase as the bond angle of the CO_2 molecule decreases and as the distance to the F^- ion decrease.

Figure 3. Quantum mechanically computed potential energy scans of the FCO_2^- molecular anion with respect to FC bond length (R_1) and CO_2 bond angle (θ).
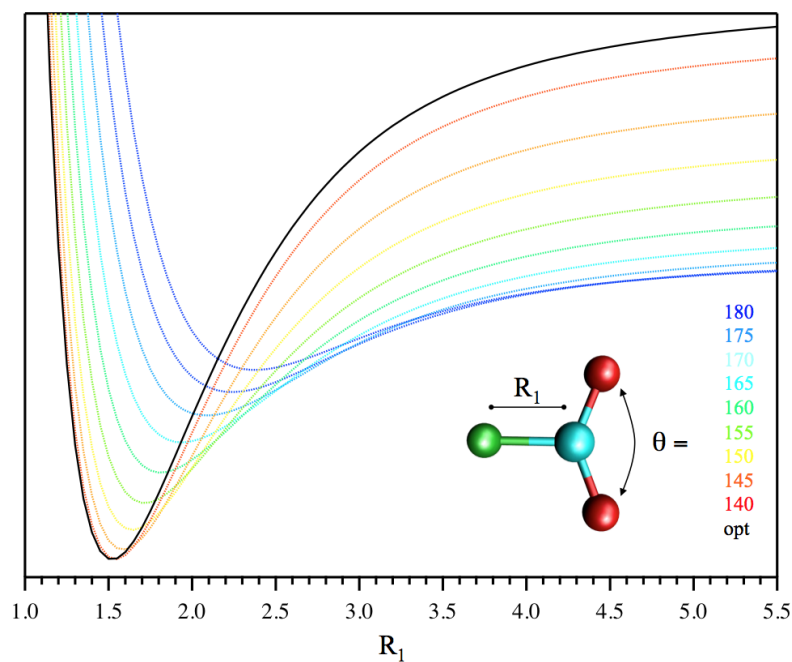
Conclusion

Although agreement between experimental spectra and our theoretical predictions is very good, infrared spectroscopic studies of messenger-tagged, mass-selected FCO_2^- and $NCCO_2^-$ cluster anions would provide much insight into the structural motifs of the anion clusters present in the experiment.

CHAPTER 9

CONCLUSION

The work presented in this dissertation has shed new light on charge accommodation in biologically relevant building blocks. Our collaborative efforts have established the solvation effects that noncovalent interactions have on the systems that were studied. The agreement between photoelectron spectroscopic results and computed electronic transitions between negative ions and the corresponding neutral ground state has elucidated the magnitude of charge accommodation in the azabenzene series. The experimental design of a Wiley-McLaren time-of-flight mass spectrometer has been modified and calibrated for water molecular clusters with an excess electron, negative CO_2 cluster anions, hydrated pyrimidine cluster anions, as well as messenger gas tagging. A tunable infrared light source (OPO/A, *LaserVision*) was also calibrated from 2400 to 4600 cm^{-1} for the BH, CH, NH and OH stretching regions so that future studies can probe mass-selected ions with tunable IR radiation. This experiment collected the first gas phase IR spectrum of the water hexamer cluster anion, $(H_2O)_6^-$, in 2013.

BIBLIOGRAPHY

1. Bailey, C. G. and M. A. Johnson (1997): "Determination of the relative photodetachment cross sections of the two isomers of (H 2 O) 6− using saturated photodetachment." *Chemical physics letters* **265** (1): 185-189.

2. Bailey, C. G., J. Kim and M. A. Johnson (1996): "Infrared Spectroscopy of the Hydrated Electron Clusters (H2O) n-, n= 6, 7: Evidence for Hydrogen Bonding to the Excess Electron." *The Journal of Physical Chemistry* **100** (42): 16782-16785.

3. Campagnola, P. J., D. J. Lavrich, M. J. DeLuca and M. A. Johnson (1991): "Photodestruction spectra of the anionic water clusters,(H2O)− n, n= 18 and 30: Absorption to the red of e− aq." *The Journal of Chemical Physics* **94** (7): 5240-5242.

4. Coe, J., G. Lee, J. Eaton, S. Arnold, H. Sarkas, K. Bowen, C. Ludewigt, H. Haberland and D. Worsnop (1990): "Photoelectron spectroscopy of hydrated electron cluster anions,(H2O)- n= 2-69." *The Journal of Chemical Physics* **92**: 3980-3982.

5. Haberland, H., C. Ludewigt, H. G. Schindler and D. R. Worsnop (1984): "Experimental observation of the negatively charged water dimer and other small (H2O)− n clusters." *The Journal of Chemical Physics* **81** (8): 3742-3744.

6. Hammer, N. I., J.-W. Shin, J. M. Headrick, E. G. Diken, J. R. Roscioli, G. H. Weddle and M. A. Johnson (2004): "How do small water clusters bind an excess electron?" *Science* **306** (5696): 675-679.

7. Kim, J., I. Becker, O. Cheshnovsky and M. A. Johnson (1998): "Photoelectron spectroscopy of themissing'hydrated electron clusters (H 2 O)− n, n= 3, 5, 8 and 9: Isomers and continuity with the dominant clusters n= 6, 7 and⩾ 11." *Chemical physics letters* **297** (1): 90-96.

8. Posey, L. A., P. J. Campagnola, M. A. Johnson, G. H. Lee, J. G. Eaton and K. H. Bowen (1989): "On the origin of the competition between photofragmentation and photodetachment in hydrated electron clusters,(H2O)− n." *The Journal of Chemical Physics* **91** (10): 6536-6538.

9. Shin, J.-W., N. Hammer, E. Diken, M. Johnson, R. Walters, T. Jaeger, M. Duncan, R. Christie and K. D. Jordan (2004): "Infrared Signature of Structures Associated with the H+ (H2O) n (n= 6 to 27) Clusters." *Science* **304** (5674): 1137-1140.

10. Douberly, G., R. Walters, J. Cui, K. D. Jordan and M. Duncan (2010): "Infrared Spectroscopy of Small Protonated Water Clusters, H+ (H2O) n (n= 2− 5): Isomers, Argon Tagging, and Deuteration." *The Journal of Physical Chemistry A* **114** (13): 4570-4579.

11. Fournier, J. A., C. J. Johnson, C. T. Wolke, G. H. Weddle, A. B. Wolk and M. A. Johnson (2014): "Vibrational spectral signature of the proton defect in the three-dimensional H+ (H2O) 21 cluster." *Science* **344** (6187): 1009-1012.

12. Fournier, J. A., C. T. Wolke, C. J. Johnson, M. A. Johnson, N. Heine, S. Gewinner, W. Schöllkopf, T. K. Esser, M. R. Fagiani and H. Knorke (2014): "Site-specific vibrational spectral signatures of water molecules in the magic H3O+ (H2O) 20 and Cs+ (H2O) 20 clusters." *Proceedings of the National Academy of Sciences* **111** (51): 18132-18137.

13. Headrick, J. M., E. G. Diken, R. S. Walters, N. I. Hammer, R. A. Christie, J. Cui, E. M. Myshakin, M. A. Duncan, M. A. Johnson and K. D. Jordan (2005): "Spectral signatures of hydrated proton vibrations in water clusters." *Science* **308** (5729): 1765-1769.

14. Heine, N., M. R. Fagiani and K. R. Asmis (2015): "Disentangling the Contribution of Multiple Isomers to the Infrared Spectrum of the Protonated Water Heptamer." *The journal of physical chemistry letters* **6** (12): 2298-2304.

15. Heine, N., M. R. Fagiani, M. Rossi, T. Wende, G. Berden, V. Blum and K. R. Asmis (2013): "Isomer-selective detection of hydrogen-bond vibrations in the protonated water hexamer." *Journal of the American Chemical Society* **135** (22): 8266-8273.

16. Lin, C.-K., C.-C. Wu, Y.-S. Wang, Y. T. Lee, H.-C. Chang, J.-L. Kuo and M. L. Klein (2005): "Vibrational predissociation spectra and hydrogen-bond topologies of H+(H 2 O) 9– 11." *Physical Chemistry Chemical Physics* **7** (5): 938-944.

17. Mizuse, K. and A. Fujii (2011): "Infrared photodissociation spectroscopy of H+(H 2 O) 6·
M m (M= Ne, Ar, Kr, Xe, H 2, N 2, and CH 4): messenger-dependent balance between H 3 O+
and H 5 O 2+ core isomers." *Physical Chemistry Chemical Physics* **13** (15): 7129-7135.

18. Mizuse, K. and A. Fujii (2013): "Infrared spectroscopy of large protonated water clusters
H+(H 2 O) 20–50 cooled by inert gas attachment." *Chemical Physics* **419**: 2-7.

19. Mizuse, K., N. Mikami and A. Fujii (2010): "Infrared Spectra and Hydrogen‐Bonded
Network Structures of Large Protonated Water Clusters H+ (H2O) n (n= 20‐200)."
Angewandte Chemie International Edition **49** (52): 10119-10122.

20. Zwier, T. S. (2004): "The structure of protonated water clusters." *Science* **304** (5674): 1119-
1120.

21. Corcelli, S., J. Kelley, J. Tully and M. Johnson (2002): "Infrared Characterization of the
Icosahedral Shell Closing in Cl-⊙ H2O⊙ Ar n (1≤ n≤ 13) Clusters." *The Journal of Physical
Chemistry A* **106** (19): 4872-4879.

22. Horvath, S., A. B. McCoy, J. R. Roscioli and M. A. Johnson (2008): "Vibrationally Induced
Proton Transfer in F−(H2O) and F−(D2O)." *The Journal of Physical Chemistry A* **112** (48):
12337-12344.

23. Odde, S., B. J. Mhin, S. Lee, H. M. Lee and K. S. Kim (2004): "Dissociation chemistry of
hydrogen halides in water." *The Journal of Chemical Physics* **120** (20): 9524-9535.

24. Pathak, A., T. Mukherjee and D. Maity (2008): "IR Spectra of Carbonate‐Water Clusters,
CO3−2 (H2O) n: A Theoretical Study." *Synthesis and Reactivity in Inorganic, Metal-Organic,
and Nano-Metal Chemistry* **38** (1): 76-83.

25. Robertson, W. H., E. G. Diken, E. A. Price, J.-W. Shin and M. A. Johnson (2003):
"Spectroscopic determination of the OH− solvation shell in the OH−·(H2O) n clusters."
Science **299** (5611): 1367-1372.

26. Robertson, W. H. and M. A. Johnson (2003): "Molecular aspects of halide ion hydration: The cluster approach." *Annual review of physical chemistry* **54** (1): 173-213.

27. Robertson, W. H., G. H. Weddle, J. A. Kelley and M. A. Johnson (2002): "Solvation of the Cl-⊙ H2O Complex in CCl4 Clusters: The Effect of Solvent-Mediated Charge Redistribution on the Ionic H-Bond." *The Journal of Physical Chemistry A* **106** (7): 1205-1209.

28. Roscioli, J. R., E. G. Diken, M. A. Johnson, S. Horvath and A. B. McCoy (2006): "Prying Apart a Water Molecule with Anionic H-Bonding: A Comparative Spectroscopic Study of the X-⊙ H2O (X= OH, O, F, Cl, and Br) Binary Complexes in the 600-3800 cm-1 Region." *The Journal of Physical Chemistry A* **110** (15): 4943-4952.

29. Szpunar, D. E., K. E. Kautzman, A. E. Faulhaber and D. M. Neumark (2006): "Photofragment coincidence imaging of small I-(H2O) n clusters excited to the charge-transfer-to-solvent state." *The Journal of Chemical Physics* **124** (5): 054318.

30. Weber, J. M., J. A. Kelley, W. H. Robertson and M. A. Johnson (2001): "Hydration of a structured excess charge distribution: Infrared spectroscopy of the O2−· (H2O) n,(1⩽ n⩽ 5) clusters." *The Journal of Chemical Physics* **114** (6): 2698-2706.

31. Woronowicz, E. A., W. H. Robertson, G. H. Weddle, M. A. Johnson, E. M. Myshakin and K. D. Jordan (2002): "Infrared Spectroscopic Characterization of the Symmetrical Hydration Motif in the⊙ H2O Complex." *The Journal of Physical Chemistry A* **106** (31): 7086-7089.

32. Dąbkowska, I., J. Rak, M. Gutowski, J. M. Nilles, S. T. Stokes, D. Radisic and K. H. Bowen Jr (2004): "Barrier-free proton transfer in anionic complex of thymine with glycine." *Physical Chemistry Chemical Physics* **6** (17): 4351-4357.

33. Denifl, S., S. Ptasinska, M. Cingel, S. Matejcik, P. Scheier and T. Märk (2003): "Electron attachment to the DNA bases thymine and cytosine." *Chemical physics letters* **377** (1): 74-80.

34. Denifl, S., S. Ptasinska, M. Probst, J. Hrušák, P. Scheier and T. Märk (2004): "Electron attachment to the gas-phase DNA bases cytosine and thymine." *The Journal of Physical Chemistry A* **108** (31): 6562-6569.

35. Eustis, S., D. Wang, S. Lyapustina and K. H. Bowen (2007): "Photoelectron spectroscopy of hydrated adenine anions." *The Journal of Chemical Physics* **127** (22): 224309.

36. Li, X., H. Wang and K. H. Bowen (2010): "Photoelectron spectroscopic study of the hydrated nucleoside anions." *The Journal of Chemical Physics* **133**: 144304.

37. Rak, J., K. Mazurkiewicz, M. Kobyłecka, P. Storoniak, M. Haranczyk, I. DĄbkowska, R. A. Bachorz, M. Gutowski, D. Radisic and S. T. Stokes (2008). Stable valence anions of nucleic acid bases and DNA strand breaks induced by low energy electrons. Radiation Induced Molecular Phenomena in Nucleic Acids, Springer**:** 619-667.

38. Xu, S., J. M. Nilles and K. H. Bowen Jr (2003): "Zwitterion formation in hydrated amino acid, dipole bound anions: How many water molecules are required?" *The Journal of Chemical Physics* **119** (20): 10696-10701.

39. Anbar, M. and E. J. Hart (1965): "The Effect of Solvent and of Solutes on the Absorption Spectrum of Solvated Electrons1a." *The Journal of Physical Chemistry* **69** (4): 1244-1247.

40. Boag, J. and E. J. Hart (1963): "ABSORPTION SPECTRA IN IRRADIATED WATER AND SOME SOLUTIONS. PART I. ABSORPTION SPECTRA OF'HYDRATED'ELECTRON." *Nature* **197**.

41. Gordon, S., E. Hart, M. Matheson, J. Rabani and J. Thomas (1963): "Reactions of the hydrated electron." *Discussions of the Faraday Society* **36**: 193-205.

42. Hart, E. J. and J. Boag (1962): "Absorption spectrum of the hydrated electron in water and in aqueous solutions." *Journal of the American Chemical Society* **84** (21): 4090-4095.

43. Rentzepis, P., R. Jones and J. Jortner (1972): "Relaxation of excess electrons in a polar solvent." *Chemical physics letters* **15** (4): 480-482.

44. Rentzepis, P., R. Jones and J. Jortner (1973): "Dynamics of solvation of an excess electron." *The Journal of Chemical Physics* **59** (2): 766-773.

45. Barnett, R., U. Landman, S. Dhar, N. Kestner, J. Jortner and A. Nitzan (1989): "Quantum simulations and abinitio electronic structure studies of (H2O)− 2." *The Journal of Chemical Physics* **91** (12): 7797-7808.

46. Ayotte, P. and M. A. Johnson (1997): "Electronic absorption spectra of size-selected hydrated electron clusters: (H2O)n−, n=6–50." *The Journal of Chemical Physics* **106** (2): 811-814.

47. Kelley, S. O. and J. K. Barton (1999): "Electron transfer between bases in double helical DNA." *Science* **283** (5400): 375-381.

48. Nikjoo, H. and D. Goodhead (1991): "Track structure analysis illustrating the prominent role of low-energy electrons in radiobiological effects of low-LET radiations." *Physics in medicine and biology* **36** (2): 229.

49. NIKJOO, P. O. N., DT GOODHEAD and H. M. TERRISSOL (1997): "Computational modelling of low-energy electron-induced DNA damage by early physical and chemical events." *International journal of radiation biology* **71** (5): 467-483.

50. Ptasińska, S., S. Denifl, S. Gohlke, P. Scheier, E. Illenberger and T. D. Märk (2006): "Decomposition of Thymidine by Low‐Energy Electrons: Implications for the Molecular Mechanisms of Single‐Strand Breaks in DNA." *Angewandte Chemie International Edition* **45** (12): 1893-1896.

51. Ray, S., S. Daube and R. Naaman (2005): "On the capturing of low-energy electrons by DNA." *Proceedings of the National Academy of Sciences* **102** (1): 15-19.

52. Winstead, C. and V. McKoy (2006): "Interaction of low-energy electrons with the purine bases, nucleosides, and nucleotides of DNA." *The Journal of Chemical Physics* **125** (24): 244302.

53. Zheng, Y., P. Cloutier, D. J. Hunting, L. Sanche and J. R. Wagner (2005): "Chemical basis of DNA sugar-phosphate cleavage by low-energy electrons." *Journal of the American Chemical Society* **127** (47): 16592-16598.

54. Zheng, Y., J. R. Wagner and L. Sanche (2006): "DNA damage induced by low-energy electrons: electron transfer and diffraction." *Physical review letters* **96** (20): 208101.

55. Bald, I., J. Kopyra and E. Illenberger (2006): "Selective Excision of C5 from D‐Ribose in the Gas Phase by Low‐Energy Electrons (0‐1 eV): Implications for the Mechanism of DNA Damage." *Angewandte Chemie International Edition* **45** (29): 4851-4855.

56. Barrios, R., P. Skurski and J. Simons (2002): "Mechanism for damage to DNA by low-energy electrons." *The Journal of Physical Chemistry B* **106** (33): 7991-7994.

57. Berdys, J., I. Anusiewicz, P. Skurski and J. Simons (2004): "Damage to model DNA fragments from very low-energy ($<$ 1 eV) electrons." *Journal of the American Chemical Society* **126** (20): 6441-6447.

58. Boudaïffa, B., P. Cloutier, D. Hunting, M. A. Huels and L. Sanche (2000): "Resonant formation of DNA strand breaks by low-energy (3 to 20 eV) electrons." *Science* **287** (5458): 1658-1660.

59. Simons, J. (2006): "How do low-energy (0.1-2 eV) electrons cause DNA-strand breaks?" *Accounts of chemical research* **39** (10): 772-779.

60. Sanche, L. (2002): "Nanoscopic aspects of radiobiological damage: Fragmentation induced by secondary low‐energy electrons." *Mass spectrometry reviews* **21** (5): 349-369.

61. Langseth, A. and R. Lord Jr (1938): "The Fine Structure of the Totally Symmetrical Raman Lines in Benzene and Benzene‐d6." *The Journal of Chemical Physics* **6** (4): 203-204.

62. Lord Jr, R. (1936): "Raman Spectrum of Benzene‐d6." *The Journal of Chemical Physics* **4** (1): 82-83.

63. Lord Jr, R., J. Ahlberg and D. Andrews (1937): "Calculation of the Heat Capacity Curves of Crystalline Benzene and Benzene‑d6." *The Journal of Chemical Physics* **5** (8): 649-654.

64. Corrsin, L., B. J. Fax and R. C. Lord (1953): "The Vibrational Spectra of Pyridine and Pyridine‑d5." *The Journal of Chemical Physics* **21** (7): 1170-1176.

65. Lord, R. C., A. L. Marston and F. A. Miller (1957): "Infra-red and Raman spectra ot the diazines." *Spectrochimica Acta* **9** (2): 113-125.

66. Takahashi, H., K. Mamola and E. K. Plyler (1966): "Effects of hydrogen bond formation on vibrations of pyridine, pyrazine, pyrimidine, and pyridazine." *Journal of Molecular Spectroscopy* **21** (1): 217-230.

67. Hobza, P. and Z. Havlas (2000): "Blue-shifting hydrogen bonds." *Chemical reviews* **100** (11): 4253-4264.

68. Hobza, P. and Z. Havlas (2002): "Improper, blue-shifting hydrogen bond." *Theoretical Chemistry Accounts* **108** (6): 325-334.

69. Joseph, J. and E. D. Jemmis (2007): "Red-, blue-, or no-shift in hydrogen bonds: a unified explanation." *Journal of the American Chemical Society* **129** (15): 4620-4632.

70. Li, X., L. Liu and H. B. Schlegel (2002): "On the physical origin of blue-shifted hydrogen bonds." *Journal of the American Chemical Society* **124** (32): 9639-9647.

71. Mo, Y., C. Wang, L. Guan, B. Braïda, P. C. Hiberty and W. Wu (2014): "On the nature of blueshifting hydrogen bonds." *Chemistry–A European Journal* **20** (27): 8444-8452.

72. Pejov, L. and K. Hermansson (2003): "On the nature of blueshifting hydrogen bonds: ab initio and density functional studies of several fluoroform complexes." *The Journal of Chemical Physics* **119** (1): 313-324.

73. Wright, A. M., A. A. Howard, J. C. Howard, G. S. Tschumper and N. I. Hammer (2013): "Charge Transfer and Blue Shifting of Vibrational Frequencies in a Hydrogen Bond Acceptor." *The Journal of Physical Chemistry A* **117** (26): 5435-5446.

74. Zierkiewicz, W., D. Michalska, Z. Havlas and P. Hobza (2002): "Study of the Nature of Improper Blue‐Shifting Hydrogen Bonding and Standard Hydrogen Bonding in the X3CH··· OH2 and XH··· OH2 Complexes (X= F, Cl, Br, I): A Correlated Ab Initio Study." *ChemPhysChem* **3** (6): 511-518.

75. Fleischmann, M., P. J. Hendra and A. McQuillan (1974): "Raman spectra of pyridine adsorbed at a silver electrode." *Chemical physics letters* **26** (2): 163-166.

76. Hager, J. S., J. Zahardis, R. M. Pagni, R. N. Compton and J. Li (2004): "Raman under nitrogen. The high-resolution Raman spectroscopy of crystalline uranocene, thorocene, and ferrocene." *The Journal of Chemical Physics* **120** (6): 2708-2718.

77. Compton, R. and N. Hammer (2014). Raman Under Liquid Nitrogen (RUN). Journal of Physics: Conference Series, IOP Publishing.

78. Bao, X., J. Wang, J. Gu and J. Leszczynski (2006): "DNA strand breaks induced by near-zero-electronvolt electron attachment to pyrimidine nucleotides." *Proceedings of the National Academy of Sciences* **103** (15): 5658-5663.

79. Gu, J., J. Wang and J. Leszczynski (2006): "Electron Attachment-Induced DNA Single Strand Breaks: C3'-O3' σ -Bond Breaking of Pyrimidine Nucleotides Predominates." *Journal of the American Chemical Society* **128** (29): 9322-9323.

80. Gu, J., Y. Xie and H. F. Schaefer (2005): "Glycosidic bond cleavage of pyrimidine nucleosides by low-energy electrons: a theoretical rationale." *Journal of the American Chemical Society* **127** (3): 1053-1057.

81. Nenner, I. and G. Schulz (1975): "Temporary negative ions and electron affinities of benzene and N‐heterocyclic molecules: pyridine, pyridazine, pyrimidine, pyrazine, and s‐triazine." *The Journal of Chemical Physics* **62** (5): 1747-1758.

82. Aflatooni, K., G. A. Gallup and P. D. Burrow (1998): "Electron Attachment Energies of the DNA Bases." *The Journal of Physical Chemistry A* **102** (31): 6205-6207.

83. Jordan, K. D. and P. D. Burrow (1978): "Studies of the temporary anion states of unsaturated hydrocarbons by electron transmission spectroscopy." *Accounts of chemical research* **11** (9): 341-348.

84. Periquet, V., A. Moreau, S. Carles, J. P. Schermann and C. Desfrançois (2000): "Cluster size effects upon anion solvation of N-heterocyclic molecules and nucleic acid bases." *Journal of Electron Spectroscopy and Related Phenomena* **106** (2–3): 141-151.

85. Hendricks, J., S. Lyapustina, H. De Clercq, J. Snodgrass and K. Bowen (1996): "Dipole bound, nucleic acid base anions studied via negative ion photoelectron spectroscopy." *The Journal of Chemical Physics* **104** (19): 7788-7791.

86. Hendricks, J. H., S. A. Lyapustina, H. L. de Clercq and K. H. Bowen (1998): "The dipole bound-to-covalent anion transformation in uracil." *The Journal of Chemical Physics* **108** (1): 8-11.

87. Lyapustina, S. A., S. Xu, J. M. Nilles and K. H. Bowen (2000): "Solvent-induced stabilization of the naphthalene anion by water molecules: A negative cluster ion photoelectron spectroscopic study." *The Journal of Chemical Physics* **112** (15): 6643-6648.

88. Coe, J. V., J. T. Snodgrass, C. B. Freidhoff, K. M. McHugh and K. H. Bowen (1986): "Photoelectron spectroscopy of the negative ion SeO−." *The Journal of Chemical Physics* **84** (2): 618-625.

89. Neumark, D. M., K. R. Lykke, T. Andersen and W. C. Lineberger (1985): "Laser photodetachment measurement of the electron affinity of atomic oxygen." *Physical Review A* **32** (3): 1890-1892.

90. Siegel, M. W., R. J. Celotta, J. L. Hall, J. Levine and R. A. Bennett (1972): "Molecular Photodetachment Spectrometry. I. The Electron Affinity of Nitric Oxide and the Molecular Constants of N<math><mrow><msup><mrow><mi

mathvariant="normal">O</mi></mrow><mrow><mo>-</mo></mrow></msup></mrow></math>." *Physical Review A* **6** (2): 607-631.

91. Travers, M. J., D. C. Cowles and G. B. Ellison (1989): "Reinvestigation of the electron affinities of O2 and NO." *Chemical physics letters* **164** (5): 449-455.

92. Becke, A. D. (1988): "A multicenter numerical integration scheme for polyatomic molecules." *The Journal of Chemical Physics* **88** (4): 2547-2553.

93. Becke, A. D. (1993): "Density‐functional thermochemistry. III. The role of exact exchange." *The Journal of Chemical Physics* **98** (7): 5648-5652.

94. Lee, C., W. Yang and R. G. Parr (1988): "Development of the Colle-Salvetti correlation-energy formula into a functional of the electron density." *Physical Review B* **37** (2): 785-789.

95. Frisch, M., G. Trucks, H. Schlegel, G. Scuseria, M. Robb, J. Cheeseman, G. Scalmani, V. Barone, B. Mennucci and G. Petersson "Gaussian 09, Revision A. 1; Gaussian, Inc: Wallingford, CT, 2009." *There is no corresponding record for this reference*.

96. Howard, J. C., N. I. Hammer and G. S. Tschumper (2011): "Structures, Energetics and Vibrational Frequency Shifts of Hydrated Pyrimidine." *ChemPhysChem* **12** (17): 3262-3273.

97. Hammer, N. I., J. R. Roscioli and M. A. Johnson (2005): "Identification of Two Distinct Electron Binding Motifs in the Anionic Water Clusters: A Vibrational Spectroscopic Study of the (H2O)6- Isomers." *The Journal of Physical Chemistry A* **109** (35): 7896-7901.

98. Hammer, N. I., J. R. Roscioli, M. A. Johnson, E. M. Myshakin and K. D. Jordan (2005): "Infrared Spectrum and Structural Assignment of the Water Trimer Anion†." *The Journal of Physical Chemistry A* **109** (50): 11526-11530.

99. Lee, H. M., S. Lee and K. S. Kim (2003): "Structures, energetics, and spectra of electron–water clusters, e−–(H2O)2–6 and e−–HOD(D2O)1–5." *The Journal of Chemical Physics* **119** (1): 187-194.

100. Rienstra-Kiracofe, J. C., G. S. Tschumper, H. F. Schaefer, S. Nandi and G. B. Ellison (2002): "Atomic and molecular electron affinities: photoelectron experiments and theoretical computations." *Chemical reviews* **102** (1): 231-282.

101. Howard, A. A., G. S. Tschumper and N. I. Hammer (2010): "Effects of hydrogen bonding on vibrational normal modes of pyrimidine." *The Journal of Physical Chemistry A* **114** (25): 6803-6810.

102. Navarro, A., M. Fernández-Gómez, J. J. López-González, M. P. Fernández-Liencres, E. Martínez-Torres, J. Tomkinson and G. J. Kearley (1999): "Inelastic Neutron Scattering Spectrum and Quantum Mechanical Calculations on the Internal Vibrations of Pyrimidine." *The Journal of Physical Chemistry A* **103** (29): 5833-5840.

103. Wright, A. M., L. V. Joe, A. A. Howard, G. S. Tschumper and N. I. Hammer (2011): "Spectroscopic and computational insight into weak noncovalent interactions in crystalline pyrimidine." *Chemical physics letters* **501** (4): 319-323.

104. Coe, J. V., G. H. Lee, J. G. Eaton, S. T. Arnold, H. W. Sarkas, K. H. Bowen, C. Ludewigt, H. Haberland and D. R. Worsnop (1990): "Photoelectron spectroscopy of hydrated electron cluster anions, $(H2O)^{-}n=2-69$." *The Journal of Chemical Physics* **92** (6): 3980-3982.

105. Abraham, M. H. (1993): "Scales of solute hydrogen-bonding: their construction and application to physicochemical and biochemical processes." *Chem. Soc. Rev.* **22** (2): 73-83.

106. Desfrançois, C., S. Carles and J. P. Schermann (2000): "Weakly Bound Clusters of Biological Interest." *Chemical reviews* **100** (11): 3943-3962.

107. Hobza, P. and J. Šponer (1999): "Structure, Energetics, and Dynamics of the Nucleic Acid Base Pairs: Nonempirical Ab Initio Calculations." *Chemical reviews* **99** (11): 3247-3276.

108. Kim, K. S., P. Tarakeshwar and J. Y. Lee (2000): "Molecular Clusters of π-Systems: Theoretical Studies of Structures, Spectra, and Origin of Interaction Energies." *Chemical reviews* **100** (11): 4145-4186.

109. Lee, H. M., P. Tarkeshwar and K. S. Kim (2004): "Structures, energetics, and spectra of hydrated hydroxide anion clusters." *The Journal of Chemical Physics* **121** (10): 4657-4664.

110. Wahl, M. C. and M. Sundaralingam (1997): "C · H⋯ O hydrogen bonding in biology."

Trends in biochemical sciences **22** (3): 97-102.

111. Xantheas, S. S. (2000): "Cooperativity and hydrogen bonding network in water clusters." *Chemical Physics* **258** (2): 225-231.

112. Nakano, S.-i., D. M. Chadalavada and P. C. Bevilacqua (2000): "General acid-base catalysis in the mechanism of a hepatitis delta virus ribozyme." *Science* **287** (5457): 1493-1497.

113. Petersen, P. B. and R. J. Saykally (2006): "On the nature of ions at the liquid water surface." *Annu. Rev. Phys. Chem.* **57**: 333-364.

114. Shen, Y. R. and V. Ostroverkhov (2006): "Sum-frequency vibrational spectroscopy on water interfaces: Polar orientation of water molecules at interfaces." *Chemical reviews* **106** (4): 1140-1154.

115. Eisenberg, D. S. and W. Kauzmann (2005). The structure and properties of water, Oxford University Press.

116. Scheiner, S. (1997): "Hydrogen bonding. A theoretical perspective."

117. Burrow, P. D., J. A. Michejda and K. D. Jordan (1987): "Electron transmission study of the temporary negative ion states of selected benzenoid and conjugated aromatic hydrocarbons." *The Journal of Chemical Physics* **86** (1): 9-24.

118. Sevilla, M. D., B. Besler and A.-O. Colson (1995): "Ab Initio Molecular Orbital Calculations of DNA Radical Ions. 5. Scaling of Calculated Electron Affinities and Ionization Potentials to Experimental Values." *The Journal of Physical Chemistry* **99** (3): 1060-1063.

119. Desfrançois, C., V. Periquet, Y. Bouteiller and J. P. Schermann (1998): "Valence and Dipole Binding of Electrons to Uracil." *The Journal of Physical Chemistry A* **102** (8): 1274-1278.

120. Kondow, T. (1987): "Ionization of clusters in collision with high-Rydberg rare gas atoms." *The Journal of Physical Chemistry* **91** (6): 1307-1316.

121. Schiedt, J., R. Weinkauf, D. M. Neumark and E. W. Schlag (1998): "Anion spectroscopy of uracil, thymine and the amino-oxo and amino-hydroxy tautomers of cytosine and their water clusters." *Chemical Physics* **239** (1–3): 511-524.

122. Nakajima, A., Y. Negishi, R. Hasumi and K. Kaya (1999): "Photoelectron spectroscopy of 7-azaindole–water cluster anions." *The European Physical Journal D - Atomic, Molecular, Optical and Plasma Physics* **9** (1): 303-307.

123. Schiedt, J., W. J. Knott, K. Le Barbu, E. W. Schlag and R. Weinkauf (2000): "Microsolvation of similar-sized aromatic molecules: Photoelectron spectroscopy of bithiophene–, azulene–, and naphthalene–water anion clusters." *The Journal of Chemical Physics* **113** (21): 9470-9478.

124. Kelly, J. T., S. Xu, J. Graham, J. M. Nilles, D. Radisic, A. M. Buonaugurio, K. H. Bowen Jr, N. I. Hammer and G. S. Tschumper (2014): "Photoelectron Spectroscopic and Computational Study of Hydrated Pyrimidine Anions." *The Journal of Physical Chemistry A*.

125. Kamrath, M. Z., R. A. Relph and M. A. Johnson (2010): "Vibrational predissociation spectrum of the carbamate radical anion, C5H5N-CO2−, generated by reaction of pyridine with (CO2) m−." *Journal of the American Chemical Society* **132** (44): 15508-15511.

126. Lee, S. H., N. Kim, D. G. Ha and S. K. Kim (2008): ""Associative" Electron Attachment to Azabenzene−(CO2) n van der Waals Complexes: Stepwise Formation of Covalent Bonds with Additive Electron Affinities." *Journal of the American Chemical Society* **130** (48): 16241-16244.

127. Dąbkowska, I., J. Rak, M. Gutowski, J. M. Nilles, S. T. Stokes and K. H. Bowen (2004): "Barrier-free intermolecular proton transfer induced by excess electron attachment to the complex of alanine with uracil." *The Journal of Chemical Physics* **120** (13): 6064-6071.

128. Eustis, S. N., D. Radisic, K. H. Bowen, R. A. Bachorz, M. Haranczyk, G. K. Schenter and M. Gutowski (2008): "Electron-Driven Acid-Base Chemistry: Proton Transfer from Hydrogen Chloride to Ammonia." *Science* **319** (5865): 936-939.

129. Eustis, S. N., A. Whiteside, D. Wang, M. Gutowski and K. H. Bowen (2010): "Ammonia−Hydrogen Bromide and Ammonia−Hydrogen Iodide Complexes: Anion Photoelectron and ab Initio Studies." *The Journal of Physical Chemistry A* **114** (3): 1357-1363.

130. Gutowski, M., I. Dabkowska, J. Rak, S. Xu, J. Nilles, D. Radisic and K. Bowen Jr (2002): "Barrier-free intermolecular proton transfer in the uracil-glycine complex induced by excess electron attachment." *The European Physical Journal D-Atomic, Molecular, Optical and Plasma Physics* **20** (3): 431-439.

131. Harańczyk, M., I. Dąbkowska, J. Rak, M. Gutowski, J. M. Nilles, S. Stokes, D. Radisic and K. H. Bowen (2004): "Excess Electron Attachment Induces Barrier-Free Proton Transfer in Anionic Complexes of Thymine and Uracil with Formic Acid." *The Journal of Physical Chemistry B* **108** (22): 6919-6921.

132. Haranczyk, M., J. Rak, M. Gutowski, D. Radisic, S. T. Stokes and K. H. Bowen (2005): "Intermolecular proton transfer in anionic complexes of uracil with alcohols." *The Journal of Physical Chemistry B* **109** (27): 13383-13391.

133. Harańczyk, M., J. Rak, M. Gutowski, D. Radisic, S. T. Stokes and K. H. Bowen (2004): "Effect of Hydrogen Bonding on Barrier-Free Proton Transfer in Anionic Complexes of Uracil with Weak Acids: (U…HCN)− versus (U…H2S)−." *Israel Journal of Chemistry* **44** (1-3): 157-170.

134. Ko, Y. J., H. Wang, R. Cao, D. Radisic, S. N. Eustis, S. T. Stokes, S. Lyapustina, S. X. Tian and K. H. Bowen (2010): "Photoelectron spectroscopy of homogeneous nucleic acid base dimer anions." *Physical Chemistry Chemical Physics* **12** (14): 3535-3541.

135. Ko, Y. J., H. Wang, D. Radisic, S. T. Stokes, S. N. Eustis, K. H. Bowen, K. Mazurkiewicz, P. Storoniak, A. Kowalczyk, M. Haranczyk, M. Gutowski and J. Rak (2010): "Barrier-free proton transfer induced by electron attachment to the complexes between 1‑methylcytosine and formic acid." *Molecular Physics* **108** (19-20): 2621-2631.

136. Mazurkiewicz, K., M. Haranczyk, M. Gutowski, J. Rak, D. Radisic, S. N. Eustis, D. Wang and K. H. Bowen (2007): "Valence anions in complexes of adenine and 9-methyladenine with formic acid: Stabilization by intermolecular proton transfer." *Journal of the American Chemical Society* **129** (5): 1216-1224.

137. Mazurkiewicz, K., M. Haranczyk, P. Storoniak, M. Gutowski, J. Rak, D. Radisic, S. N. Eustis, D. Wang and K. H. Bowen (2007): "Intermolecular proton transfer induced by excess electron attachment to adenine(formic acid)n (n = 2, 3) hydrogen-bonded complexes." *Chemical Physics* **342** (1–3): 215-222.

138. Radisic, D., K. H. Bowen, I. Dąbkowska, P. Storoniak, J. Rak and M. Gutowski (2005): "AT Base Pair Anions versus (9-Methyl-A)(1-Methyl-T) Base Pair Anions." *Journal of the American Chemical Society* **127** (17): 6443-6450.

139. Storoniak, P., K. Mazurkiewicz, M. Haranczyk, M. Gutowski, J. Rak, S. N. Eustis, Y. J. Ko, H. Wang and K. H. Bowen (2010): "The Anionic (9-Methyladenine)−(1-Methylthymine) Base Pair Solvated by Formic Acid. A Computational and Photoelectron Spectroscopy Study." *The Journal of Physical Chemistry B* **114** (34): 11353-11362.

140. Szyperska, A., J. Rak, J. Leszczynski, X. Li, Y. J. Ko, H. Wang and K. H. Bowen (2009): "Valence Anions of 9-Methylguanine−1-Methylcytosine Complexes. Computational and

Photoelectron Spectroscopy Studies." *Journal of the American Chemical Society* **131** (7): 2663-2669.

141. Szyperska, A., J. Rak, J. Leszczynski, X. Li, Y. J. Ko, H. Wang and K. H. Bowen (2010): "Low-Energy-Barrier Proton Transfer Induced by Electron Attachment to the Guanine···Cytosine Base Pair." *ChemPhysChem* **11** (4): 880-888.

142. Zhang, X., Y. Wang, H. Wang, A. Lim, G. Gantefoer, K. H. Bowen, J. U. Reveles and S. N. Khanna (2013): "On the Existence of Designer Magnetic Superatoms." *Journal of the American Chemical Society* **135** (12): 4856-4861.

143. Ho, J., K. M. Ervin and W. C. Lineberger (1990): "Photoelectron spectroscopy of metal cluster anions: Cu−n, Ag−n, and Au−n." *The Journal of Chemical Physics* **93** (10): 6987-7002.

144. Frisch, M. J., G. W. Trucks, H. B. Schlegel, G. E. Scuseria, M. A. Robb, J. R. Cheeseman, G. Scalmani, V. Barone, B. Mennucci, G. A. Petersson, H. Nakatsuji, M. Caricato, X. Li, H. P. Hratchian, A. F. Izmaylov, J. Bloino, G. Zheng, J. L. Sonnenberg, M. Hada, M. Ehara, K. Toyota, R. Fukuda, J. Hasegawa, M. Ishida, T. Nakajima, Y. Honda, O. Kitao, H. Nakai, T. Vreven, J. A. Montgomery Jr., J. E. Peralta, F. Ogliaro, M. J. Bearpark, J. Heyd, E. N. Brothers, K. N. Kudin, V. N. Staroverov, R. Kobayashi, J. Normand, K. Raghavachari, A. P. Rendell, J. C. Burant, S. S. Iyengar, J. Tomasi, M. Cossi, N. Rega, N. J. Millam, M. Klene, J. E. Knox, J. B. Cross, V. Bakken, C. Adamo, J. Jaramillo, R. Gomperts, R. E. Stratmann, O. Yazyev, A. J. Austin, R. Cammi, C. Pomelli, J. W. Ochterski, R. L. Martin, K. Morokuma, V. G. Zakrzewski, G. A. Voth, P. Salvador, J. J. Dannenberg, S. Dapprich, A. D. Daniels, Ö. Farkas, J. B. Foresman, J. V. Ortiz, J. Cioslowski and D. J. Fox (2009). Gaussian 09. Wallingford, CT, USA, Gaussian, Inc.

145. Zhao, Y. and D. G. Truhlar (2008): "Density Functionals with Broad Applicability in Chemistry." *Accounts of chemical research* **41** (2): 157-167.

146. Zhao, Y. and D. G. Truhlar (2008): "How Well Can New-Generation Density Functionals Describe the Energetics of Bond-Dissociation Reactions Producing Radicals?" *The Journal of Physical Chemistry A* **112** (6): 1095-1099.

147. Zhao, Y. and D. G. Truhlar (2008): "The M06 suite of density functionals for main group thermochemistry, thermochemical kinetics, noncovalent interactions, excited states, and transition elements: two new functionals and systematic testing of four M06-class functionals and 12 other functionals." *Theoretical Chemistry Accounts* **120** (1-3): 215-241.

148. Allodi, M. A., M. E. Dunn, J. Livada, K. N. Kirschner and G. C. Shields (2006): "Do Hydroxyl Radical−Water Clusters, OH(H2O)n, n = 1−5, Exist in the Atmosphere?" *The Journal of Physical Chemistry A* **110** (49): 13283-13289.

149. Anderson, J. A. and G. S. Tschumper (2006): "Characterizing the Potential Energy Surface of the Water Dimer with DFT: Failures of Some Popular Functionals for Hydrogen Bonding." *The Journal of Physical Chemistry A* **110** (22): 7268-7271.

150. Bates, D. M., J. R. Smith, T. Janowski and G. S. Tschumper (2011): "Development of a 3-body:many-body integrated fragmentation method for weakly bound clusters and application to water clusters (H2O)n = 3 − 10, 16, 17." *The Journal of Chemical Physics* **135** (4): -.

151. Bates, D. M., J. R. Smith and G. S. Tschumper (2011): "Efficient and Accurate Methods for the Geometry Optimization of Water Clusters: Application of Analytic Gradients for the Two-Body:Many-Body QM:QM Fragmentation Method to (H2O)n, n = 3–10." *Journal of Chemical Theory and Computation* **7** (9): 2753-2760.

152. Bates, D. M. and G. S. Tschumper (2009): "CCSD(T) Complete Basis Set Limit Relative Energies for Low-Lying Water Hexamer Structures." *The Journal of Physical Chemistry A* **113** (15): 3555-3559.

153. Dahlke, E. E., R. M. Olson, H. R. Leverentz and D. G. Truhlar (2008): "Assessment of the Accuracy of Density Functionals for Prediction of Relative Energies and Geometries of

Low-Lying Isomers of Water Hexamers." *The Journal of Physical Chemistry A* **112** (17): 3976-3984.

154. Shields, R. M., B. Temelso, K. A. Archer, T. E. Morrell and G. C. Shields (2010): "Accurate Predictions of Water Cluster Formation, (H2O)n=2−10." *The Journal of Physical Chemistry A* **114** (43): 11725-11737.

155. Harańczyk, M., J. Rak, M. Gutowski, D. Radisic, S. T. Stokes and K. H. Bowen (2005): "Intermolecular Proton Transfer in Anionic Complexes of Uracil with Alcohols." *The Journal of Physical Chemistry B* **109** (27): 13383-13391.

156. Lee, G. H., S. T. Arnold, J. G. Eaton, H. W. Sarkas, K. H. Bowen, C. Ludewigt and H. Haberland (1991): "Negative ion photoelectron spectroscopy of solvated electron cluster anions, (H2O) n − and (NH3) n −." *Zeitschrift für Physik D Atoms, Molecules and Clusters* **20** (1): 9-12.

157. Puiatti, M., D. M. A. Vera and A. B. Pierini (2008): "Species with negative electron affinity and standard DFT methods. Finding the valence anions." *Physical Chemistry Chemical Physics* **10** (10): 1394-1399.

158. Desfrancois, C., B. Baillon, J. Schermann, S. Arnold, J. Hendricks and K. Bowen (1994): "Prediction and observation of a new, ground state, dipole-bound dimer anion: The mixed water/ammonia system." *Physical review letters* **72** (1): 48.

159. Harańczyk, M., R. Bachorz, J. Rak, M. Gutowski, D. Radisic, S. T. Stokes, J. M. Nilles and K. H. Bowen (2003): "Excess Electron Attachment Induces Barrier-Free Proton Transfer in Binary Complexes of Uracil with H2Se and H2S but Not with H2O." *The Journal of Physical Chemistry B* **107** (31): 7889-7895.

160. Kim, J. H., J. K. Song, H. Park, S. H. Lee, S. Y. Han and S. K. Kim (2003): "Photoelectron spectroscopy of s-triazine anion clusters: Polarization-induced electron binding in aza-aromatic molecule." *The Journal of Chemical Physics* **119** (8): 4320-4327.

161. Song, J. K., N. K. Lee and S. K. Kim (2002): "Photoelectron spectroscopy of pyrazine anion clusters." *The Journal of Chemical Physics* **117** (4): 1589-1594.

162. Wang, X.-B. and S. R. Kass (2014): "Anion A− • HX Clusters with Reduced Electron Binding Energies: Proton vs Hydrogen Atom Relocation upon Electron Detachment." *Journal of the American Chemical Society* **136** (49): 17332-17336.

163. Green, W. H., S. M. Gorun, G. Fitzgerald, P. W. Fowler, A. Ceulemans and B. C. Titeca (1996): "Electronic structures and geometries of C60 anions via density functional calculations." *The Journal of Physical Chemistry* **100** (36): 14892-14898.

164. Kato, T., T. Kodama and T. Shida (1993): "Spectroscopic studies of the radical anion of C< sub> 60</sub>. Detection of the fluorenscence and reinvestigation of the ESR spectrum." *Chemical physics letters* **205** (4): 405-409.

165. Koga, N. and K. Morokuma (1992): "Ab initio MO study of the C< sub> 60</sub> anion radical: the Jahn—Teller distortion and electronic structure." *Chemical physics letters* **196** (1): 191-196.

166. Voora, V. K., L. S. Cederbaum and K. D. Jordan (2013): "Existence of a correlation bound s-type anion state of C60." *The journal of physical chemistry letters* **4** (6): 849-853.

167. Wang, X.-B., H.-K. Woo and L.-S. Wang (2005): "Vibrational cooling in a cold ion trap: Vibrationally resolved photoelectron spectroscopy of cold C60− anions." *The Journal of Chemical Physics* **123** (5): 051106.

168. Zakrzewski, V. G., O. Dolgounitcheva and J. V. Ortiz (2014): "Electron Propagator Calculations on the Ground and Excited States of C⁻ 60." *The Journal of Physical Chemistry A.*

169. ElSohly, A. M., G. S. Tschumper, R. A. Crocombe, J. T. Wang and F. Williams (2005): "Computational and ESR Studies of Electron Attachment to Decafluorocyclopentane, Octafluorocyclobutane, and Hexafluorocyclopropane: Electron Affinities of the Molecules

and the Structures of Their Stable Negative Ions as Determined from 13C and 19F Hyperfine Coupling Constants." *Journal of the American Chemical Society* **127** (30): 10573-10583.

170. Hameka, H. F., G. W. Robinson and C. J. Marsden (1987): "Structure of the hydrated electron." *The Journal of Physical Chemistry* **91** (12): 3150-3157.

171. Abel, B., U. Buck, A. L. Sobolewski and W. Domcke (2012): "On the nature and signatures of the solvated electron in water." *Physical Chemistry Chemical Physics* **14** (1): 22-34.

172. Sobolewski, A. L. and W. Domcke (2002): "Hydrated hydronium: a cluster model of the solvated electron?" *Physical Chemistry Chemical Physics* **4** (1): 4-10.

173. Huh, Y. S., A. J. Chung and D. Erickson (2009): "Surface enhanced Raman spectroscopy and its application to molecular and cellular analysis." *Microfluidics and nanofluidics* **6** (3): 285-297.

174. Joya, K. S. and X. Sala (2015): "In situ Raman and surface-enhanced Raman spectroscopy on working electrodes: spectroelectrochemical characterization of water oxidation electrocatalysts." *Physical Chemistry Chemical Physics* **17** (33): 21094-21103.

175. Kneipp, K., Y. Wang, H. Kneipp, L. T. Perelman, I. Itzkan, R. R. Dasari and M. S. Feld (1997): "Single molecule detection using surface-enhanced Raman scattering (SERS)." *Physical review letters* **78** (9): 1667.

176. Le Ru, E. and P. Etchegoin (2008). Principles of Surface-Enhanced Raman Spectroscopy: and related plasmonic effects, Elsevier.

177. Maher, R., C. Galloway, E. Le Ru, L. Cohen and P. Etchegoin (2008): "Vibrational pumping in surface enhanced Raman scattering (SERS)." *Chemical Society Reviews* **37** (5): 965-979.

178. Nie, S. and S. R. Emory (1997): "Probing single molecules and single nanoparticles by surface-enhanced Raman scattering." *Science* **275** (5303): 1102-1106.

179. Porter, M. D., R. J. Lipert, L. M. Siperko, G. Wang and R. Narayanan (2008): "SERS as a bioassay platform: fundamentals, design, and applications." *Chemical Society Reviews* **37** (5): 1001-1011.

180. Radziuk, D. and H. Moehwald (2015): "Prospects for plasmonic hot spots in single molecule SERS towards the chemical imaging of live cells." *Physical Chemistry Chemical Physics* **17** (33): 21072-21093.

181. Smith, W. (2008): "Practical understanding and use of surface enhanced Raman scattering/surface enhanced resonance Raman scattering in chemical and biological analysis." *Chemical Society Reviews* **37** (5): 955-964.

182. Campion, A. and P. Kambhampati (1998): "Surface-enhanced Raman scattering." *Chemical Society Reviews* **27** (4): 241-250.

183. Dasary, S. S. R., A. K. Singh, D. Senapati, H. Yu and P. C. Ray (2009): "Gold Nanoparticle Based Label-Free SERS Probe for Ultrasensitive and Selective Detection of Trinitrotoluene." *Journal of the American Chemical Society* **131** (38): 13806-13812.

184. Moskovits, M. (1985): "Surface-enhanced spectroscopy." *Reviews of Modern Physics* **57** (3): 783-826.

185. Rowe, J., C. Shank, D. Zwemer and C. Murray (1980): "Ultrahigh-vacuum studies of enhanced Raman scattering from pyridine on Ag surfaces." *Physical review letters* **44** (26): 1770.

186. Tiwari, V. S., T. Oleg, G. K. Darbha, W. Hardy, J. Singh and P. C. Ray (2007): "Non-resonance SERS effects of silver colloids with different shapes." *Chemical physics letters* **446** (1): 77-82.

187. Fang, Y., N.-H. Seong and D. D. Dlott (2008): "Measurement of the distribution of site enhancements in surface-enhanced Raman scattering." *Science* **321** (5887): 388-392.

188. Lombardi, J. R., R. L. Birke, T. Lu and J. Xu (1986): "Charge‑transfer theory of surface enhanced Raman spectroscopy: Herzberg–Teller contributions." *The Journal of Chemical Physics* **84** (8): 4174-4180.

189. Osawa, M., N. Matsuda, K. Yoshii and I. Uchida (1994): "Charge transfer resonance Raman process in surface-enhanced Raman scattering from p-aminothiophenol adsorbed on silver: Herzberg-Teller contribution." *The Journal of Physical Chemistry* **98** (48): 12702-12707.

190. Yamada, H., H. Nagata, K. Toba and Y. Nakao (1987): "Charge-transfer band and SERS mechanism for the pyridine-Ag system." *Surface science* **182** (1): 269-286.

191. Chen, L., Y. Gao, H. Xu, Z. Wang, Z. Li and R.-Q. Zhang (2014): "The mechanism of N–Ag bonding determined tunability of surface-enhanced Raman scattering of pyridine on MAg (M= Cu, Ag, Au) diatomic clusters." *Physical Chemistry Chemical Physics* **16** (38): 20665-20671.

192. Kong, X.-k., Q.-w. Chen and Z.-y. Sun (2013): "Enhanced SERS of the complex substrate using Au supported on graphene with pyridine and R6G as the probe molecules." *Chemical physics letters* **564**: 54-59.

193. Li, J.-F., Y.-J. Zhang, A. V. Rudnev, J. R. Anema, S.-B. Li, W.-J. Hong, P. Rajapandiyan, J. Lipkowski, T. Wandlowski and Z.-Q. Tian (2015): "Electrochemical Shell-Isolated Nanoparticle-Enhanced Raman Spectroscopy: Correlating Structural Information and Adsorption Processes of Pyridine at the Au (hkl) Single Crystal/Solution Interface." *Journal of the American Chemical Society* **137** (6): 2400-2408.

194. Wu, D.-Y., X.-M. Liu, S. Duan, X. Xu, B. Ren, S.-H. Lin and Z.-Q. Tian (2008): "Chemical enhancement effects in SERS spectra: A quantum chemical study of pyridine interacting with copper, silver, gold and platinum metals." *The Journal of Physical Chemistry C* **112** (11): 4195-4204.

195. Zhao, L., L. Jensen and G. C. Schatz (2006): "Pyridine-Ag20 cluster: a model system for studying surface-enhanced Raman scattering." *Journal of the American Chemical Society* **128** (9): 2911-2919.

196. Fales, A. M., H. Yuan and T. Vo-Dinh (2011): "Silica-coated gold nanostars for combined surface-enhanced Raman scattering (SERS) detection and singlet-oxygen generation: a potential nanoplatform for theranostics." *Langmuir* **27** (19): 12186-12190.

197. Hesse, E. and J. Creighton (1999): "Investigation by surface-enhanced Raman spectroscopy of the effect of oxygen and hydrogen plasmas on adsorbate-covered gold and silver island films." *Langmuir* **15** (10): 3545-3550.

198. Suh, J. and M. Moskovits (1986): "Surface-enhanced Raman spectroscopy of amino acids and nucleotide bases adsorbed on silver." *Journal of the American Chemical Society* **108** (16): 4711-4718.

199. Centeno, S. P., I. Lopez-Tocon, J. F. Arenas, J. Soto and J. C. Otero (2006): "Selection rules of the charge transfer mechanism of surface-enhanced Raman scattering: The effect of the adsorption on the relative intensities of pyrimidine bonded to silver nanoclusters." *The Journal of Physical Chemistry B* **110** (30): 14916-14922.

200. Centeno, S. P., I. Lopez-Tocon, J. Roman-Perez, J. F. Arenas, J. Soto and J. C. Otero (2012): "Franck–Condon dominates the surface-enhanced Raman scattering of 3-methylpyridine: propensity rules of the charge-transfer mechanism under reduced symmetry." *The Journal of Physical Chemistry C* **116** (44): 23639-23645.

201. Schlücker, S., J. Koster, R. Singh and B. Asthana (2007): "Hydrogen-bonding between pyrimidine and water: A vibrational spectroscopic analysis." *The Journal of Physical Chemistry A* **111** (24): 5185-5191.

202. Singh, D. K., S. Mishra, A. K. Ojha, S. K. Srivastava, S. Schlücker, B. Asthana, J. Popp and R. K. Singh (2011): "Hydrogen bonding in different pyrimidine–methanol clusters probed

by polarized Raman spectroscopy and DFT calculations." *Journal of Raman Spectroscopy* **42** (4): 667-675.

203. Takahashi, H., K. Mamola and E. K. Plyler (1966): "Effects of hydrogen bond formation on vibrations of pyridine, pyrazine, pyrimidine, and pyridazine." *Journal of Molecular Spectroscopy* **21** (1-4): 217-230.

204. Arenas, J. F., M. S. Woolley, I. L. Tocón, J. C. Otero and J. I. Marcos (2000): "Complete analysis of the surface-enhanced Raman scattering of pyrazine on the silver electrode on the basis of a resonant charge transfer mechanism involving three states." *The Journal of Chemical Physics* **112** (17): 7669-7683.

205. Barsberg, S. (2015): "Identification of the best DFT functionals for a reliable prediction of lignin vibrational properties." *Theoretical Chemistry Accounts* **134** (3): 1-12.

206. Pagliai, M., L. Bellucci, M. Muniz-Miranda, G. Cardini and V. Schettino (2006): "A combined Raman, DFT and MD study of the solvation dynamics and the adsorption process of pyridine in silver hydrosols." *Physical Chemistry Chemical Physics* **8** (1): 171-178.

207. Becke, A. D. (1988): "Density-functional exchange-energy approximation with correct asymptotic behavior." *Physical Review A* **38** (6): 3098-3100.

208. Jensen, L., L. L. Zhao and G. C. Schatz (2007): "Size-Dependence of the Enhanced Raman Scattering of Pyridine Adsorbed on Agn (n = 2−8, 20) Clusters." *The Journal of Physical Chemistry C* **111** (12): 4756-4764.

209. Van Duyne, R., J. Hulteen and D. Treichel (1993): "Atomic force microscopy and surface‐enhanced Raman spectroscopy. I. Ag island films and Ag film over polymer nanosphere surfaces supported on glass." *The Journal of Chemical Physics* **99** (3): 2101-2115.

VITA

John T. Kelly
Department of Chemistry and Biochemistry
University of Mississippi

Education

2016 Doctors of Philosophy (Physical Chemistry)	University of Mississippi
2011 Bachelors of Science (Chemistry)	Georgia Southern University

Research Experience

Gaseous Molecular Cluster Spectroscopy	University of Mississippi
Advisor: Nathan I. Hammer	2011 – 2016
Characterization of Biofuel by NMR	Georgia Southern University
Advisor: David I. Kreller	Fall/Spring 2010
Molten Salt Synthesis and XRD Analysis	Georgia Southern University
Advisor: James Burgess (REU)	Summer 2008

Teaching Experience

Summer Research Mentor	University of Mississippi
Research Experience for Undergraduates	2011 – 2016
Assistant Student Lecturer	University of Mississippi
Course: Physical Chemistry I/II	2011 – 2016
Graduate Teaching Assistantship	University of Mississippi
Course: Physical Chemistry I/II	2011 – 2013
Laboratory Teaching Assistant	Georgia Southern University
Course: Physics I	Fall 2008

Appointments, Honors, and Awards

Associate Member	American Chemical Society
Younger Chemist Committee	2016
Outstanding Graduate Research Award	American Chemical Society
Local Section (Ole Miss)	2016
Local Section Founder/President	American Chemical Society
Younger Chemist Committee	2014